

**BIOENGINEERING TARGETED NANODRUGS FOR HEMATOLOGIC
MALIGNANCIES: AN INNOVATION IN PEDIATRIC ONCOLOGY**

by

Vinu Krishnan

A dissertation submitted to the Faculty of the University of Delaware
in partial fulfillment of the requirements for the degree of Doctor of Philosophy in
Materials Science and Engineering

Spring 2015

Copyright 2015 Vinu Krishnan
All Rights Reserved

ProQuest Number: 3718344

All rights reserved

INFORMATION TO ALL USERS

The quality of this reproduction is dependent upon the quality of the copy submitted.

In the unlikely event that the author did not send a complete manuscript and there are missing pages, these will be noted. Also, if material had to be removed, a note will indicate the deletion.



ProQuest 3718344

Published by ProQuest LLC (2015). Copyright of the Dissertation is held by the Author.

All rights reserved.

This work is protected against unauthorized copying under Title 17, United States Code
Microform Edition © ProQuest LLC.

ProQuest LLC.
789 East Eisenhower Parkway
P.O. Box 1346
Ann Arbor, MI 48106 - 1346

**BIOENGINEERING TARGETED NANODRUGS FOR HEMATOLOGIC
MALIGNANCIES: AN INNOVATION IN PEDIATRIC ONCOLOGY**

by

Vinu Krishnan

Approved: _____
Darrin J. Pochan, Ph.D.
Chair of the Department of Materials Science and Engineering

Approved: _____
Babatunde Ogunnaike, Ph.D.
Dean of the College of Engineering

Approved: _____
James G. Richards, Ph.D.
Vice Provost for Graduate and Professional Education

I certify that I have read this dissertation and that in my opinion it meets the academic and professional standard required by the University as a dissertation for the degree of Doctor of Philosophy.

Signed:

Ayyappan K. Rajasekaran, Ph.D.
Chair and Professor in charge of dissertation

I certify that I have read this dissertation and that in my opinion it meets the academic and professional standard required by the University as a dissertation for the degree of Doctor of Philosophy.

Signed:

Xinqiao Jia, Ph.D.
Co-chair and Professor in charge of dissertation

I certify that I have read this dissertation and that in my opinion it meets the academic and professional standard required by the University as a dissertation for the degree of Doctor of Philosophy.

Signed:

Robert W. Mason, Ph.D.
Member of dissertation committee

I certify that I have read this dissertation and that in my opinion it meets the academic and professional standard required by the University as a dissertation for the degree of Doctor of Philosophy.

Signed:

Millicent O. Sullivan, Ph.D.
Member of dissertation committee

I certify that I have read this dissertation and that in my opinion it meets the academic and professional standard required by the University as a dissertation for the degree of Doctor of Philosophy.

Signed:

David C. Martin, Ph.D.
Member of dissertation committee

ACKNOWLEDGMENTS

First and foremost, I am most deeply indebted to my research advisor Prof. A. K. Rajasekaran (Raj) for his constant support, encouragement and guidance. This work would not have been possible without his vision to save children with cancer and his confidence in my abilities to realize that vision. I am thankful to Raj for providing me all the necessary resources, including collaborations and facilities, to complete this dissertation. I am also grateful to him for helping me expand my horizons in cancer research and for involving me extensively during grant submissions and manuscript writing process. Raj has been phenomenal as a mentor and a friend in uplifting my confidence, especially in tough situations and for nurturing my skills and acumen too. This has given me the ability to think analytically and to be a good critique with the big picture in mind. I am obliged to Raj for giving me this opportunity to contribute to the field of nanomedicine, which would benefit every child affected with cancer and their families around the world.

I wish to thank Dr. Xinqiao Jia, for her firm support, words of inspiration and advice throughout my graduate life. Her patience and aggressiveness are the most important traits that I would hold onto when I take the next step in my career. No words can do justice to my gratitude towards her for giving me the opportunity to work in her lab and for supporting the successful completion of this dissertation. I will forever appreciate her efforts and hope to remain in touch with her.

I am extremely grateful to Dr. Robert W. Mason at the Nemours Alfred I duPont Hospital for Children who helped me to think and gain an overall perspective of my research from a clinical point of view. I learnt from him the basics of assay development and how to decide the appropriate controls that were critical to this study. I sincerely appreciate his time and effort in providing valuable guidance and support at critical moments in my life. I am glad that I got the opportunity to work and discuss extensively with him about this work right from the beginning.

I would like to thank my committee members Prof. David C. Martin from the Department of Materials Science and Engineering and Prof. Millicent O. Sullivan from the Department of Chemical and Biomolecular Engineering for their time and effort in reviewing this dissertation. Constructive ideas, insights and suggestions from them significantly increased my knowledge, and the quality of this work. I am also grateful to our collaborators, Prof. Scott A. Waldman and Dr. Adam Snook from Thomas Jefferson University for their scientific input and critical thinking in developing this project.

I should also mention all of my past and current colleagues in the Raj, Jia and Mason groups, to whom I am obliged for their help in planning the studies, exchanging ideas through discussions, and for all their support, encouragement and friendship. I am most indebted to Dr. Thu P. Huynh, Daniel Wolle, Dr. Seung Joon Lee, Dr. Valerie B. Sampson and Dr. Sonali P. Barwe – all previously with the Raj Lab – for helping me to start the project and for training me in cell biology and *in vivo* techniques. I also owe special thanks to Dr. Justin M. David, Pratima U. Patil

and Sona Lakshme Balasubramaniam for their critical and helpful insights on my project while we enjoyed our times together outside the lab. From the Jia group, Dr. Xian Xu, Dakota Kelly and Xiaowei Yang deserve special mention and recognition; for without their contribution, this project could not have advanced to the point where it stands today. In addition, I would like to thank Dr. Shuang Liu for her critical and valuable perceptions on this study. From the Mason Lab, I am very grateful to Dr. Bruce D. Korant for sharing with me a copy of any interesting publication that he came across by leaving it either on my desk or in my mailbox. Suzanne Purfield, Lisa G. Glazewski and Guizhen Liu have been the most helpful in taking care of all administrative needs, ordering of lab supplies and maintenance of equipments required to complete this project. I deeply enjoyed working in all the three labs in an interdisciplinary manner, and this has increased my confidence and the willingness to explore uncharted territories as I move forward.

I would like to thank Dr. Gwen Talham, Frank M. Warren and Minh A. Pham for providing access to valuable resources at the University of Delaware's Office of Laboratory Animal Medicine. I would also like to acknowledge Prof. Randall L. Duncan, Dr. Mary Boggs and Jim Farmer from the Department of Biological Sciences for giving me the permission to use their tissue culture room facility in McKinley Lab.

I would like to express my gratitude to the Department of Materials Science and Engineering current and past staff members (Charles O. Garbini, Robin J. Buccos, Kathleen A. Forwood, Christine A. Williamson, Naima Hall and Dionne M. Putney) for their assistance with administrative work and laboratory safety.

I am extremely grateful for my friends at the University of Delaware, in the United States, and everywhere else, for without their encouragement, I would not have been able to work here miles away from home.

I would like to thank my parents, my sister and brother-in-law for their prayers and sacrifices while pursuing my dreams. I am also indebted to my parents-in-law and brother-in-law for their constant love and care during this endeavor.

Finally, mere words can never sum up the gratitude I have for the love of my life - Priyanka, for putting up with my tantrums and me while completing this work. Her unconditional love, patience, support and belief in me have always been an inspiration. This work could not have been completed without her.

Thank you so much everyone!

TABLE OF CONTENTS

LIST OF TABLES	xiii
LIST OF FIGURES	xiv
LIST OF ABBREVIATIONS	xvi
ABSTRACT	xix
Chapter	
1 INTRODUCTION	1
1.1 Acute Lymphoblastic Leukemia (ALL) and the Chemotherapy Conundrum	1
1.2 Pediatric Leukemia – Pathophysiology.....	2
1.3 Treatment for ALL.....	3
1.3.1 Chemotherapy:	4
1.3.2 Radiation Therapy and Stem Cell Transplant:	7
1.3.3 Targeted Therapies:.....	7
1.3.4 Immunotherapy:	8
1.4 Side Effects in Treatment of ALL.....	10
1.5 Cancer Nanomedicine	13
1.5.1 Types of Nanocarriers:.....	13
1.5.2 Nanocarriers-based Drug Delivery:	15
1.6 Dissertation Summary	22
2 DEXAMETHASONE-LOADED BLOCK COPOLYMER NANOPARTICLES INDUCE LEUKEMIA CELL DEATH AND ENHANCES THERAPEUTIC EFFICACY <i>IN VITRO</i> AND <i>IN VIVO</i> * ..	28
2.1 Introduction.....	28
2.2 Experimental Section	31
2.2.1 Reagents, Cell Lines and Mouse Models:.....	31
2.2.2 Polymer Synthesis:.....	32
2.2.3 Particle Formulation and Drug/Dye Encapsulation:	32
2.2.4 Characterization of NPs:	33
2.2.5 Drug/Dye Loading and Release:	34
2.2.6 <i>In Vitro</i> Toxicity:	35
2.2.7 Hemolytic Activity and <i>in Vivo</i> Tolerability:	35

2.2.8	Dexamethasone Bioactivity Assay:	36
2.2.9	Cytotoxicity Evaluation of Dex-NPs:	36
2.2.10	Evaluation of Apoptosis:.....	37
2.2.11	Measurement of Glucocorticoid Receptor (GR) Phosphorylation:	38
2.2.12	Determination of Cellular Uptake of ECT2-NPs:.....	39
2.2.13	<i>In Vivo</i> Pharmacokinetics and Biodistribution:	39
2.2.14	<i>In Vivo</i> Antitumor Efficacy:.....	41
2.2.15	Statistical Analysis:.....	41
2.3	Results.....	42
2.3.1	NP Formulation and Characterization:	42
2.3.2	Drug/Dye Loading and Release:	44
2.3.3	ECT2-NPs are Non-toxic <i>in Vitro</i> and <i>in Vivo</i> :	45
2.3.4	Dex-NPs Deliver Bioactive Dexamethasone and Induce Apoptosis in Leukemia Cells:	48
2.3.5	ECT2-NPs are Bound to and Internalized by Leukemia Cells:	50
2.3.6	ECT2-NPs Deliver Dexamethasone to Leukemia Cells at Sustained Rates:	51
2.3.7	Biodistribution and Clearance of ECT2-NPs in Mice:	53
2.3.8	Dex-NPs Enhance Therapeutic Efficacy in a Pre-clinical ALL Mouse Model:	54
2.4	Discussion	56
2.5	Conclusion	61
3	CD19-TARGETED NANODELIVERY OF DOXORUBICIN ENHANCES THERAPEUTIC EFFICACY IN ACUTE LYMPHOBLASTIC LEUKEMIA.....	62
3.1	Introduction	62
3.2	Experimental Section	66
3.2.1	Reagents, cell lines and mouse models:.....	66
3.2.2	Preparation of DOX-loaded NPs with or without the targeting Ab:	67
3.2.2.1	Polymer synthesis:.....	67
3.2.2.2	Synthesis of avidin-palmitic acid conjugates (avidin-PA):.....	67
3.2.2.3	Preparation of drug/dye-loaded NPs:	68
3.2.2.4	Preparation of drug-loaded Ab-conjugated NPs:	68

3.2.3	NP characterization:	69
3.2.3.1	Particle size and surface charge:.....	69
3.2.3.2	Drug/dye loading and <i>in vitro</i> release:	69
3.2.3.3	Quantifying anti-CD19Abs on NPs:.....	70
3.2.4	Analyzing CD19 cellular levels:	71
3.2.4.1	Immunoblot:	71
3.2.4.2	Flow cytometry.....	72
3.2.5	Cell uptake of non-targeted and targeted NPs:	72
3.2.5.1	Treatment with NPs, CD19-NPs and IgG-NPs:.....	72
3.2.5.2	Treatment with endocytic inhibitors:.....	73
3.2.6	Cytotoxicity evaluation of DOX formulations:	74
3.2.6.1	Evaluation of toxicity:	74
3.2.6.2	Evaluation of apoptosis:	74
3.2.7	HPLC/MS/MS analysis of cell associated DOX (intracellular and cell surface bound) levels in targeted and non-targeted cells:	75
3.2.8	<i>In vivo</i> pharmacokinetics and biodistribution:	76
3.2.9	Measurement of agility and monitoring of survival:	77
3.2.10	Statistical Analysis:.....	77
3.3	Results	78
3.3.1	NP formulation and characterization:	78
3.3.2	Drug/dye loading and release:.....	80
3.3.3	CD19-specific targeting and uptake of anti-CD19Ab-conjugated NPs:	82
3.3.4	Competition assays confirmed specific binding and uptake of anti-CD19Ab-conjugated NPs:	83
3.3.5	Analysis of endocytic mechanism for anti-CD19Ab-conjugated NPs:	84
3.3.6	CD19-mediated induction of apoptosis in leukemia cells:	86
3.3.7	CD19 targeting increases the cell-associated DOX (intracellular and cell surface bound) levels in RS4;11 cells:	87
3.3.8	Plasma levels and biodistribution of anti-CD19Ab-conjugated NPs in mice.....	91

3.3.9	CD19-DOX-NPs Enhance Therapeutic Efficacy in a Pre-clinical Mouse Model of ALL:.....	92
3.4	Discussion	94
3.5	Conclusion	98
4	CONCLUSIONS AND FUTURE WORK.....	99
4.1	Conclusions.....	99
4.2	Future Work	101
4.2.1	Nanomaterials Design and Characterization for ‘ALL’ Therapy	102
4.2.1.1	Size and Shape of Nanocarriers:.....	102
4.2.1.2	Blood Half-life of Nanocarriers.....	103
4.2.1.3	Active Targeting of Nanocarriers to Leukemic Cells.....	103
4.2.1.4	Drug Release Kinetics of Nanocarriers:	104
4.2.1.5	Mathematical Modeling:	104
4.2.1.6	Combinatorial Treatment Studies:.....	105
4.3	Nanomedicine for Pediatric Leukemia – A Final Perspective	105
	REFERENCES	108
	Appendix	
A	PERMISSION LETTERS	125
B	CALCULATIONS	129
C	ANIMAL SUBJECTS PROTOCOL REVIEW AND APPROVAL BY INSTITUTIONAL REVIEW BOARD (IRB)	131

LIST OF TABLES

Table 1.1	Anticancer agents for the treatment of acute lymphoblastic leukemia (ALL)	6
Table 1.2	Non-targeted NPs clinically approved or advanced in clinical trials	17
Table 1.3	Targeted NPs in clinical trials	21
Table 3.1	Summary of size, loading content and encapsulation efficiency of different types.....	79

LIST OF FIGURES

Figure 1.1.	Comparison of chemo- and nano- therapy in childhood leukemia treatment.....	12
Figure 1.2.	Nanocarriers for drug delivery applications.....	14
Figure 1.3.	Illustration of non-targeted nanocarriers.....	23
Figure 1.4.	Illustration of targeted nanocarriers.....	27
Figure 2.1.	(A) Chemical structure of ECTx copolymer consisting of a hydrophilic PEG block and a hydrophobic PCL segment carrying randomly distributed cyclic ketals. Analysis of particle size (B and C) and morphology (D):	43
Figure 2.2.	<i>In vitro</i> release profiles of Dex (square), Nile red (diamond) and DiR (triangle) from nanoparticles in PBS (pH 7.4) at ambient temperature	45
Figure 2.3A.	Effect of ECT2-NPs on the viability of leukemia and carcinoma cell lines.....	46
Figure 2.3B.	<i>In vitro</i> hemolytic analysis of ECT2-NPs on human blood	47
Figure 2.3C.	<i>In vivo</i> biocompatibility of ECT2-NPs in C57BL/6 mice (3 per group):	47
Figure 2.4A.	Bioactivity of Dex is retained post encapsulation:	49
Figure 2.4B.	Dose-response curves of free Dex and Dex-NPs at 48h.....	49
Figure 2.4C.	Cleaved PARP and cleaved caspase-3 levels confirm Dex-NP induced apoptosis in RS4;11 cells at 48h	50
Figure 2.5.	NR-NPs bind and internalize by non-specific uptake	51
Figure 2.6.	Dex-NPs act as sustained-release formulations when treated with leukemia cells <i>in vitro</i>	52
Figure 2.7.	ECT2-NPs in mice. Balb/c mice (3 per group) were intravenously injected with DiR-NPs (0.2mg/kg DiR):	53
Figure 2.8.	Dex-NPs enhance therapeutic efficacy and prolongs survival in pre-clinical leukemia mouse models	55
Figure 2.9.	CLSM images of Nalm6 leukemic cells treated with free Nile-red (L) and NR-NP (R).....	59
Figure 3.1.	A representative immunoblot used to quantify biotinylated anti-CD19Ab levels on NPs.	80
Figure 3.2.	<i>In vitro</i> release profiles from non-targeted and targeted NPs.....	81

Figure 3.3.	Quantification of CD19 total and surface expression levels in REH and RS4;11 B-ALL cells	82
Figure 3.4.	CD19 specific targeting and uptake of anti-CD19Ab conjugated NPs.....	84
Figure 3.5.	Analysis of endocytic mechanism for anti-CD19Ab conjugated NPs.....	85
Figure 3.6.	CD19-mediated induction of apoptosis in leukemia cells.....	86
Figure 3.7.	Treatment of REH cells with free DOX or CD19-DOX-NPs (\approx 100nM, 1 μ M or 10 μ M DOX) for 1h at 37°C.....	88
Figure 3.8.	Treatment of RS4;11 cells with free DOX or CD19-DOX-NPs (\approx 100nM, 1 μ M or 10 μ M DOX) for 1h at 37°C.....	88
Figure 3.9.	CD19-targeting increases the cell associated DOX (intracellular and cell surface bound, caDOX) levels in RS4;11 cells.....	89
Figure 3.10.	CD19-targeting achieves similar cell associated DOX (intracellular and cell surface bound, caDOX) levels in RS4;11 cells.....	90
Figure 3.11.	CD19-targeting reduces the cell associated DOX (intracellular and cell surface bound, caDOX) levels in REH cells.....	90
Figure 3.12.	Plasma levels and biodistribution of anti-CD19Ab conjugated NPs in mice.....	91
Figure 3.13.	CD19-DOX-NPs enhance therapeutic efficacy and prolongs survival in pre-clinical leukemia mouse models.....	93
Figure 3.14.	CD19-DOX-NPs maintained high agility factor in leukemic mice.....	94
Figure 4.1.	Nanoparticle design (size, shape and blood-half-life) requirements to target sites of leukemia-cell proliferation.....	106

LIST OF ABBREVIATIONS

6-MP	6-mercaptopurine
Ab	Antibody
ABC	Accelerated Blood Clearance
ADCC	Antibody Dependent Cellular Cytotoxicity
ALL	Acute Lymphoblastic Leukemia
AML	Acute Myeloid Leukemia
APC	Allophycocyanin
AUC _{blood}	Area under the drug versus time concentration curve in blood from time of administration
BBB	Blood Brain Barrier
CDC	Complement Dependent Cytotoxicity
CML	Chronic Myeloid Leukemia
CNS	Central Nervous System
COG	Children's Oncology Group
CPT	Camptothecin
Dex	Dexamethasone
DOX	Doxorubicin
DOX-HCL	doxorubicin hydrochloride
DiR	1,1'-dioctadecyl-3,3,3',3' tetramethylindotricarbocyanine iodide
DRR	Drug Release Rates

DLS	Dynamic Light Scattering
Dtxl	Docetaxel
EDTA	Ethylenediaminetetraacetic Acid
EE	Encapsulation Efficiency
EPR	Enhanced Permeability and Retention
FBS	Fetal Bovine Serum
FITC-CD19	Fluorescein Isothiocyanate-CD19
FITC-Tf	Fluorescein Isothiocyanate-transferrin
GVHD	Graft-versus-Host Disease
IACUC	Institutional and Animal Care Use Committee
HPLC	High-performance Liquid Chromatography
IC50	Half Maximal Inhibitory Concentration
IRRs	Infusion-Related Reactions
LC	Loading Content
mAbs	Monoclonal Antibodies
MDR	Multi-Drug Resistance
Mn	Number-Average Molecular Weight
MPS	Mononuclear Phagocyte System
MTD	Maximum Tolerated (Tolerable) Dose
MTX	Methotrexate
NHS-PA	Palmitic acid N-hydroxysuccinimide ester
NK	Natural Killer Cells

NP	Nanoparticle
NR	Nile Red
OHA	Oxaliplatin
PBS	Phosphate Buffered Saline
PCL	Poly(ϵ -caprolactone)
PDI	Polydispersity Index
PEG	Poly(ethylene glycol)
Ph+/-	Philadelphia Chromosome Positive or Negative
PK	Pharmacokinetics
PLGA	Poly(lactic-co-glycolic)
PSMA	Prostate Specific Membrane Antigen
RBCs	Red Blood Cells
t _{1/2}	Terminal Half-life
TEM	Transmission Electron Microscopy
Tf	Transferrin
TSU	1,4,8-trioxaspiro-[4,6]-9-undecanone
Vcr	Vincristine Sulfate
VOD	Veno-Occlusive Disease
WBCs	White Blood Cells

ABSTRACT

Chemotherapy for pediatric cancers employs combinations of highly toxic drugs. This has achieved 5-year survival rates exceeding 90% in children treated for leukemia – the most prominent form of pediatric cancer. However, delayed onset of harmful side effects in more than 60% of survivors result in death or low quality of life post therapy. This is primarily due to the non-specific effect of drugs on healthy dividing cells in a growing child. Nanomedicine has advanced tremendously to improve adult cancer therapy, but as yet has had minimal impact in pediatric oncology. There is a pressing need for innovative therapeutic strategies that can reduce life-threatening side effects caused by conventional chemotherapy in the clinic. Targeting chemotherapeutic agents specifically to leukemia cells may alleviate treatment-related toxicity in children. The research objective of this dissertation is to bioengineer and advance preclinically a novel nanotherapeutic approach that can specifically target and deliver drugs into leukemic cells.

Dexamethasone (Dex) is one of the most commonly used chemotherapeutic drugs in treating pediatric leukemia. For the first part in this study, we encapsulated Dex in polymeric NPs and validated its anti-leukemic potential *in vitro* and *in vivo*. NPs with an average diameter of 110 nm were assembled from an amphiphilic block copolymer of poly(ethylene glycol) (PEG) and poly(ϵ -caprolactone) (PCL) bearing pendant cyclic ketals (ECT2). The blank NPs were

nontoxic to cultured cells *in vitro* and to mice *in vivo*. Encapsulation of Dex into the NPs (Dex-NP) did not compromise the bioactivity of the drug. Dex-NPs induced glucocorticoid phosphorylation and showed cytotoxicity similar to free drug when treated with leukemic cells. Studies using NPs labeled with fluorescent dyes revealed leukemic cell surface binding and internalization. *In vivo* biodistribution studies showed NP accumulation in the liver and spleen with subsequent clearance of particles with time. In a preclinical model of leukemia, Dex-NPs significantly improved the quality of life and survival of mice compared to the group treated with free Dex.

In the second section, we demonstrate, that doxorubicin (DOX, an anthracycline commonly used in pediatric leukemia therapy) when encapsulated within 80 nm sized NPs and modified with targeting ligands against CD19 (a B-lymphoblast antigen, CD19-DOX-NPs) can be delivered in a CD19-specific manner to leukemic cells. The CD19-DOX-NPs were internalized via receptor-mediated endocytosis and imparted cytotoxicity in a CD19-dependent manner in CD19 positive (CD19+) leukemic cells. Leukemic mice treated with CD19-DOX-NPs survived significantly longer and manifested a higher degree of agility indicating reduced apparent systemic toxicity during treatment compared to mice treated with free DOX. This study for the first time shows the efficacy of polymeric NPs to target and deliver chemotherapeutic drugs in pediatric oncology and suggests that targeted nanotherapy can potentially improve the therapeutic efficacy of conventional chemotherapy and reduce treatment-related side effects in children.

Chapter 1

INTRODUCTION*

1.1 Acute Lymphoblastic Leukemia (ALL) and the Chemotherapy Conundrum

Leukemia is the most common type of cancer in children. The disease accounted for one-third of all cancer deaths in children <15 years of age in 2012. The two major types of leukemia common in children are acute lymphoblastic leukemia (ALL) and acute myeloid leukemia (AML) (1). ALL is the most prevalent childhood malignancy accounting for over 75% of all forms of leukemia in children and adolescents younger than 20 years of age (1).

Significant improvements in pediatric cancer treatment led to extraordinary success in achieving an overall five-year relative survival rate of over 90% for pediatric ALL (1). This success is tempered by delayed onset of treatment-related complications; including relapse, secondary cancers, cognitive and/or growth impairment, cardiac disease and pulmonary disease in more than 60% of childhood cancer survivors (2). Low target specificity, limited diffusion across cancer cell membranes, and low therapeutic index require high doses of anticancer agents that induce treatment-related toxic side effects and jeopardize the clinical outcome of cancer patients. Novel clinical strategies are needed to optimize the effective

* Reprinted (adapted) with permission from (<http://onlinelibrary.wiley.com/doi/10.1038/clpt.2013.174/abstract>), *Clinical Pharmacology & Therapeutics*, 2014, 95 (2), pp 168–78). © 2014 American Society for Clinical Pharmacology and Therapeutics

therapeutic dose to minimize side effects. This could be achieved by localizing the agents' pharmacological activity to the site of action (an organ, tumor or a metastatic cancer cell). Drug delivery systems can be designed to distribute drugs in (i) controlled and (ii) targeted fashion.

Although current chemotherapeutic regimens in childhood leukemia have improved prognosis dramatically, the drugs used presently in the clinic do not discriminate between actively dividing normal cells and uncontrollably dividing leukemic cells. Targeting clinically approved chemotherapeutic drugs specifically to leukemic cells should alleviate toxic effects on normal cells and prevent treatment-related side effects in children. The clinical impact of nanomedicine is clearly evident as several of these approaches are presently being used to effectively combat adult cancers (3, 4). While the rationale is clear and the need is pressing, there has been minimal development and research to utilize nanotechnology for combating childhood cancers.

1.2 Pediatric Leukemia – Pathophysiology

Acute lymphocytic leukemia (ALL) is a form of leukemia characterized by uncontrolled proliferation of malignant immature white blood cells or lymphoid cells in the bone marrow. The origin of the disease may involve the occurrence of a transformation event in a single progenitor cell which may either be an early precursor cell or a committed lymphoid B-or T-cell that give rise to different subtypes of ALL. The subsequent continuous clonal expansion of the initial leukemogenic event results in massive proliferation of immature lymphoid cells. These tumor cells can damage internal organs and cause death by disrupting

growth of normal and essential cells (hematopoiesis) including red blood cells (RBCs), white blood cells (WBCs) and platelets in the bone marrow. Common symptoms in patients with ALL include massive blast infiltration in (a) the bone marrow and periosteum resulting in bone and joint aches; (b) the lymphoid system characterized by enlarged lymph nodes (lymphadenopathy), liver and spleen (hepatosplenomegaly); (c) and the central nervous system (CNS) resulting in symptoms such as frequent headaches, sixth-nerve palsy, edema and vomiting. In cases of recurrent ALL, the malignant blasts may appear in the testicular regions as well. This tissue infiltration, combined with the body's lack of ability to fight infections due to neutropenia (neutrophil count $<500/\text{mm}^3$) in a majority of cases at presentation, and leukocytosis (leukocyte count $>50,000/\text{mm}^3$) in approximately 20% of cases can result in additional complications during disease progression. The condition of ALL also results in severe anemia ($\text{Hb}<7\text{g/dL}$) and thrombocytopenia (platelet count $<50,000/\text{mm}^3$) causing excessive bruising and bleeding, fever, and fatigue accompanied with loss of appetite and gradual weight loss.

1.3 Treatment for ALL

Existing treatment protocols involve the combined use of chemotherapeutics administered at maximum tolerated dose (MTD). The use of such combinatorial regimens was far more effective than using single drugs in achieving complete and long-term remission. With single agents, only 60% of patients achieved complete remission, while the remainder did not respond or relapse within 6-9 months (5). The combination therapies help prevent

proliferation of tumor cells that mutate to become resistant to single agents during therapy, a problem faced by more than 50% of newly diagnosed cancer cases (6).

1.3.1 Chemotherapy:

Some of the most commonly used chemotherapeutic drugs to treat ALL are listed in Table 1.1. These agents belong to the class of glucocorticoids (*dexamethasone, prednisone, prednisolone*) (7); genotoxic drugs (*daunorubicin, doxorubicin, idarubicin, mitoxantrone, ifosamide, cyclophosphamide and carboplatin*) (8, 9) spindle inhibitors (*vincristine and vindesine*) (10); and antimetabolites (*methotrexate, 6-mercaptopurine, 6-thioguanine, cytarabine, fludarabine, clofarabine, cladribine, azacitidine and hydroxyurea*) (11-13). The drugs are administered in various combinations (chemotherapy regimens) at different phases of the therapy and the type of regimen adopted usually depends on the patient's age and risk factors.

(A) Stages in Chemotherapy:

Treatment of ALL using chemotherapy generally involves three different phases – (1) Induction Therapy (2) Consolidation Therapy and (3) Maintenance Therapy. Induction therapy is the first phase of chemotherapy in ALL. The objective of this phase is to bring the disease into remission by eliminating the leukemic blasts in the blood and bone marrow. The induction phase is highly intense since the treatment regimen lasts about a month. Consolidation therapy begins when the disease is in remission. The purpose here is to prevent relapse by wiping out remaining malignant cells in the blood and bone marrow. The

consolidation phase is also intense since the combinatorial regimens are administered for at least four to eight months. The final phase of chemotherapy in ALL is the maintenance therapy. The goal here is to achieve obliteration of all residual tumor cells within the patient. This final phase is expected to complete the patient's return to a healthy state with normal blood counts. The maintenance therapy is less intense when compared to the previous two phases since reduced doses of chemotherapeutic regimens are administered for two to three years to ensure that any residual tumor cells are eradicated.

At standard doses, chemotherapeutic agents do not cross the blood-brain barrier (BBB). To destroy leukemic cells in the CNS and prevent relapse, children with ALL receive higher doses of drugs, either by injecting directly into the spinal fluid or by implanting a drug reservoir device (Omaya reservoir) beneath the scalp. This treatment is referred to as intrathecal therapy or CNS sanctuary therapy that serves to prophylactically treat the sanctuary site preventing the risk of CNS relapse. It is usually combined with induction or consolidation and in certain cases the maintenance therapy. Despite attaining remission in 95% of children after induction therapy; the extensive systemic exposure to the non-specific effect of anticancer agents is evident in each phase of the treatment. Consequently, deleterious treatment-related side effects are induced, reducing the quality of life

Table 1.1: Anticancer agents for the treatment of acute lymphoblastic leukemia (ALL).

Mode of therapy	Class of Drugs	Trade Name	Common Side Effects (for the class)	References
Chemotherapy	(1) Glucocorticoids (Synthetic Hormones)	Dexamethasone Prednisone Prednisolone	Immunodeficiency, Osteoporosis, Hyperglycemia, Cushing's Syndrome	7
	(2) Genotoxic Drugs	Daunorubicin (Cerubidine®) Doxorubicin (Adriamycin®) Idarubicine (Idamycin®) Mitoxantron (Novatrone®) Ifosamide (Ifex) ® Cyclophosphamide(Cytoxan) ® Carboplatin (Paraplatin) ® Vincristine (Oncovin®, Vincasar PFS®, Vincrex®) Vindesine (Eldisine, Fildesin)	Cardiotoxicity, Myelosuppression, Nausea, Vomiting, Diarrhea, Mucositis, Encephalopathy, Hemorrhagic Cystitis, Hypersensitivity, Nephrotoxicity	8, 9
	(3) Spindle Inhibitors	Methotrexate (Trexal®) 6-Mercaptopurine (Purinethol®) 6-Thioguanine Cytarabine (Cytosar-U®) Fludarabine (Fludara®) Clofarabine (Clolar®) Cladribine (2-CdA; Leustatin®) Azacitidine (Vidaz®) Hydroxyurea (Hydrea®)	Peripheral Neuropathy, Hyponatremia, Nausea, Vomiting, Myelosuppression	10
	(4) Antimetabolites	Imatinib Mesylate (Gleevec®) Dasatinib (Sprycel®) Nilotinib (Tasigna®) Asparaginase (Elspar®) Topotecan (Hycamtin®) Etoposide (VP-16, VePesid®, Etopophos®)	Oral/Gastrointestinal Mucositis, Neurotoxicity, Nephrotoxicity, Hepatotoxicity, Myelosuppression, Nausea and Vomiting	11-13
Targeted Therapies	1) BCR-ABL Tyrosine Kinase Inhibitors 2) Enzyme Activators 3) Enzyme Inhibitors	Alemtuzumab (Campath®)/CD52 Epratuzumab/CD22 Rituximab (Rituxan®)/CD20 SAR3419/CD19	Hypersensitivity Typhlitis, Diarrhea, Mucositis, Nausea, Vomiting, Hypersensitivity	14 15 16
Immunotherapy	Antibody Dependant Cellular Cytotoxicity			21-29

in children both during therapy and for many years after.

1.3.2 Radiation Therapy and Stem Cell Transplant:

Occasionally in patients with advanced or recurrent ALL, radiation bursts or high energy X-rays are applied to the brain, spinal cord or the testicular region to prevent relapse. However, radiation therapy affects the growth and mental development of children subjected to chemotherapy. Another form of treatment in patients with high risk ALL constitutes transplantation of stem cells from a matching healthy donor after intensive chemotherapy and radiation therapy. Stem-cell transplantation is often associated with serious complications including graft-versus-host disease (GVHD) where the transplanted immune cells identify the host's normal cells as foreign and destroy them. Hence, the therapy does not form part of the treatment plan in a majority of cases.

1.3.3 Targeted Therapies:

The severe treatment-related side effects due to chemotherapy led to the evolution of targeted therapies that comprised of novel small molecules to target cancer cells and not normal cells. Some of the standard targeted drugs that have been approved by the FDA and novel compounds that are in clinical trials for treating childhood ALL are listed in Table 1.1. These include BCR-ABL tyrosine kinase inhibitors (*imatininib mesylate, dasatinib, nilotinib*) (14); enzyme activators (*aspariginase*) (15); and enzyme inhibitors (*topotecan, etoposide*) (16). However, such anticancer agents were effective only when combined with chemotherapeutic agents.

A major drawback associated with use of targeted therapeutics was the multi-drug resistance acquired by cancer cells. Cancer cells can acquire multi-drug resistance (MDR) that may depend upon pharmacologic factors and cell mechanisms involved in cancer cell function and survival (17, 18). For instance, the development of mutations in the kinase domain of BCR-ABL (a fusion between BCR, break point cluster gene at chromosome 22 and ABL, Abelson tyrosine kinase gene at chromosome 9) in Philadelphia chromosome positive (Ph+) ALL and Chronic Myeloid Leukemia (CML) patients lead to therapeutic inefficacy of *imatinib mesylate* (Gleevec®) (14, 19). The drug was originally approved as a tyrosine kinase inhibitor for treating patients affected with CML and Ph+ALL and was effective as single agent or in combination therapy (14, 20). Additional factors that contribute to imatinib resistance are decreased permeability or increased efflux of the drug from the leukemic cells, activation of alternate signaling pathways (SRC family kinases), elevated BCR-ABL expression levels, and evolution of leukemic clones with new chromosomal aberrations (19).

1.3.4 Immunotherapy:

Significant advances in understanding the biology of immune response in the past two decades has led to the rise of cancer immunotherapy. This is now combined with chemotherapy and other treatment protocols for treating cancer. Use of monoclonal antibodies (mAbs) to target tumor-specific antigens have led to the evolution of clinical-based molecular and cell mediated therapeutic approaches. Therapeutic mAbs are humanized to target tumor cell antigens preferentially expressed on leukemic cells and not on normal hematopoietic stem cells (HSCs) or

other normal tissues. This makes mAb therapies a safe and highly specific approach in cancer therapy.

Antibodies can be used to treat ALL, causing cell death by Complement Dependent Cytotoxicity (CDC) and Antibody Dependent Cellular Cytotoxicity (ADCC). mAbs target proteins or antigens on surface of cancer cells, inducing complement fixation to the tumor cell- surface. Complement activation results in CDC while recruitment of natural killer cells (NK), neutrophils and monocytes results in ADCC. The humanized mAb alemtuzumab (Campath®) directed against the antigen CD52 found on T and B-lymphocytes is effective in treating T-cell prolymphocytic leukemia (21), cutaneous T-cell lymphomas (22), and fludarabine-refractory chronic lymphocytic leukemia (23, 24). Recent findings suggest its' clinical activity in treating ALL as well (25). Childrens Oncology Group (COG) clinically evaluated the activity of epratuzumab, a mAb that binds to the glycoprotein CD22 of mature and malignant B-cells, in combination with chemotherapy to treat pediatric ALL in relapse (26, 27). Other examples include Rituximab that targets CD20 in mature B-ALL (28) and SAR3419 directed against CD19, a ubiquitous B-cell marker (29). Despite the high specificity of immunotherapy, improved survival in cases of relapsed or refractory ALL can be achieved only in combination with intensified chemotherapy. These facts reinforce that despite deleterious treatment related side effects in children treated for cancer, chemotherapy is essential to control disease progression and save lives.

1.4 Side Effects in Treatment of ALL

Conventional chemotherapeutics induce cytotoxicity to rapidly dividing cells (a characteristic trait of cancer). However, such agents will affect cellular division and viability of normal cells and tissues. This results in commonly observed side effects such as myelosuppression (reduced blood cells and platelets), immunosuppression (reduced efficacy of the immune system), mucositis (inflammation of mucous membranes that line the digestive tract), alopecia (hair loss) and a host of other effects as listed in Table 1.1(7-13, 15, 16, 30-53).

Glucocorticoids are normally administered in all phases of ALL therapy. This class of drugs induces apoptosis of normal and malignant B and T lymphocytes resulting in a weakened immune system. This places a child undergoing chemotherapy at risk of succumbing to infections. Glucocorticoids also induce a wide array of severe side effects including osteoporosis, Cushing's syndrome, hyperglycemia, facial swelling, and depression (30). Steroid induced behavioral changes are probably the most common side effect parents deal with. This can be subtle or in its extreme a true psychosis (7).

Prolonged administration of genotoxic drugs such as daunorubicine and doxorubicin (anthracyclines) results in cumulative dose-dependent cardiomyopathy and congestive heart failure (8, 9, 31). Therapeutic doses of daunorubicin are also known to induce severe myelosuppression. Vincristine (VCR), a vinca alkaloid that belongs to the class of spindle inhibitors causes neurotoxicity leading to numbness, tingling of fingers and toes, and muscle weakness. The principal dose-limiting toxicity of VCR is sensorimotor peripheral neuropathy caused by microtubule dysfunction in peripheral and autonomic nerves; where disruption of

intracellular transport ultimately leads to axonal degeneration (10). The peripheral neuropathy is variably reversible but, if persistent, can lead to permanent impairment of quality of life in cancer survivors (36). The major adverse side effects of methotrexate (MTX), a folic acid antagonist, are myelosuppression, oral and gastrointestinal mucositis (11). While MTX is known to induce nephrotoxicity in certain cases; the drug causes neurotoxicity following intrathecal chemotherapy in children treated for ALL (38, 39). While drugs like 6-mercaptopurine (6-MP), an antimetabolite cause significant myelosuppression, hepatotoxicity, nausea, vomiting, anorexia (in approximately 25% patients) and pancreatitis (in approximately 3% of patients); 6-thioguanine, an antimetabolite causes jaundice and hepatic veno-occlusive disease (VOD) in children treated for ALL (40-42). Targeted therapeutics such as imatinib, desatinib and nilotinib also induce dose-dependent toxicities (45-51). However, further clinical investigations are warranted to address the long-term effects of such therapeutics in childhood ALL.

Children affected with leukemia when subjected to high doses of “ionizing radiation” suffer from radiation induced severe side effects that range from cognitive impairment to formation of secondary tumors (53, 54). The extensive array of side effects seen with current therapeutic regimens for ALL (Table 1.1) exemplify the necessity of developing effective approaches to deliver existing chemotherapeutics specifically to the cancer cell to reduce side effects and enhance the quality of life for pediatric ALL patients (Figure 1.1).

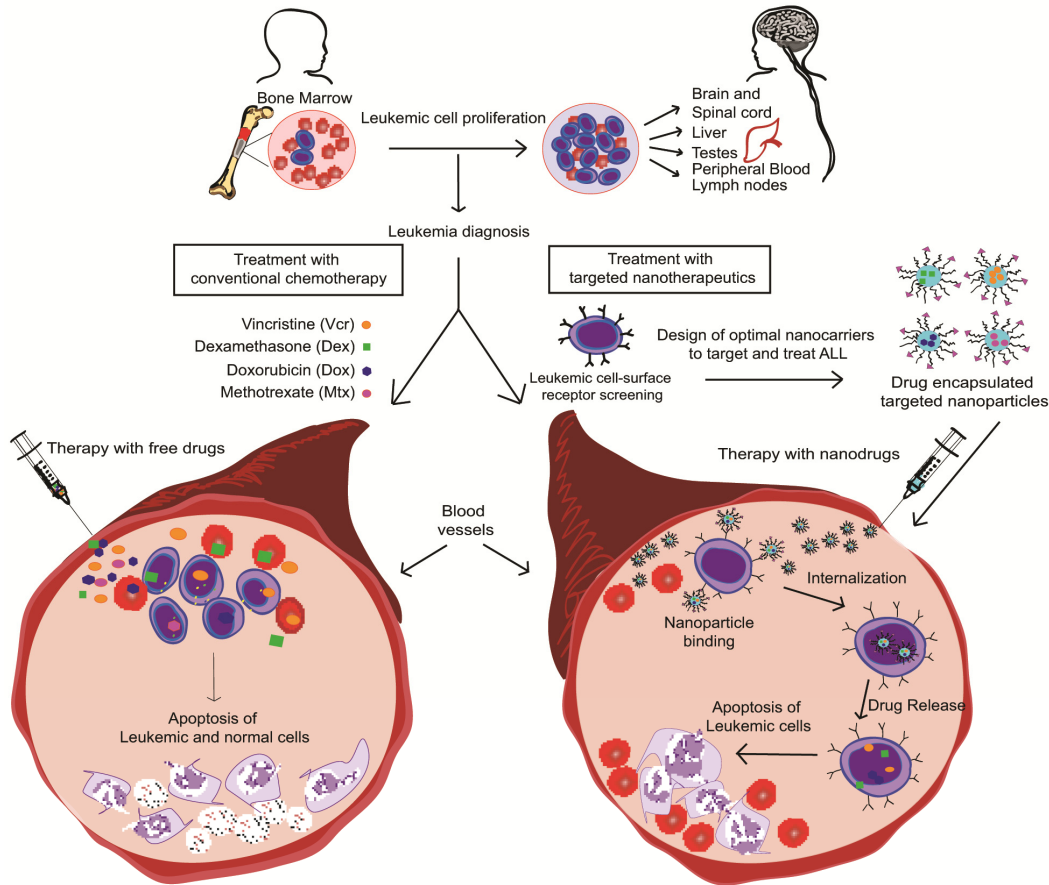


Figure 1.1. Comparison of chemo- and nano- therapy in childhood leukemia treatment: (a) leukemia cells originate in the bone marrow and rapidly proliferate to peripheral blood, spleen, liver, lymph nodes, testes and the CNS. Conventional chemotherapeutic agents administered during therapy indiscriminately kill malignant and normal cells (RBCs or lymphocytes) in the body. This causes deleterious treatment-related side effects and reduces the quality of life in a child subjected to therapy. Nanoparticle mediated targeted delivery of chemotherapeutic agents in children treated for leukemia induces selective apoptosis of malignant cells without harming the normal cells. This would reduce treatment-related side effects and enhance the quality of life in a child during and post therapy.

1.5 Cancer Nanomedicine

Nanotechnology is the manipulation of material properties at the nanometer level. The prerequisite for designing a nanomaterial is to have an effective dimension within the range of 1 to 100 nanometers (nm) (55). The practical application of such materials in the field of medicine is termed as “nanomedicine”. The high surface area to volume ratio of nanomaterials enables the accommodation of favorable quantities of targeting ligands for cell or organelle-specific delivery and hydrophilic polymers to render “stealth-like” properties for extended *in vivo* circulation. Thus significant advantages such as (i) targeted delivery of clinical agents, (ii) reduced dosage, (iii) reduced frequency of dosing, (iii) improved drug solubility, (iv) reduced immunogenicity and (v) superior half-life of clinical agents *in vivo* led to the unprecedented evolution of nanotherapeutics.

1.5.1 Types of Nanocarriers:

The majority of nanomaterial-based drug delivery systems that advanced to clinical development are based on liposomes or polymers. Liposomes are artificial biocompatible vesicles composed of amphiphatic lipid bilayer membranes that can encapsulate water-soluble agents within the central polar cavity, and oil-soluble agents within the lipid bilayer (Figure 1a). Polymeric formulations are derived from biocompatible polymers to form (i) polymer-drug conjugates (Figure 1b) or (ii) micelles that self assemble from amphiphilic block copolymers in aqueous media to form hydrophilic outer corona and hydrophobic inner core for drug encapsulation (Figure 1c) or (iii) dendrimers composed of highly branched

structures that rise from a central core to form particles of nano-sized dimensions (Figure 1d).

Therapeutic payloads can be integrated into such engineered nanoparticles (NPs) via covalent bonds that are stable or degrade in response to environmental stimuli (eg. endosomal pH) or physical entrapment. It should be emphasized that targeted NPs can be loaded with significantly more drug molecules than the classic antibody or ligand-drug conjugates. These, formulations have shown promising results in achieving increased circulation; therapeutic efficacy and superior antitumor activity in clinical applications (see Tables 1.2 and 1.3).

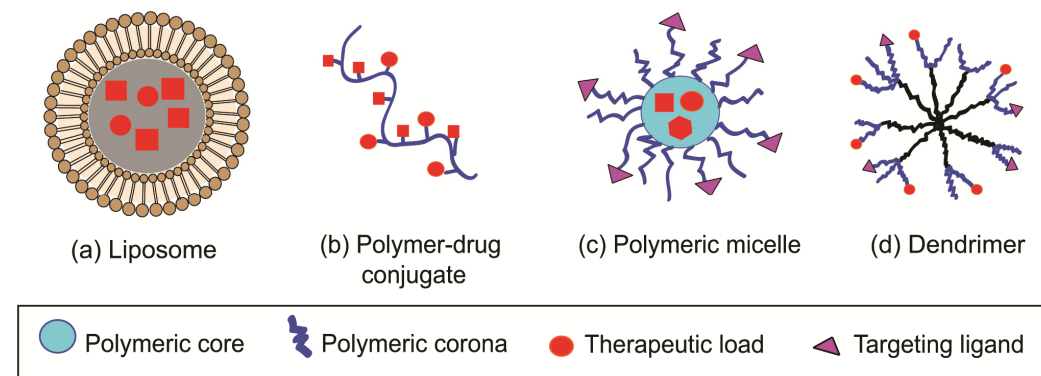


Figure 1.2. Nanocarriers for drug delivery applications: (a) liposomes are artificial biocompatible vesicles of amphiphatic lipid bilayer membranes (b) polymer-drug conjugates are nanosized particles where the drug may be covalently linked to a polymeric backbone (c) micelles self assemble from amphiphilic block copolymers in aqueous media to form hydrophilic outer corona and hydrophobic inner core (d) dendrimers are highly branched structures that rise from a central core to form nanoparticles.

1.5.2 Nanocarriers-based Drug Delivery:

Nanotherapeutics based on liposomes, micelles or proteins have evolved through three generations to date. The first generation nanocarriers were primarily evaluated for biocompatibility with living systems, ability to encapsulate drugs and cell uptake rates. Despite enhancing the solubility of hydrophobic drugs incorporated within; clinical advancement of first generation NPs were hindered by drawbacks such as instability and lack of prolonged circulation half-lives. These limitations were overcome by modifying the nanomaterial composition to improve stability and the surface chemistry to enhance *in vivo* circulation rates, giving rise to the second generation of nanotherapeutics.

Clinical trials of first and second generation NP-based “smart drugs” (**Table 1.2**) include liposomal or polymeric formulations of (a) anthracyclines (*Dauno Xome*[®], *Myocet*[®], *CPX-351*, *DOXIL*[®], *SP1049C* and *NK911*) (56-61); (b) spindle or mitotic inhibitors (*Marqibo*[®], *EndoTAG*[®]-1, *LEP-ETU*, *Abraxane*[®], *Genexol-PM*[®], *NK105*, and *Opaxio*TM) (62-69); (c) naturally occurring alkaloids (*OSI-211*, *S-CKD-602*[®], *CRLX101*) (70-72); (e) metabolites of enzyme inhibitors (*NK012*) (73) or (d) platinum containing anti-cancer drugs (*NC6004 Nanoplatin*TM) (74). Such systems have improved therapeutic properties of anticancer drugs (**Table 1.2**). The enhanced stability and extended *in vivo* circulation half-lives of second generation nanocarriers was achieved by coating the surface with linear chains of poly(ethylene glycol) (PEG) - the process termed as PEGylation. For example, the terminal half-life ($t_{1/2}$) of *DOXIL*[®] is 65 fold greater and the area under the plasma drug concentration-time curve from time of administration (AUC_{blood}) is 2-3 times larger than conventional DOX at identical doses (59). Likewise, *NK012* possess a

$t_{1/2}$ 16 times more and AUC_{blood} 14.09 fold larger than the native form of SN-38 (an active metabolite of the camptothecin derivative, irinotecan) (73). However,

Table 1.2 Non-targeted NPs clinically approved or advanced in clinical trials.

Formulation	NP Design Characteristics			Drugs (Trade Name®)	Pharmacological Benefits	Cancer Type	Current Status	References
	Size and Shape	PK ($t_{1/2}$; AUC _{blood})*	DRR					
Non-PEGylated Liposomes	45nm; spherical	5.72; 35	Controlled	Daunorubicin (DaunoXome®)	Extended PK, High response rates, Reduced cardiotoxicity	Kaposi's sarcoma	FDA approved	56
	100-250nm; spherical	9; 20	Controlled	Doxorubicin (Myocet®)	No IRRs, High response rates, Reduced cardiotoxicity	Kaposi's sarcoma, Metastatic breast cancer (phase I/II)	Phase III	57
	115nm; spherical	~100; 1273	Controlled	Vincristine Sulfate Liposome (Marqibo®)	Extended PK	Acute lymphocytic leukemia (ALL),- Hodgkin's lymphoma (NHL)	FDA approved (Ph- adult ALL), Phase II (NHL), Phase I (pediatric ALL)	62
	100nm; spherical	-Increased -	Controlled	Cytarabine/Daunorubicin (CPX-351)	Extended PK, High response rates	Acute myeloid leukemia (AML)	Phase III	58
	160-180nm; spherical	1.29; 134	Controlled	Paclitaxel (EndoTAG®-1)	Stable disease	Various solid tumors	Phase III	63
	150nm; spherical	- Increased with inter-patient variability -	Controlled	Lurtotecan (OSI-211 or NX211)	Reduced myelosuppression, High response rates	Ovarian cancer	Phase II completed	70
	150nm; spherical	0.84; 0.74	Controlled	Paclitaxel (LEP-ETU)	No IRRs*, High response rates	Metastatic breast cancer	Phase II completed	64
PEGylated Liposomes	88nm; spherical	65; 2-3	Controlled	Doxorubicin (PEGylated DOX or DOXIL®)	Extended PK, High response rates, Reduced cardiotoxicity	Variety of cancers	FDA approved	59
	100nm; spherical	Increased; 68	Controlled	Camptothecin (S-CKD-602®)	Extended PK	Advanced solid tumors	Phase I/II	71
	130nm; spherical	No change;	Controlled	Paclitaxel (Abraxane®)	No hypersensitivity, High response rates,	Metastatic breast cancer	FDA approved	65
Protein-Drug Conjugates	<50nm; spherical	Significant ↑ with dose escalation -	Controlled	Paclitaxel (Genexol-PM®)	Delayed tumor progression	Metastatic breast cancer, Urothelial carcinoma	Approved (Korea); Phase II/III (USA)	66, 67
	85nm; spherical	0.62; 0.74	Controlled	Paclitaxel (NK105)	Increased paclitaxel MTD, High response rates	Gastrointestinal cancer	Phase III	68
Polymeric Micelles	30nm; spherical	No change; - Significant ↑ with dose escalation -	Controlled	Doxorubicin (SP1049C)	Extended PK, High response rates, Reduced hypersensitivity	Advanced adenocarcinoma of esophagus and gastroesophageal system	Phase I completed	60
	40nm; spherical	2.62; 28.88	Controlled	Doxorubicin (NK911)	High response rates, No hand foot syndrome	Metastatic / Recurrent solid tumors	Phase II (Asia)	61
	10-150nm; spherical	- Significant ↑ with dose escalation -	Controlled	Paclitaxel-poliglumex (Opaxio™)	Extended PK	Ovarian cancer	Phase III	69
	20-50nm; spherical	0.8; 9	Controlled	Camptothecin (CRLX101)	Extended PK, High response rates	Advanced solid tumors	Phase Ib/Ia	72
	20nm; spherical	16.41; 14.09	Controlled	SN-38 (NK012)	Extended PK, Stable disease	Solid tumors	Phase I/II	73
	30nm; spherical	0.19; 64.77	Controlled	Cisplatin (NC-6004 Nanoplatin™)	Extended PK, Stable disease	Advanced / metastatic pancreatic cancer	Phase I/II (Asia)	74

PK – Pharmacokinetics; $t_{1/2}$ – Terminal Half-life; AUC_{blood} - Area under the drug versus time concentration curve in blood from time of administration; DRR – Drug Release Rate; IRRs – Infusion-Related Reactions; Ph- – Philadelphia Chromosome Negative; MTD – Maximum Tolerable Dose; *PK parameters indicate fold change over free form of the drug; **AUC was 15 fold larger at 150 mg m⁻² than conventional paclitaxel at 210 mg m⁻²

production of PEG-specific antibodies can result in Accelerated Blood Clearance (ABC) phenomena (75). This could attribute to the size, surface charge; composition and time interval between doses of drug-encapsulated NPs (75-79). Yet, the aforementioned issue of ABC can be overcome via smart design and engineering, as has been demonstrated by the clinical success of DOXIL® (59).

Prime limitations of second-generation nanocarriers are lack of control over drug release and poor tumor cell uptake. Drug delivery systems may exhibit “burst-release” effects when in contact with body fluids or tissues (80). Consequently, premature drug release from the carrier in minimal time post administration results in excessive levels of free drug in the blood. This causes drug accumulation at non-specific sites undermining the very significance of developing drug delivery strategies to treat any form of disease. The second generation systems rely heavily on the concept of passive targeting driven by Enhanced Permeability and Retention effect or (EPR) caused by leaky tumor vasculature and impaired lymphatic system, leading to preferential accumulation of macromolecular agents at tumor sites (81). The permeation and accumulation rates could vary further depending on the tumor microenvironment’s heterogeneity and interstitial pressures at the tumor core (82). This prevents uniform and substantial accumulation of NPs throughout the tumor interstitium resulting in reduced effective doses of anticancer agents. These drawbacks led to the development of NPs with increased cellular and sub-cellular targeting capabilities. Such particles can be retained at active sites while possessing long circulating half-lives in the blood and reduced clearance rates. Thus, a third generation of NP mediated therapeutic carriers was born.

Targeted nanocarriers employ ligands (monoclonal antibodies, peptides, single-chain variable fragments, oligonucleotides or aptamers etc.), generally located

on the outer corona for selective cell-surface targeting (Figure 1.2). By virtue of these ligands; NPs readily interact with biomolecules or receptors overexpressed on the targeted cell-surface and undergo receptor-mediated endocytosis. A significant rise in the cell uptake rates are observed in contrast to non-targeted NPs (83). The NPs then release the cargo only within the targeted region of the cell. The nanomaterial composition can therefore be adjusted to modulate the release kinetics in response to environmental cues such as low pH in endosomes. While sustained-release formulations ensure that drug release is maintained at steady rates for extended intervals; pH-responsive NPs readily disintegrate within the endosomal compartments of malignant cells or the tumor microenvironment. The superior therapeutic implications of such systems have been established by a comparative study between pH-sensitive and insensitive nanoformulations (84). Thus, ligand mediated targeting enhances the therapeutic efficacy of encapsulated drugs in comparison with the previous generations of nanodrugs. To date, five targeted NP formulations (three liposomal – *MCC-465*, *MBP-426*, *SGT53-01* and two polymeric-based – *BIND-014[®]*, *CALAA-01*) (85-89) have advanced to clinical trials for treating cancers. These systems have demonstrated great tumor specificity, enhanced efficacy and most importantly reduced toxicity in adult cancer treatments (Table 1.3). For instance, oxaliplatin (OHA) induced peripheral neuropathy was not observed in any of the patients administered with MBP-426 during Phase I/II clinical trials. A significantly improved pharmacokinetic (PK) profile and an increase in effective dose ($130 \text{ mg/m}^2 \rightarrow 226 \text{ g/m}^2$) without inducing neurotoxicity were attained for OHA. This could attribute to the unique physicochemical properties of MBP-426. While human transferrin (Tf) ligands on the liposomal surface specifically targeted OHA to cancer cells that overexpress Tf receptor, the pH-responsive coating of N-glutaryl

phosphatidylethanolamine on liposomes ensured the particles' rapid disintegration in acidic conditions to release the drug within the endosomes of cancer cells (86). Similarly, Phase I clinical trials of BIND-014® in patients treated for advanced solid tumors revealed prolonged and elevated levels of Docetaxel (Dtxl) in the plasma. This ensured Dtxl accumulation at the tumor site and an enhanced antitumor activity at 20% of the recommended dose of the drug in its conventional form. Simultaneous evaluation of physicochemical properties (size, PEG density and molecular weight, surface charge etc.) determined the most optimal formulation for BIND-014 with extended PK and efficient targeting capabilities (88). BIND-014 is presently undergoing Phase II clinical trials in treatment of second-line docetaxel-naïve non-small cell lung cancer and first-line chemotherapy-naïve castrate-resistant prostate cancer. This reinforce utilizing such novel therapeutic strategies in treating childhood malignancies where existing survival rates of 90% can still be achieved or increased while significantly reducing side effects.

Table 1.3 Targeted NPs in clinical trials.

Formulation	NP Design Characteristics			Drugs (Trade Name®)	Pharmacological Benefits	Ligand/Receptor	Type of Cancer	Current Status	References
	Size and Shape	PK ($t_{1/2}$; AUC_{blood})*	DRR						
Liposomes	143nm; spherical	- Identical to Doxil -	Controlled	Doxorubicin (MCC-465)	No hand-foot syndrome or cardiotoxicity, Stable disease	F(ab') ₂ fragment of human mAb GAH or Tumor specific antigen Transferrin/Transferrin receptor	Metastatic stomach cancer	Phase I (discontinued)	85
	180nm; spherical	- Significant ↑ with dose escalation -	Controlled and pH dependent	Oxaliplatin (MBP-426)	Extended PK, Stable disease		Advanced/Metastatic solid tumors	Phase I/II	86
	400nm; spherical	N.A.***	Controlled	p53 gene (SGT53-01)	Improved response rates	scFv/Transferrin receptor	Solid tumors	Phase Ib	87
Polymeric Micelles	100nm; spherical	Significant ↑**	Controlled and pH dependent	Docetaxel (BIND-014®)	Enhanced therapeutic efficacy, partial response/stable disease	peptide/PSMA	Solid tumors	Phase I completed	88
	70nm; spherical	N.A.***	pH dependent	siRNA (CALAA-01)	Stable disease, no DLTs	Transferrin/Transferrin receptor	Solid tumors	Phase I	89

21

PK – Pharmacokinetics; $t_{1/2}$ – Terminal Half-life; AUC_{blood} - Area under the drug versus time concentration curve in blood from time of administration; DRR – Drug Release Rate; DLTs – Dose-Limiting Toxicities; PSMA – Prostate Specific Membrane Antigen

*PK parameters indicate comparison with free form of the drug

** - results yet to be published

*** - ongoing

1.6 Dissertation Summary

A 90% survival rate in children treated for ALL strongly suggests that the current treatment approaches are successful in saving lives. However, as described earlier, a key predicament associated with this success is the induction of treatment-related side effects in children (**Table 1.1**). Today there are at least 328,000 childhood cancer survivors in the United States alone (90). More than 60% of these survivors are expected to have a life-threatening event emanating from their treatment. This is a major emotional stress to the child, the family and a significant economic burden to society. Nanotechnology-based targeted delivery of currently used chemotherapeutics to leukemic cells should improve the therapeutic outcome in children. While nanotechnology approaches have advanced and are well documented for adult cancers, these approaches have not yet progressed to pre-clinical or clinical development in treating childhood malignancies.

The dissertation work describes the engineering and preclinical development of a polymeric based nanotherapeutic approach to target and deliver some of the most commonly used chemotherapeutic agents in pediatric oncology to leukemic cells. This should reduce treatment-related toxicity and alleviate life-threatening side effects in children treated for leukemia. In Chapter 1, titled **“Dexamethasone-loaded block copolymer nanoparticles induce leukemia cell death and enhance therapeutic efficacy in childhood acute lymphoblastic leukemia”**, multi-step chemical transformations were employed to construct amphiphilic block copolymers consisting of hydrophilic polyether (poly(ethylene glycol), PEG) and hydrophobic polyester (poly(ϵ -caprolactone), PCL) bearing

pendant cyclic ketals. This was achieved via PEG-initiated ring-opening copolymerization of CL and 1,4,8-trioxaspiro-[4,6]-9-undecanone (TSU) using Sn(Oct)₂ as the catalyst. The incorporation of such pendant cyclic ketal groups on the hydrophobic portion on the polymer backbone increased the chain flexibility while decreasing polymer crystallinity. This improved the drug loading capacity and the release profile which sustained for over a week. It was identified that NPs formulated from block copolymers composed of 14 mol% TSU showed moderate crystallinity with effective control over drug release and this composition was used throughout the project. The block copolymers self-assemble into micelles with a core-shell architecture composed of a segregated PCL core, which was used to encapsulate the payload and a sterically stabilized PEG shell to conjugate targeting moieties (Figure 1.2) (95). In this chapter, the ability of non-targeted nanoformulations to induce leukemia cell death was examined both *in vitro* and *in vivo*. The steroidal drug, dexamethasone (Dex) and fluorescent-dye (Nile red (NR) or DiR) encapsulated nanoparticles (NPs) were formulated by nanoprecipitation.

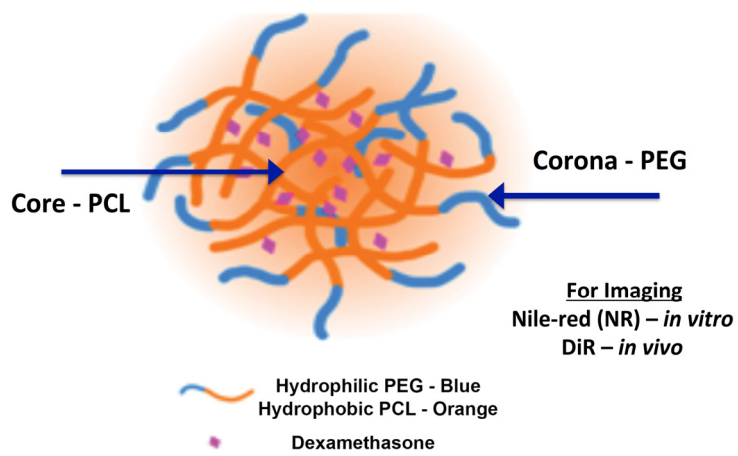


Figure 1.3. Illustration of non-targeted nanocarriers.

Dynamic light scattering (DLS) analysis revealed the size of all formulations (Blank-NPs, Dex-NPs, NR-NPs and DiR-NPs) to be within the range of 100-120 nm. The loading content and encapsulation efficiency for Dex within the NPs was 58.4 ± 5 ($\mu\text{g}/\text{mg}$) and $52.6 \pm 4\%$, respectively. On the other hand, the loading content and encapsulation efficiency for NR and DiR were estimated as 7.9 ± 1.2 $\mu\text{g}/\text{mg}$; $78.8 \pm 12.3\%$ and 3.1 ± 0.4 $\mu\text{g}/\text{mg}$; $79.5 \pm 10\%$ respectively. *In vitro* release profiles of DEX from NPs incubated in PBS under sink conditions at ambient temperature revealed an initial release of 60.1 ± 1.9 wt% of encapsulated Dex within the first 48h. This was followed by a slower release with an average rate of 17.2 wt% from day 2 to day 4 and 14.1 wt% from day 4 to day 7, respectively. By the end of a week, approximately 91.4 ± 2.9 wt% of the initially loaded drug was released.

The formulated blank NPs were confirmed to be biocompatible when tested at increasing concentrations with multiple platforms: (a) epithelial and lymphocytic cell lines, (b) human blood and (c) in mice. The bioactivity of encapsulated Dex was confirmed by the drug's insensitivity towards the epithelioid carcinoma cell line, Hela in contrast to its apoptotic effect on RS4;11 B-cell acute lymphoblastic leukemia (B-ALL) cells following endocytosis of Dex-NPs. The steady levels of glucocorticoid-receptor phosphorylation inside RS4;11 B-All cells when incubated with Dex-NPs, indicated a sustained-release pattern for Dex from NPs. This was in complete agreement with a similar trend observed for the drug release kinetics of Dex-NPs incubated in PBS. In mice, the NPs were detected in the blood plasma at sustained levels for approximately 2h and were found to accumulate within the

liver and spleen from where they completely cleared off in 2 weeks. The therapeutic efficacy of these novel nanoparticle-based formulations was finally confirmed in a pre-clinical mouse model of ALL by showing that Dex-NPs reduced the disease symptoms and significantly extended survival compared to groups treated with Saline ($P=0.0009$) or free Dex ($P=0.0229$). Overall, the results successfully demonstrate for the first time the suitability and promising potential of polymeric NPs to deliver Dex and reduce systemic toxicity in ALL therapy.

In Chapter 2, titled **“CD19-Targeted Nanodelivery of Doxorubicin Enhances Therapeutic Efficacy in B-Cell Acute Lymphoblastic Leukemia Therapy”**, the surface of 80 nm sized NPs were modified to display antibodies (Abs) directed against CD19 (a B-lymphoblast cell surface antigen) that is expressed on leukemic cells and is absent on pluripotent stem cells. To immobilize the CD19-targeting ligand, avidin was chemically modified with a fatty acid (i.e. palmitic acid) group, and then incorporated onto the surface of NPs via the nanoprecipitation method. The fatty acid group preferentially partitions within the hydrophobic PCL core of NPs, and the hydrophilic avidin head group is presented on the surface alongside PEG. Biotinylated anti-CD19Abs were then linked to the NP surface (CD19-NPs, Figure 1.3) via the anchored avidin, the amount of which was estimated to be at $8.2 \mu\text{g}/\text{mg}$ of NPs. The level of anti-CD19Abs conjugated to the surface of NPs was quantified to be approximately 120 ng or approximately 77×10^{10} molecules per mg of NPs or 3 antibody molecules per NP.

Prior to the encapsulation process, the anthracycline, doxorubicin-hydrochloride (DOX-HCL) was desalted to achieve increased loading. DLS

analysis revealed the size of all non-targeted nanoformulations (DOX-NPs, NR-NPs and DiR-NPs) to be within the range of 77-85 nm. Incorporation of anti-CD19Abs to the NP surface slightly increased the size of all formulations to the range of 80-89 nm. The zeta potential values for non-targeted and CD19-NPs were estimated to be at -5mV and -42mV respectively. Conjugating an irrelevant isotype matched IgG to the NPs reduced the surface charge to -50mV. The loading content and encapsulation efficiency for DOX was approximately 71.3 ± 4.7 $\mu\text{g}/\text{mg}$ and 42.8 ± 2.8 % for non-targeted-NPs, and of 72.1 ± 6.4 $\mu\text{g}/\text{mg}$ and 45.4 ± 2.1 % for anti-CD19Ab-NPs. The loading content and encapsulation efficiency for ‘NR’ in non-targeted and anti-CD19Ab conjugated formulations were similar. These values were estimated to be approximately 3.4 ± 0.4 $\mu\text{g}/\text{mg}$ and 34.4 ± 4.0 %, respectively. For ‘DiR’ loaded non-targeted and CD19-NPs, the loading content and encapsulation efficiency values were 3.1 ± 0.3 $\mu\text{g}/\text{mg}$ and 86.4 ± 8.4 %, respectively. *In vitro* release kinetic studies were performed by incubating targeted or non-targeted nanoformulations in PBS under sink conditions at 37°C. For DOX-NPs, an average of 18.5 ± 2.7 wt% of the drug was released per day within the first 72h, and an average of 8.4 ± 4.8 wt% per day followed during the next 72h. By the end of a week, 88.9 ± 4.8 wt% of the encapsulated DOX was released. The release rate of DOX from CD19-DOX-NPs was estimated to be around 15.8 ± 2.2 wt% and 12.2 ± 2.7 wt% from day 0 to day 3 and day3 to day 7, respectively.

The ability of CD19-NPs to deliver DOX specifically to targeted cells was examined by utilizing B-lymphocytic cell lines (RS4;11 and REH) that express highly contrasting levels of the CD19 receptor. Confocal imaging revealed that

significantly high levels of CD19-NPs were internalized by CD19+ RS4;11 cells in contrast to CD19- REH cells. The CD19-NPs were internalized in a CD19-dependent manner via clathrin-mediated endocytosis and could deliver DOX specifically into CD19+ RS4;11 cells to induce cell-death via apoptosis. HPLC/MS/MS quantification revealed that CD19 targeting could achieve elevated levels of cell-associated DOX in RS4;11 cells compared to the non-targeted REH cells. *In vivo* plasma profiling revealed detectable levels of 80 nm-sized CD19-NPs for atleast 8h; a significant improvement over the 2h period identified for the previous generation of 110 nm sized NPs. In a preclinical mouse model of ALL, the CD19-DOX-NPs treated leukemic mice survived longer and manifested higher degree of agility, indicating reduced apparent systemic toxicity compared to mice treated with free DOX. This suggests that targeted delivery of chemotherapeutic agents used in the clinic should improve or sustain current survival rates with reduced side effects in children treated for leukemia.

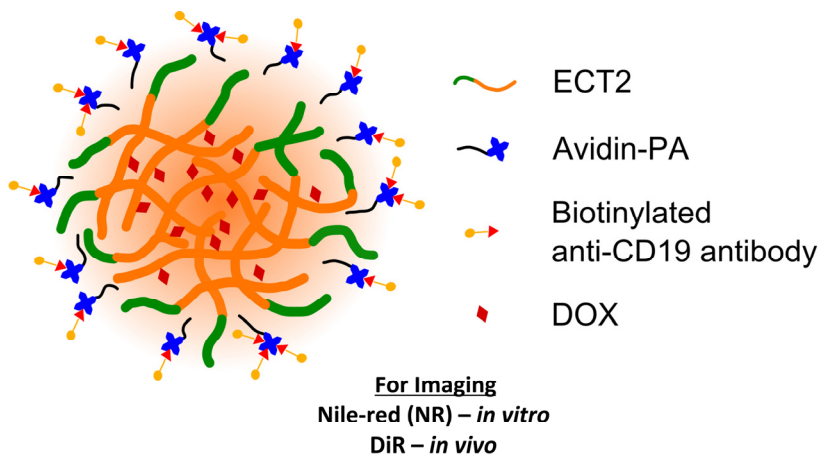


Figure 1.4. Illustration of targeted nanocarriers.

Chapter 2

DEXAMETHASONE-LOADED BLOCK COPOLYMER NANOPARTICLES INDUCE LEUKEMIA CELL DEATH AND ENHANCES THERAPEUTIC EFFICACY *IN VITRO* AND *IN VIVO* **

2.1 Introduction

Cancer nanotechnology is an emerging multi-disciplinary field that involves novel and practical application of materials or devices on the nanometer scale while integrating concepts in biology, chemistry, engineering and medicine for early cancer diagnosis and therapy. Unprecedented growth of research in this field has led to significant advances in various biomedical applications; especially in the field of drug delivery. Nanosized drug delivery systems not only enhance the pharmacokinetics and pharmacodynamic properties of anti-cancer agents; but also ensure specific delivery of chemotherapeutic agents to cancer cells (3, 4). The existence of a subtle balance in achieving therapeutic efficacy and reducing deleterious side effects in any form of therapy raises the need to maintain control over drug release for extended periods of time. Attaining this control is paramount and a key design factor in engineering novel drug delivery systems prior to targeting them. Over the years, numerous nanoscaled drug delivery systems have been formulated and explored for treating cancers. These systems include polymeric nanoparticles and micelles, liposomes, gold nanoshells, dendrimers, quantum dots and fullerenes (3, 4).

** Reprinted (adapted) with permission from
(<http://pubs.acs.org/doi/abs/10.1021/mp300350e>, *Mol. Pharmaceutics*, 2013, 10 (6), pp 2199–2210). Copyright (2013) American Chemical Society.

Acute lymphoblastic leukemia (ALL) is the most common form of pediatric leukemia. It is characterized by malignant proliferation of immature lymphoblasts, curbing the development of healthy blood cells comprising of (i) red blood cells or RBCs that carry oxygen and nutrients throughout the body via the circulatory system; (ii) platelets that prevent excessive bleeding in case of injuries and (iii) white blood cells (WBCs) that are essential for strengthening the body's immune system to fight infections. The proliferation of the malignant cells further leads to massive infiltration of immature lymphoblasts to various sites in the body including the lymphoid system – liver and spleen (hepatosplenomegaly); the bone marrow (joint aches) and the central nervous system. The disease accounts for 76% of all childhood and adolescent leukemia with incidence rates that peak at the age of 5 years (1). Although chemotherapeutic regimens in combination with radiation therapy and hematopoietic stem cell transplantation have increased 5-year relative survival rates for children with ALL to 90.5%; leukemia is still the leading cause of cancer-related death in children in the age category 0-14 (1, 91). The use of combination chemotherapy to treat and cure leukemia inflicts a severe toll on the child's health in the form of acute or delayed onset of treatment related side effects that often result in fatality. Although advances in nanotechnology for drug delivery has resulted in pharmaceutical formulations that effectively combat adult cancers, little research has been performed to develop innovative therapeutic strategies for childhood cancers.

Dexamethasone (Dex), a glucocorticoid class steroid hormone, is widely used as a potent anti-inflammatory and bone growth steroid (92). Dex is also one

of the most commonly used chemotherapeutic drugs to treat childhood leukemia (93, 94). It induces apoptosis of B and T lymphocytes and consequently kills a large population of leukemic cells. However, long-term systemic exposure to Dex causes adverse side effects. These include fluid retention, slowed growth, stomach and intestinal bleeding due to ulcers, damage to the joints that can result in pain and loss of motion usually involving the hip and knee (osteoporosis), high blood sugar (Cushing's syndrome), high blood pressure (hypertension), increased pressure in the eyes and most important of all; the body's inability to fight infections due to non-specific killing of normal T and B lymphocytes (immunosuppression). To date the potential of nanocarriers to deliver Dex for ALL has not been explored.

The procedure for the synthesis of amphiphilic block copolymers consisting of hydrophilic poly(ethylene glycol) (PEG) and hydrophobic polyester bearing pendant cyclic ketals via PEG-initiated ring-opening copolymerization of ϵ -caprolactone (CL) and 1,4,8-trioxaspiro-[4,6]-9-undecanone (TSU) using Sn(Oct)₂ as the catalyst was adopted from Wang, X. et al 2010 (95). The resultant copolymers, referred to as ECTx with x indicating the monomer feed ratio, assembled into nanoparticles (NPs) capable of encapsulating Camptothecin (CPT). Particularly, nanoparticles derived from ECT2 (20% (w/w) TSU in monomer feed) offered the best control for CPT release, and the released CPT effectively induced dose-dependent apoptosis in prostate cancer cells. In this chapter, the ECT2-NPs were examined and validated as a novel biocompatible carrier that can deliver Dex at a controlled rate and induce apoptotic cell death in leukemia cell lines. The

results also demonstrate that Dex encapsulated ECT2-NPs (Dex-NPs) induce leukemia cell apoptosis *in vitro* and show enhanced therapeutic efficacy *in vivo*. The ability to sensitize leukemia cells with this novel system highlights significant therapeutic implications for NPs for the future treatment of childhood leukemia.

2.2 Experimental Section

2.2.1 Reagents, Cell Lines and Mouse Models:

All chemicals necessary for the synthesis of the amphiphilic copolymers were purchased from Sigma-Aldrich (St Louis, MO) and were used as received unless otherwise indicated. Dexamethasone for *in vitro* studies was purchased from Tocris Biosciences (Minneapolis, MN) and clinical grade Dex for *in vivo* studies was obtained through Nemours-A.I. duPont Hospital for Children's Pharmacy. Nile red was purchased from Sigma-Aldrich (St Louis, MO). DilC18 (7) tricarbocyanine probe (DiR) was acquired from Life Technologies (Grand Island, NY). Cell lines, RS4;11 (established from an ALL patient); Nalm6 (established from a patient with ALL at relapse) and Hela (established from epitheloid cervical carcinoma), were purchased from the American Type Culture Collection (ATCC, Manassas, VA). RS4;11, Nalm6 cells were maintained in RPMI media (Life Technologies) supplemented with 20% fetal bovine serum (FBS) and Hela cells were maintained in DMEM media (Life Technologies) supplemented with 10% FBS, glutamine and penicillin/streptomycin. All cells were maintained at 37°C under a humidified atmosphere of 95% air and 5% CO₂. Whole blood samples were drawn from healthy volunteers into blood collection tubes with heparin in

accordance with Institutional Review Board approved protocols. C57BL/6 mice used for *in vivo* tolerability studies, BALB/c mice used for *in vivo* pharmacokinetic analysis, and immune-compromised NSG-B2m mice used to develop pre-clinical acute lymphoblastic leukemia mouse models for efficacy studies were all purchased from Jacksonville Laboratories, U.S.A. C57BL/6 and BALB/c mice were bred in-house. Animal studies were approved by the Institutional Animal Care and Use Committee (IACUC) at the Nemours-Alfred I. duPont Hospital for Children.

2.2.2 Polymer Synthesis:

ECT copolymers were synthesized following a previously reported procedure (95). As determined by ^1H NMR (polymers were dissolved in CDCl_3 and the spectrum was recorded on a Bruker AV400 NMR spectrometer) and gel permeation chromatography (the system comprised of a Waters 515 pump, a Waters Styragel® HR column and a Waters 2414 refractive index detector and mobile phase; tetrahydrofuran), the resultant copolymer showed a composition of $\text{EG}_{113}\text{CL}_{497}\text{TSU}_{85}$, a number-average molecular weight (M_n) of 64.2 kg/mol, and polydispersity index (PDI) of 1.39.

2.2.3 Particle Formulation and Drug/Dye Encapsulation:

NPs were formulated using a nanoprecipitation method. To a vigorously stirred (900 rpm) aqueous phase (5 ml DI water) was added an acetone solution of ECT (16 mg/ml, 1.4 ml). The mixture was allowed to stabilize overnight under constant agitation at room temperature to obtain blank or ECT2-NPs. Dex- or Nile

red-loaded NPs were prepared using an acetone solution of ECT containing 1.8 mg/ml Dex or 0.16 mg/ml Nile red, respectively. Similarly, DiR dye was dissolved in DMSO at a concentration of 0.9 mg/ml. The DiR dye solution (100 μ l) was then mixed with the ECT solution (16 mg/ml, 1.4 ml) in acetone. The resulting dye/polymer mixtures were used for nanoprecipitation as described above. Centrifugation (4,000 rpm for 10min) was applied to all types of NP suspension to remove large aggregates formed from the polymer. The supernatant containing NPs was collected and then additional centrifugation was performed (14,000 rpm for 10min) to spin down the NPs. Subsequently, NPs were thoroughly washed with PBS for three times by centrifugation and immediately used for the characterization and biological studies.

2.2.4 Characterization of NPs:

The hydrodynamic diameters of ECT2- and Dex-NPs were measured using the Zetasizer nanoZS (Malvern Instruments) via dynamic light scattering (DLS). Z-average particle size and size distribution were analyzed by using Malvern's DTS software (v.5.02). Transmission electron microscopy (TEM) was used for the morphological examination of the NPs. TEM samples were prepared by applying a drop of NP suspension (3 μ l) directly onto a carbon-coated copper TEM grid. Samples were allowed to dry under ambient condition prior to imaging using a Tecnai G2 12 Twin TEM (FEI Company).

2.2.5 Drug/Dye Loading and Release:

Aliquots (1 ml each) of the Dex-NP, Nile red-NP and DiR-NP suspension were collected and lyophilized. The dried powder was weighed accurately before being dissolved in DMSO (1 ml). The drug/dye concentration was determined using a UV-Vis spectrometer (Agilent Technologies, King of Prussia, PA) at 254 nm (Dex), 520 nm (Nile red) and 750 nm (DiR). Drug loading content was defined as the amount of drug (μ g) loaded per milligram of Dex-NPs. Drug encapsulation efficiency (EE, as percentage of the total) was calculated by dividing the amount of Dex loaded into the NPs with the amount of Dex initially added during the nanoprecipitation process. All measurements were carried out in triplicate and the results were indicated as the mean \pm SD.

The *in vitro* release behaviors of Dex, Nile red and DiR were analyzed under sink conditions following a previous method (95). Briefly, freshly formulated NP suspensions were loaded into hydrated dialysis cassettes with a molecular weight cut-off of 10,000 Da. The cassettes were subsequently immersed in the release media (100 ml PBS) under gentle stirring. At predetermined time points, 10 ml of the release media was collected and 10 ml fresh PBS was replenished to maintain a constant volume (100 ml). Media containing the released Dex or dyes collected from each time point was lyophilized and the resultant solid was re-dissolved in DMSO. Subsequently, the concentrations of Dex or the dyes were determined by UV-Vis. Three repeats were performed for each time point and the cumulative release profile was calculated by dividing the amount of drug or dyes released in one specific measurement time by the total mass initially loaded.

2.2.6 *In Vitro* Toxicity:

The toxicity of ECT2-NPs was tested in two ALL cell lines (RS4; 11 and Nalm6) and an epitheloid carcinoma cell line (Hela). The leukemia cells were seeded at 50,000 cells per well and Hela cells were seeded at 5,000 cells per well in 100 μ l of cell culture media containing ECT2-NPs at a dosage ranging from 0.07 μ g/ml to 70 μ g/ml (1 to 1000 fold), corresponding to 10nM to 10 μ M Dex equivalents encapsulated within Dex-NPs, in 96-well cell culture plates. The plates were then incubated for 72h at 37°C in 5% CO₂ atmosphere. At the end of incubation, cell viability was measured by Cell Titer-Blue® Assay (Promega, Madison, WI) following manufacturer's instruction. The fluorescence measurements were recorded on a micro plate reader (Perkin Elmer Victor™, USA). Assays were repeated to obtain an average of 6 replicates and the data were expressed as the percentage of viable cells compared to the survival of a control group (untreated cells to define maximum cell viability).

2.2.7 Hemolytic Activity and *in Vivo* Tolerability:

Hemolytic properties were evaluated by incubating ECT2-NPs at varying concentrations (0.1, 1, 2.5 mg/ml) for 240min at 37°C with human heparinized whole blood samples drawn from three different subjects. Blood samples treated with 1% Triton X-100 and PBS were included as positive and negative controls, respectively. Sample tubes were gently inverted every 30min during the incubation period, after which the tubes were centrifuged at 800 g for 15min at room temperature to remove unlysed RBCs. The supernatants obtained were then mixed with a cyanmethemoglobin reagent and analyzed at 540 nm with a micro

plate reader to quantify the hemoglobin concentration. The percentage hemolysis was then determined by calculating ratio of the relative absorbance of samples and Triton X-100 with respect to PBS.

For *in vivo* toxicity evaluation of ECT2-NPs, NPs (100 µl of 0.5, 5 and 50 mg/kg of NPs in PBS) were intravenously injected to C57BL/6 mice (3/group) twice a week for 1 month. All mice were evaluated twice weekly for eight weeks post-treatment for clinical symptoms of toxicity. To monitor change in body weights of mice in all treatment groups, the ratio of values recorded each week to the pre-treatment values were calculated and compared with the ratios obtained for the group that received the vehicle (control).

2.2.8 Dexamethasone Bioactivity Assay:

The bioactivity of the encapsulated Dex was analyzed by treating RS4;11 cells seeded at 50,000 cells per well and Hela cells at 5,000 cells per well in 100 µl of cell culture media composed of Dex-NPs at multiple doses (1-1000 fold) that correspond to 10nM to 10µM of Dex equivalents encapsulated within NPs in 96-well cell culture plates. The plates were incubated for 72h at 37°C in 5%CO₂ atmosphere and cell viability was subsequently analyzed by Cell Titer-Blue® Assay as described in *in vitro* toxicity assay.

2.2.9 Cytotoxicity Evaluation of Dex-NPs:

The cytotoxic effect of Dex-NPs or Dex in free form was tested and compared between ALL cell lines RS4;11 and Nalm6. The cells were seeded at an initial density of 50,000 cells per well in 100 µl of cell culture media constituted

with Dex-NPs or free Dex at increasing doses ranging from 1 to 10^7 fold (1pM to 10 μ M Dex equivalents). The assays were performed in 96-well cell culture plates which were maintained at 37°C in 5% CO₂ atmosphere for 24h, 48h, 72h and 96h. At the end of each incubation point; cell viability was measured by Cell Titer-Blue® Assay. The measurements were then expressed as the percentage of viable cells compared to the survival of respective control groups (untreated cells for Dex-NP and 0.01% DMSO treated cells for Dex in free form) defined as the maximum cell viability. The data obtained was further analyzed using Prism nonlinear regression software (Graphpad Software) for the curve-fitting and determination of IC50 values.

2.2.10 Evaluation of Apoptosis:

RS4;11 cells were plated in 10 cm dishes at a density of 5×10^6 cells/dish and were incubated with Dex-NPs at dosages ranging from 1pM to 10 μ M Dex equivalents encapsulated within NPs for 48h. Leukemia cells treated with 0.01% DMSO or 10 μ M Dex in free form was considered as negative and positive experimental controls respectively. Post incubation, cells were collected, washed with cold PBS twice and centrifuged at 2,000 rpm for 5min. The cell pellets were resuspended in a lysis buffer (20mM Tris-HCl, pH 7.5; 150mM NaCl; 1mM EDTA; 1mM EGTA; 1mM β -Glycerol Phosphate; 1mM Sodium Vanadate; 1.25mM Sodium Pyrophosphate; 1% (w/v) Triton X-100) with a 1% protease inhibitor cocktail (100mM Phenylmethylsulfonyl Fluoride, 1:100; 15 mg/ml mixture of Antipain, Leupeptin, Pepstatin, 1:1000; Sigma-Aldrich. St Louis, MO) at 4°C for 30min. The cell lysates were then prepared from the homogenates by

sonication and centrifugation at 12,000 rpm and 4°C for 15min. The protein concentration in the lysates was determined using a protein assay kit (DC protein assay reagent, Bio-Rad, Hercules, CA, USA). Equal amounts of protein (90 µg) were resolved on 15% SDS-PAGE gels and transferred overnight onto nitrocellulose membranes (Bio-Rad) in 20% methanol, 25mM Tris, and 192mM glycine. After transfer, the membranes were blotted with a rabbit polyclonal against active + pro caspase-3 antibody (1:1000, Cell Signaling, Danvers, MA) and a mouse monoclonal antibody against actin (1:10000, Cell Signaling) and visualized by HRP-conjugated secondary antibodies and Enhanced Chemiluminescence Plus reagent (GE Healthcare, Piscataway, NJ) followed by exposure to X-ray film (Amersham Biosciences, Piscataway, NJ).

2.2.11 Measurement of Glucocorticoid Receptor (GR) Phosphorylation:

ALL cell lines RS4;11 and Nalm6 were plated in 10 cm dishes at an initial seeding density of 5×10^6 cells/dish with RPMI media containing 20% charcoal-stripped FBS. Cells were briefly exposed to Dex-NPs and free Dex at 10µM Dex encapsulated for 0.08, 0.25, 0.5, 1, 2 and 6h. Cells treated with 0.01% DMSO was considered as the experimental control. The cell lysates were prepared and protein concentrations were estimated as described earlier. Equal amounts of protein (45 µg) were resolved on 10% SDS-PAGE gels and transferred overnight onto nitrocellulose membranes and blotted with a rabbit polyclonal to phospho-GR antibody (1:1000, Cell Signaling, MA) as explained above.

2.2.12 Determination of Cellular Uptake of ECT2-NPs:

NPs containing encapsulated Nile red ($485_{\text{Ex}}/525_{\text{Em}}$) (NR-NPs) were used to determine cellular uptake of NPs. For flow cytometry (FCM) and confocal laser scanning microscopy analysis (CLSM), 1×10^6 RS4;11 and Nalm6 cells/ml were seeded in 12 well plates and incubated in the presence or absence of NR-NPs (final concentration $70.1 \mu\text{g}/\text{ml}$) at 37°C for 6h. Cells were then washed three times with cold PBS and subjected to FCM analysis with BD Acuri C6 Flow Cytometer® System. Thereafter, the Nile-red fluorescence emitted by the particles bound or internalized by the leukemia cells was analyzed in the FL-1 channel at a wavelength of 530 nm and the data were generated using BD Accuri CFlow® software. To visualize cellular uptake of NPs, the NP treated cells were washed three times with cold PBS and transferred to Poly Prep Slides™ (Sigma Aldrich, St. Louis, USA). Cells were then fixed for 5min with 2% paraformaldehyde solution and embedded in ProLong Antifade Kit® mounting medium (Life Technologies, Grand Island, NY). Images were acquired by sequential scanning using a Leica TCS SP5 laser-scanning confocal microscope and processed by merging of the fluorescence channels using the software LSM (Leica Microsystems, Mannheim, Germany).

2.2.13 *In Vivo* Pharmacokinetics and Biodistribution:

To investigate biodistribution and clearance rates of ECT2-NPs, female BALB/c mice (4-6 weeks of age; 3 per group) received intravenous injections of $100\mu\text{l}$ of DiR-NPs (0.2mg/kg DiR). Subsequently, liver, spleen, heart, lung, kidney, intestine, gonads, bladder and brain were dissected out after euthanizing

the mice at 2h, 15h, 24h, 48h, 96h, 1 week, 2 weeks and a month post administration for subsequent *ex vivo* imaging using Carestream Multi-spectral *in vivo* Imaging System. Additionally, the organs were lysed in tissue lysis buffer (20mM Tris-HCL, pH 7.5; 150mM Sodium Chloride; 1mM EDTA; 1mM EGTA; 1mM β-Glycerol Phosphate; 1mM Sodium Vanadate; 2.5mM Sodium Pyrophosphate; 1% (w/v) Triton X-100; 1% (w/v) IGEPAL; 0.5% (w/v) Deoxycholate; 1% (w/v) SDS) and 1% protease inhibitor cocktail (100mM Phenylmethylsulfonyl Fluoride, 1:100; 15 mg/ml mixture of Antipain, Leupeptin, Pepstatin, 1:1000; Sigma-Aldrich, St Louis, MO) at 4°C for 1h. The lysates were used to quantify the DiR-NP fluorescence levels in various organs using the imaging software and the NP levels were estimated by comparing with standards prepared in tissue lysis buffer. BALB/c mice treated with saline were included as controls for the experiment and to establish imaging settings based on background fluorescence for each measurement.

For analyzing plasma pharmacokinetics; a lipophilic “far-red” dye DiR ($750_{\text{Ex}}/830_{\text{Em}}$) was encapsulated in ECT2-NPs (DiR-NPs). A cohort of female BALB/c mice (4-6 weeks of age; 3/group) was injected via the tail vein with a single dose of 100 μ l of DiR-NPs (0.2mg/kg DiR)_resuspended in PBS. At 0, 0.08, 0.25, 0.5, 1, 2, 6, 8 and 12h after nanoparticle injection, peripheral blood was collected from the mice by submandibular bleeding in tubes containing 20 μ l of sodium citrate to prevent blood from clogging. Blood was then centrifuged and plasma was analyzed by multi-label microplate reader (Plate Chameleon V, Hidex,

Finland) to assess the plasma half-life of DiR-NPs. The NP levels were then estimated by comparing with standards prepared in plasma.

2.2.14 *In Vivo* Antitumor Efficacy:

RS4;11 cells (5×10^6) were injected via the tail vein into female NSG-B2m mice (6 - 8 weeks old; 7 per group). Weekly submandibular bleeding was used to monitor disease progression, calculating the percentage of human cells in mouse peripheral blood by flow cytometry using fluorescein isothiocyanate (FITC)-conjugated anti-human CD45 and allophycocyanin (APC)-conjugated anti-mouse CD45. Two weeks after leukemia cell injection, the mice received intravenous treatments of saline, free Dex, or Dex-NPs suspended in saline at Dex equivalents of 5 mg/kg every other day for 4 weeks. The treatment efficacy was determined using Kaplan-Meier curves, sacrificing animals when they depicted signs of morbidity, including hind-limb paralysis or excessive weight loss, according to IACUC guidelines.

2.2.15 Statistical Analysis:

All data are indicated as mean \pm SD unless otherwise indicated. The IC₅₀ values were compared by the student's *t*-test. Survival data were presented using Kaplan-Meier plots and were analyzed using "Log-rank (Mantel-Cox) Test". A p < 0.05 was considered significant.

2.3 Results

2.3.1 NP Formulation and Characterization:

Amphiphilic block copolymers containing a hydrophilic PEG block and a hydrophobic PCL block randomly decorated with cyclic ketals were synthesized by ring opening polymerization of CL and TSU using mPEG as the initiator (Figure 2.1A). ECT2 with 14 mol% TSU in the hydrophobic block and an average molecular weight of 62kDa was used for Dex encapsulation. Blank or ECT2-NPs and Dex-loaded NPs were prepared using the acetone/water system. Particle size analysis by DLS (Figure 2.1) showed that the ECT2-NPs exhibited an intensity-average size of 111 ± 4 nm (Figure 2.1B) and a volume-average size of 98 ± 3 nm (Figure 2.1C). Dex encapsulation increased the average size to 127 ± 1 nm (Figure 2.1B) and 124 ± 2 nm (Figure 2.1C) by intensity and by volume, respectively. The average size from intensity and volume were in agreement with each other for both ECT2-NPs and Dex-NPs, and reflected the size of the major nanoparticle population. In addition, NPs exhibited a narrow size distribution as shown by the low PDI values of 0.14 and 0.05 for ECT2-NPs and Dex-NPs, respectively.

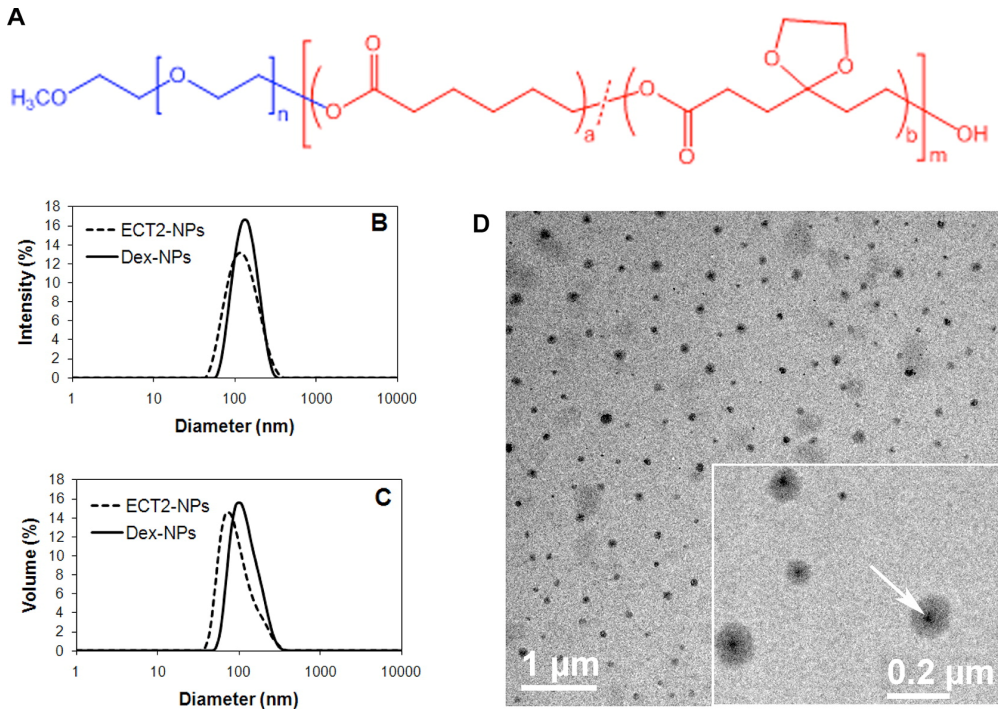


Figure 2.1. (A) Chemical structure of ECTx copolymer consisting of a hydrophilic PEG block and a hydrophobic PCL segment carrying randomly distributed cyclic ketals. Analysis of particle size (B and C) and morphology (D): DLS analysis of ECT2-NPs (dash line) and Dex-NPs (solid line): (B) intensity-based size distribution and (C) volume-based size distribution. (D) Transmission electron micrograph of Dex-NPs formulated through nanoprecipitation. (D) Insert: TEM showing higher magnification of NPs with entrapped Dex in the core (white arrow).

Inspection of Dex-NPs by TEM revealed the presence of spherical nanoparticles with an estimated diameter of 110 nm (Figure 2.1D), in good agreement with the measured size by DLS (Figures 2.1B, 2.1C). Higher magnification image (Figure 2.1D, insert) revealed the presence of a dense core (arrow) and a diffuse corona for Dex-loaded NPs, confirming the successful entrapment of Dex in the interior of the NPs. Nile red and DiR-labeled NPs showed similar size distributions as Dex-NPs (data not shown). All three types of

NPs were stable upon dilution and prolonged incubation (up to 4.5 months) under experimental conditions employed in the study.

2.3.2 Drug/Dye Loading and Release:

Dex was effectively entrapped in ECT2-NPs with a loading content and encapsulation efficiency of 58.4 ± 5 ($\mu\text{g}/\text{mg}$) and $52.6 \pm 4\%$, respectively. Comparable values were obtained by other studies using amphiphilic polymers as carriers for hydrophobic drugs (96, 97). *In vitro* release was evaluated by incubating Dex-NPs in PBS under sink conditions at ambient temperature for up to 7 days. The release profile shown in Figure 2.2 revealed that 60.1 ± 1.9 wt% of the initially loaded Dex was released during the first two days, followed by a slower release with an average rate of 17.2 wt% and 14.1 wt% from day 2 to day 4 and day 4 to day 7, respectively. By day 7, 91.4 ± 2.9 wt% of the initially loaded Dex was released. Separately, *in vitro* release of Nile red and DiR loaded NPs were also performed (Figure 2.2).

The loading content for Nile red and DiR were estimated as 7.9 ± 1.2 and 3.1 ± 0.4 $\mu\text{g}/\text{mg}$ respectively, with the encapsulation efficiency as $78.8 \pm 12.3\%$ and $79.5 \pm 10\%$ for the corresponding dye loaded NPs. Only 2.8 ± 1.3 wt% and 0.5 ± 0.1 wt% of hydrophobic dyes were released after the first 6 h for Nile red and DiR respectively. By day 7 when the experiment was terminated, a total cumulative release of 10.5 ± 0.5 wt% and 8.5 ± 2.0 wt% were detected for Nile red and DiR respectively. This limited release has been attributed to the strong hydrophobicity of these dyes (98, 99). The high retention of hydrophobic fluorescent probes by NPs demonstrates the feasibility to use Nile red and DiR to

track the fate of NPs within cellular environments without undesirable premature leaking.

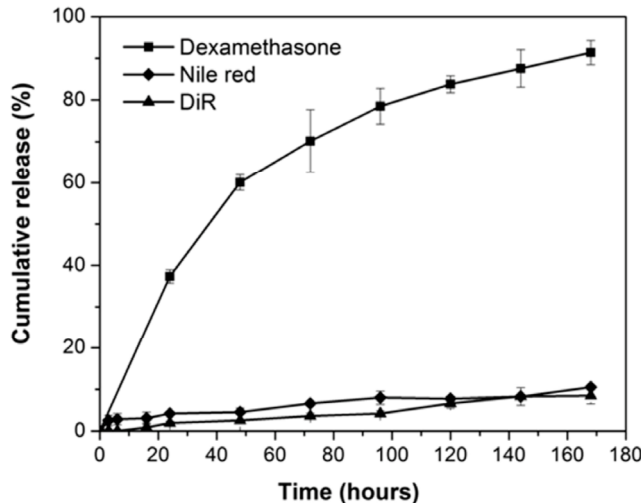


Figure 2.2. In vitro release profiles of Dex (square), Nile red (diamond) and DiR (triangle) from nanoparticles in PBS (pH 7.4) at ambient temperature: Data shown is average of three independent experiments.

2.3.3 ECT2-NPs are Non-toxic *in Vitro* and *in Vivo*:

Three different test platforms including cultured cells, human blood, and live animals were utilized to confirm the biocompatibility of ECT2-NPs. Two leukemia (RS4; 11, Nalm6) and one carcinoma (Hela) cell lines were used to test the biocompatibility of ECT2-NPs. As depicted in Figure 2.3A, cell viability remained unaffected in the presence of ECT2-NPs at concentrations ranging from 0.07 to 70 µg/ml, demonstrating their non-toxic nature towards leukemia cells and the adherent epithelial cancer cells. *In vitro* hemolytic evaluation was carried out by incubating ECT2-NPs with human whole blood samples drawn from three different individuals. Contrary to Triton X-100 (positive control), ECT2-NPs did not induce any hemolysis at concentrations of 0.1, 1.0 and 2.5 mg/ml (Figure

2.3B). In addition, the *in vivo* biocompatibility of ECT2-NPs was examined by monitoring changes of body weight or behavioral patterns in mice during the treatment. The body weight ratios remained stable and normal eating, drinking, grooming and physical activities continued throughout the duration of treatment and for 3 weeks post treatment (Figure 2.3C). The mice did not exhibit any symptoms of pain or hematuria and no damage was observed at the injection sites on lateral tail veins due to the intravenous dosing of NPs. These observations confirm ECT2-NPs as a biocompatible carrier for therapeutic agents.

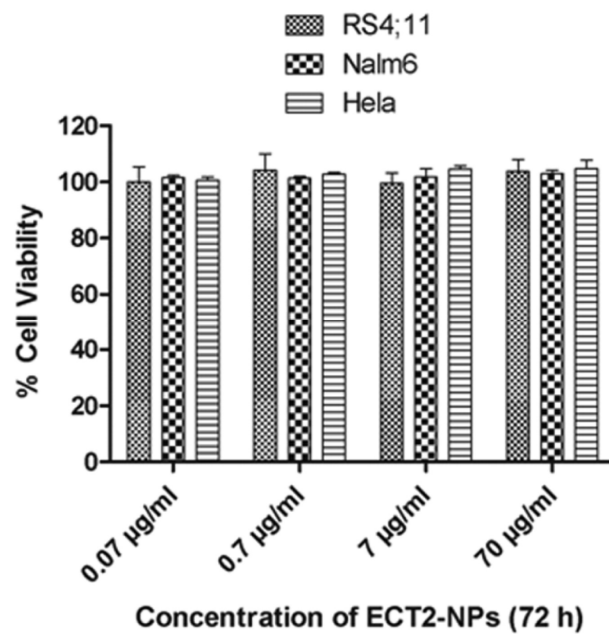


Figure 2.3A. Effect of ECT2-NPs on the viability of leukemia and carcinoma cell lines.

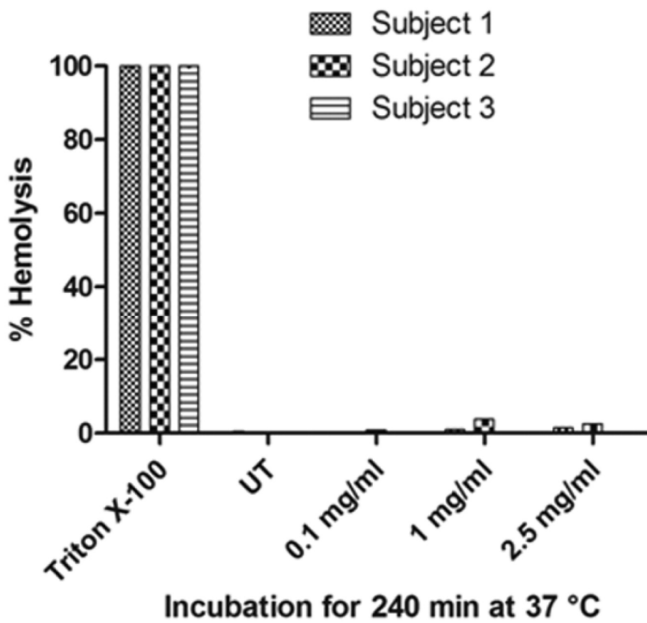


Figure 2.3B. *In vitro* hemolytic analysis of ECT2-NPs on human blood: ECT2-NPs do not induce hemolysis in contact with human blood.

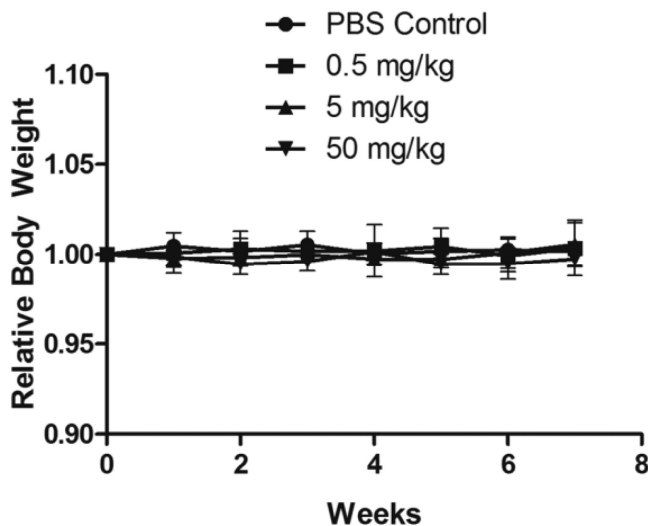


Figure 2.3C. *In vivo* biocompatibility of ECT2-NPs in C57BL/6 mice (3 per group): Absence of changes in relative body weight of mice validates the safety of ECT-NPs.

2.3.4 Dex-NPs Deliver Bioactive Dexamethasone and Induce Apoptosis in Leukemia Cells:

RS4; 11 cells are highly sensitive to Dex while HeLa cells are not (100, 101). As expected, close to 100% viability was observed from Dex-NP-treated HeLa cells at equivalent Dex concentrations of 10nM to 10 μ M (Figure 2.4). By contrast, RS4;11 cells showed 10-30% viability after 72h of Dex-NP treatment at the same concentration range. Interestingly, 100nM of Dex-NPs caused close to 90% cell death and further increase in NP dosage (1 μ M and 10nM) did not induce a significant change in cell viability (Figure 2.4A). Dose-dependent cytotoxicity studies with free Dex or Dex-NPs on RS4;11 and Nalm6 revealed a similar pharmacological activity (Figure 2.4B). The IC50 values [(a) 1.7nM (free Dex) and 2.4nM (Dex-NP) for RS4;11, P = 0.16 and (b) 6.7nM (free Dex) and 5.08nM (Dex-NP) for Nalm6, P = 0.6] were not significantly different between either form of treatment in both cell lines. It is well established that Dex induces cell death in leukemic cells by apoptosis (102). Dex-NPs induced dose-dependent cleavage of caspase-3 protein and its substrate PARP (Figure 2.4C), indicating apoptotic cell death. Taken together, the results validate that ECT2-NPs deliver bioactive Dex and induce cytotoxicity in leukemia cells.

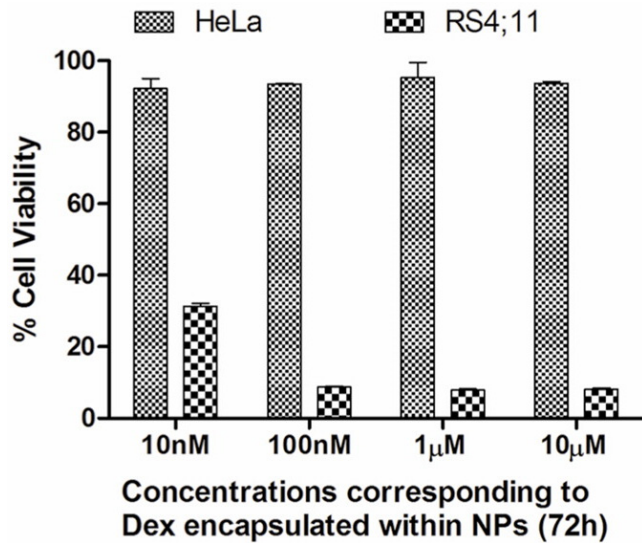


Figure 2.4A. Bioactivity of Dex is retained post encapsulation: Hela cells are insensitive to Dex and RS4;11 leukemia cells are sensitive to Dex.

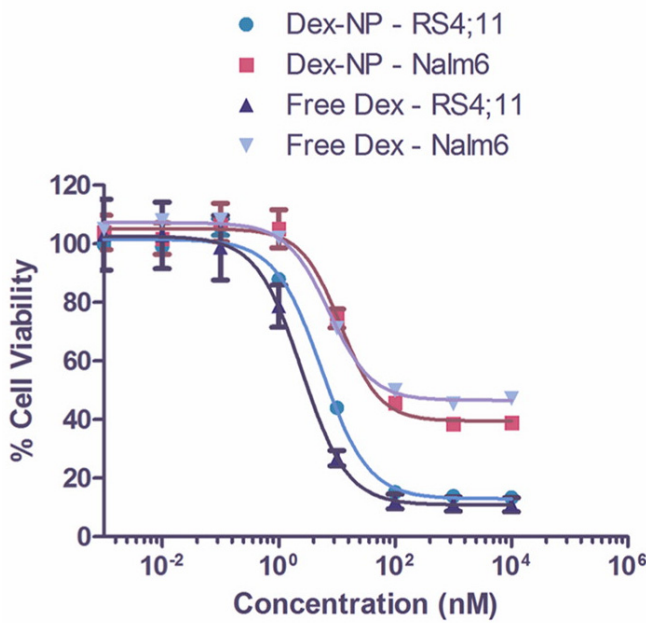


Figure 2.4B. Dose-response curves of free Dex and Dex-NPs at 48h.

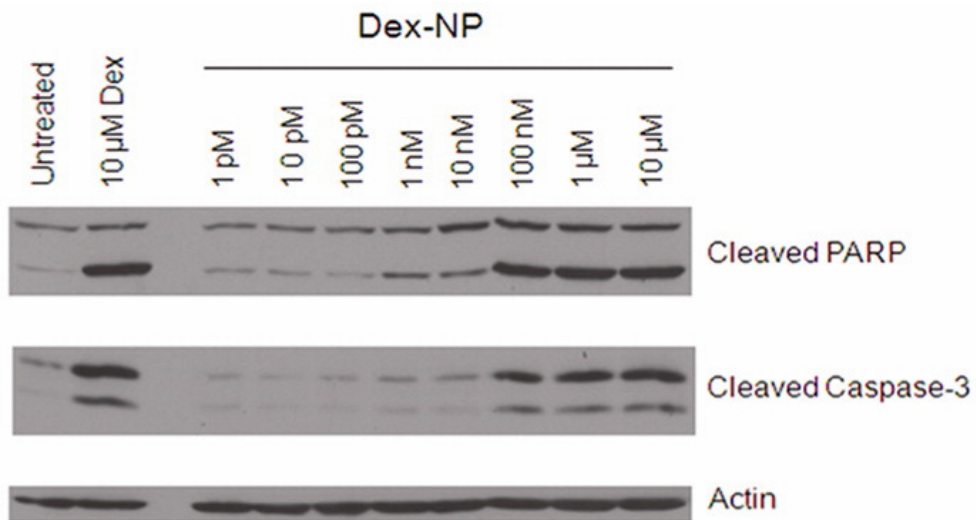


Figure 2.4C. Cleaved PARP and cleaved caspase-3 levels confirm Dex-NP induced apoptosis in RS4;11 cells at 48h.

2.3.5 ECT2-NPs are Bound to and Internalized by Leukemia Cells:

To investigate the potential of ECT2-NPs as drug carriers, cellular binding and uptake studies were performed on two leukemia cell lines (RS4;11, Nalm6) using NR-NPs at a concentration of 70.1 μ g/ml. The shift in fluorescence peak from the untreated group (orange trace) to the treated samples (pink trace) in the FCM plot (Figure 2.5) confirms the binding of NR-NPs to leukemia cells. Further, CLSM revealed NR-NPs internalized and localized within RS4;11 and Nalm6 cells after 6h post-treatment at 37°C (Figures. 2.5A and 2.5B).

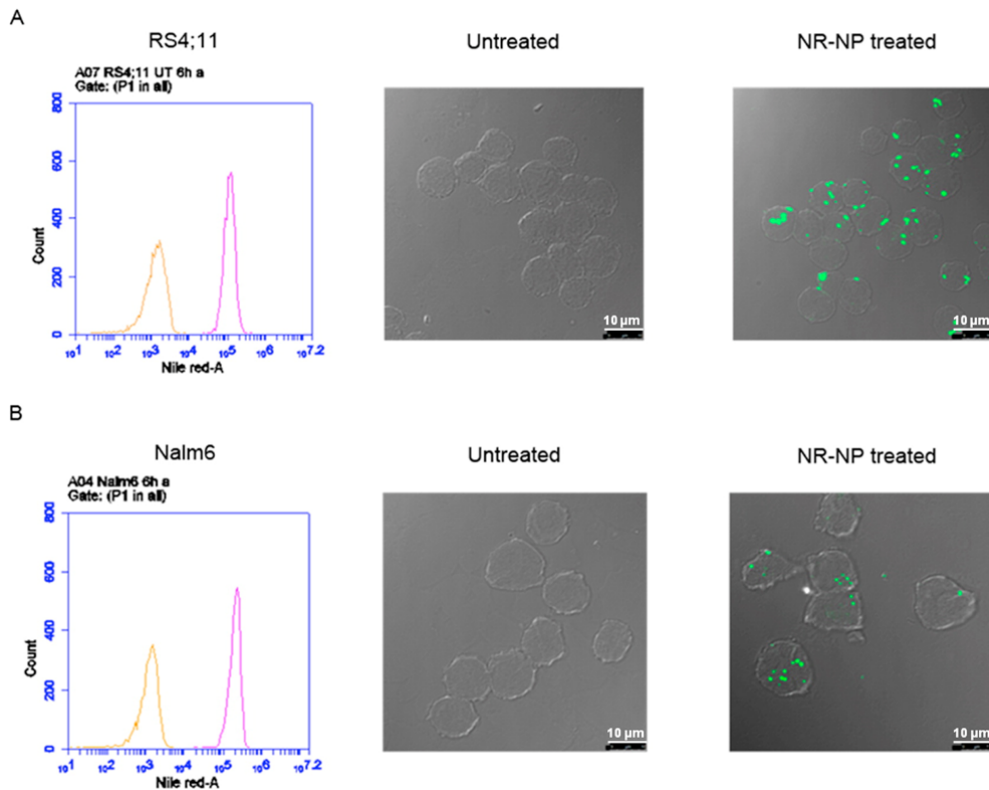


Figure 2.5. NR-NPs bind and internalize by non-specific uptake: Flow cytometry analysis of leukemia cells RS4;11 (A; upper left) and Nalm6 (B; lower left) depict untreated (orange trace) and cell-surface binding of NR-NPs at 6h (pink trace). CLSM images of leukemia cells RS4;11 (A) and Nalm6 (B) represent untreated (middle) and NR-NP treated (right) in 6 h. Scale Bar: 10 μ m

2.3.6 ECT2-NPs Deliver Dexamethasone to Leukemia Cells at Sustained Rates:

Binding of Dex to the glucocorticoid receptor (GR) induces its phosphorylation, subsequently leading to cell apoptosis (103). Therefore, release of Dex from the NPs within the cells could be monitored by the extent of phosphorylation of GR. Free Dex should induce GR phosphorylation as soon as it enters the cell. Thus, GR phosphorylation was used to gauge the intracellular functionality of Dex. RS4;11 cells were incubated with either 10 μ M of free Dex or

equivalent amounts of Dex encapsulated within the ECT2-NPs or Dex-NPs (70.1 $\mu\text{g/ml}$) for 0.08, 0.25, 0.5, 1, 2, and 6h. Quantification of the blots revealed higher GR phosphorylation levels within 5min and it remained high for 6h in cells treated with free Dex. By contrast, in Dex-NP treated cells GR phosphorylation levels increased gradually over the first two hours and by 6h were only 50% of the free Dex treated cells (Figures 2.6A and B). This result suggests that a slow and sustained release of Dex occurs when it is encapsulated in NPs.

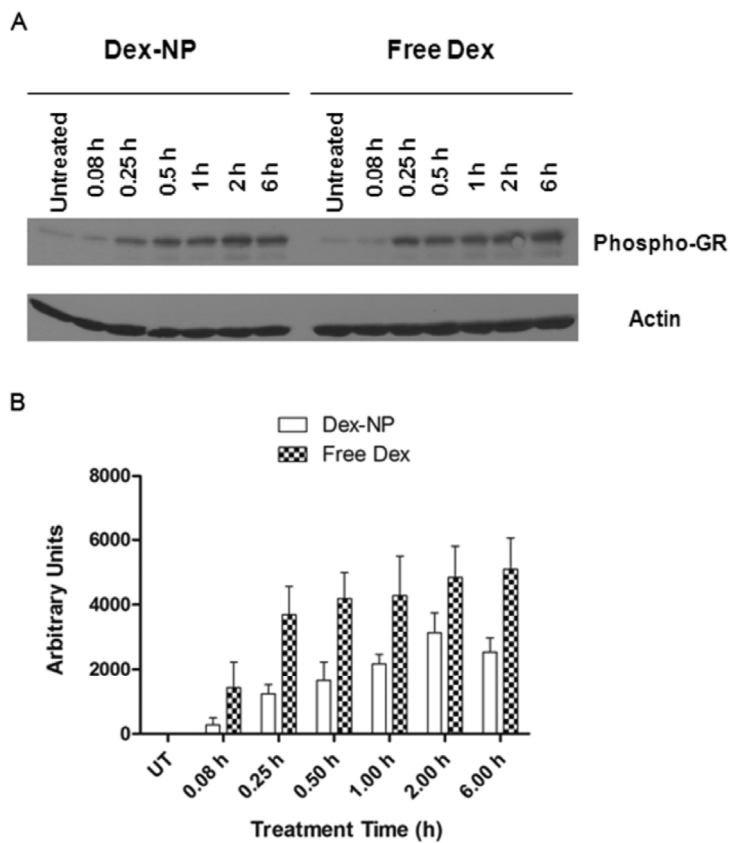


Figure 2.6. Dex-NPs act as sustained-release formulations when treated with leukemia cells *in vitro*: (A) A representative immunoblot depicting GR phosphorylation levels in RS4;11 leukemia cells treated with Dex-NPs corresponding to 10 μM of drug encapsulated within or 10 μM of free Dex. (B) Quantified GR phosphorylation levels in RS4;11 cells highlight Dex-NPs as sustained-release formulations *in vitro* from three independent experiments.

2.3.7 Biodistribution and Clearance of ECT2-NPs in Mice:

To assess tissue distribution levels, BALB/c mice injected via the tail vein with DiR-NPs (0.2 mg/kg DiR) were euthanized at a range of time points to harvest liver, spleen, heart, lung, kidneys, intestine, gonads, bladder and brain. The *ex vivo* imaging of harvested tissues revealed maximum NP accumulation in liver and spleen, reduced levels in kidneys and no accumulation in other organs. The DiR-NP fluorescence levels detected in the liver, spleen and kidneys reduced one week later, decreased further in two weeks and cleared almost completely a month later (Figure 2.7A). The signals detected in the images correlated with DiR-NP levels extracted from tissue lysates (Figure 2.7B).

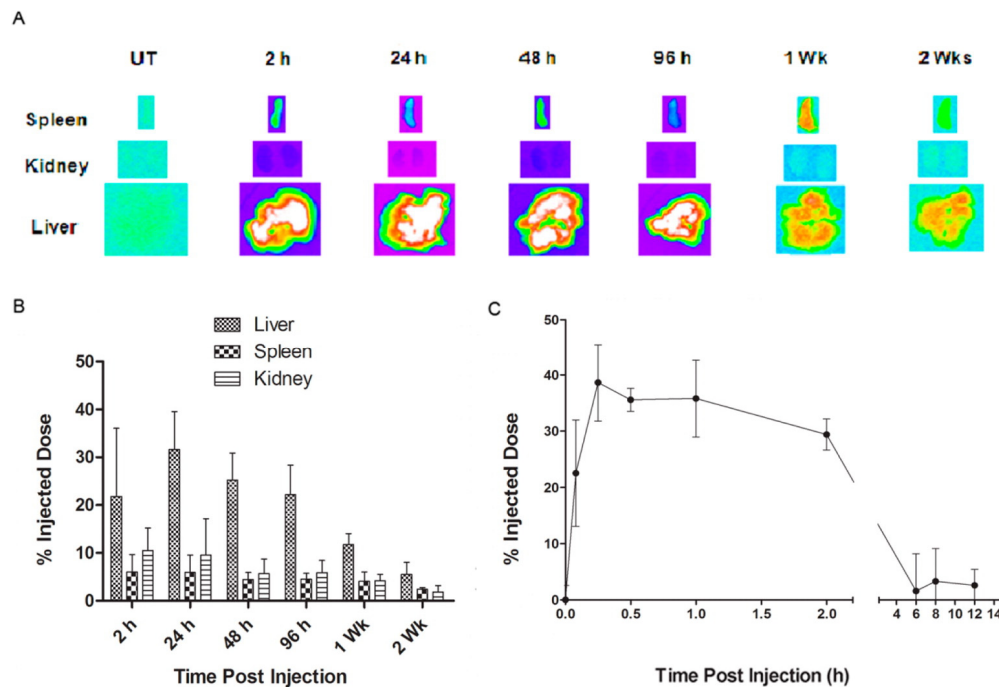


Figure 2.7. Biodistribution and subsequent clearance of ECT2-NPs in mice. Balb/c mice (3 per group) were intravenously injected with DiR-NPs (0.2mg/kg DiR): Subsequently, DiR-NP levels were monitored (A) by *ex vivo* imaging of spleen, kidney, and liver. (B) DiR-NP levels in tissue lysates reveal in vivo biodistribution and clearance. (C) DiR-NP levels in blood plasma.

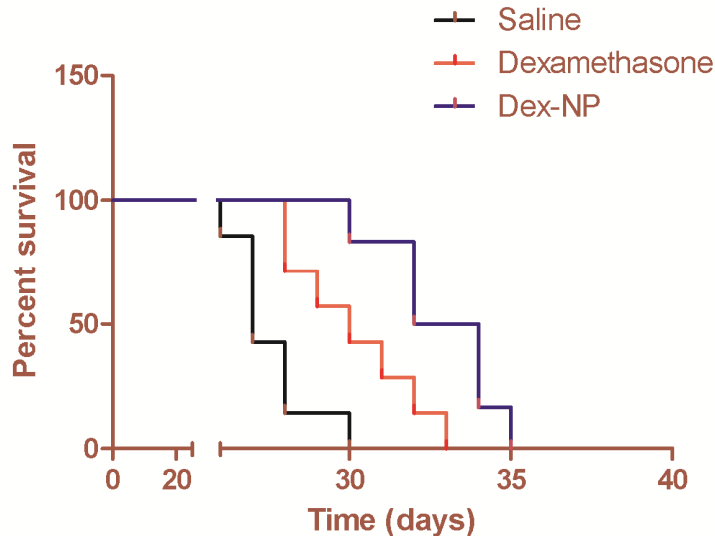
In order to evaluate plasma levels of DiR-NPs, peripheral blood samples drawn from mice at various time points were assessed for “DiR” fluorescence levels. As revealed in Figure 2.7B, there was an initial spike of DiR-NPs, which sustained circulation in the blood plasma for at least 2h and then reduced at 6h post injection indicating biodistribution of DiR-NPs to various tissues from blood or clearance from the system. Overall, the results indicate time-dependent clearance of ECT2-NPs.

2.3.8 Dex-NPs Enhance Therapeutic Efficacy in a Pre-clinical ALL Mouse Model:

To confirm the *in vivo* efficacy of Dex-NPs, ALL human xenograft models, developed in NSG-B2m mice, received intravenous injections at 5 mg/kg every other day for 4 consecutive weeks. The dose administered is one-third the usual recommended daily dose for controlling leukemia progression in pre-clinical models of mice described previously (104, 105). Following injection of RS4;11 leukemia cells, treatment was initiated after the successful engraftment, as determined by the percentage (>1%) of human cells detected in mouse blood (106).

Mice were randomized into three groups (7/group) to receive saline, clinical grade Dex in free form or Dex-NPs. Kaplan-Meier survival curves show that mice that received intravenous administrations of Dex-NPs survived longer (Median Survival = 33 days) than those treated with saline (Median Survival = 27 days P = 0.0009) or the group treated with free Dex (Median Survival = 30 days, P = 0.0229) (Figure 2.8). Moreover, the group that received Dex-NPs manifested no

disease symptoms and were active until the beginning of the 5th week whereas mice treated with free Dex depicted symptoms in 3.5 weeks and were lethargic during the treatment.



Untreated = 7 mice Median survival = 27 days

Dex = 7 mice Median survival = 30 days

Dex-NP = 6 mice Median survival = 33 days

"Log-rank (Mantel-Cox) Test"

P value = 0.0229 between Dex and Dex-NP,

P value = 0.0128 between Untreated and Dex,

P value = 0.0009 between Untreated and Dex-NP

Figure 2.8. Dex-NPs enhance therapeutic efficacy and prolongs survival in pre-clinical leukemia mouse models: Efficacy of Dex-NPs in xenograft model of ALL. (Survival rate is presented in a Kaplan-Meier plot). Dex-NPs (5 mg/kg Dex) significantly prolonged survival in comparison with groups treated with saline and free Dex (5 mg/kg). This highlights the therapeutic efficacy of ECT based Dex-NP formulations *in vivo*.

2.4 Discussion

Dex is widely used as an anti-inflammatory and bone growth steroid. Drug delivery systems that promote osteoblast growth and enhance local treatment of arthropathies have been formulated (107, 108). Dex loaded polymeric implants or NPs have demonstrated tolerance for extended and controlled intravitreal release *in vitro* and *in vivo* (109, 110). In addition, dexamethasone-eluting stents have been used in clinical trials for treating angina (111, 112). To date the potential of using nanocarriers to deliver Dex for ALL has not been explored.

In this study, Dex-loaded NPs were successfully prepared from amphiphilic block copolymers *via* a nanoprecipitation approach. The results show that ECT2-NPs are not toxic *in vitro* or *in vivo*. Dex-NPs induce dose-dependent cytotoxicity by apoptosis and act as a controlled release formulation for Dex. The efficacy of these novel nanoparticle-based formulations in inducing cytotoxicity is confirmed by both *in vitro* studies with cell lines and *in vivo* studies in a pre-clinical leukemia mouse model. Dex-NPs were significantly more toxic than free Dex *in vivo*. Overall, these results demonstrate the suitability and promising potential of ECT2-NPs for delivery of Dex for acute lymphoblastic leukemia therapy.

Preclinical models using subcutaneous xenografts have contributed significantly to nanomedicine (113, 114). Although subcutaneous models are easy to create and evaluate tumor progression in response to a treatment, this approach does not reflect the *in vivo* situation *viz* all tumors are not subcutaneous. The ALL pre-clinical model used in this study accurately mimics the *in vivo* disease condition where the malignant cells are in the blood and are directly accessed by the intravenously administered therapeutics. This situation closely resembles the

treatment received by the ALL patients in the clinic and suggests that this pre-clinical model will be a valuable tool in the evaluation of nanotherapeutics for hematological malignancies.

Owing to their biocompatibility and biodegradability, PCL-based polymeric nanoparticles have been widely used for the delivery and controlled release of anti-cancer drugs (115-118). The incorporation of a cyclic ketal group to the hydrophobic portion of the polymer backbone did not compromise the non-toxic nature of PCL, but allowed to enhance the chain flexibility while decreasing the polymer crystallinity, offering the opportunity to fine-tune the drug release profile (95). The NPs, which varied in size from 100-120 nm, were taken up by leukemia cells *in vitro* and produced a better outcome in leukemic mice. The loading efficiency of Dex in ECT2-NPs was comparable to previously reported values for polymeric nanoparticles (119). Although the incorporation of pendant cyclic ketals reduced the crystallinity of PCL (95), the low affinity of polymer for Dex may have compromised the overall drug loading. Future modification and adjustment of the polymer composition should allow increased loading and controlled release of Dex *in vitro* and *in vivo*.

In B-cell lymphoma, IC50s of the non-targeted liposomal formulations of doxorubicin were higher than the free drug (120). This may be expected because there would be a time delay due to nonspecific cellular uptake and subsequent release of the drug from liposomes compared to simple diffusion of the free drug. Although there appears to be a small difference in IC50 values for free and encapsulated Dex, the changes were not significant. The results obtained in this

study are consistent with a notion that there is a time delay to initiate events leading to apoptosis in Dex treated cells and that this time delay is similar irrespective of the type of treatment. Since IC₅₀ values are dependent on toxicity of the drug and cell viability, which is the endpoint, a time delay in inducing cytotoxicity is a critical factor in justifying the lack of significant differences in the IC₅₀ values between free and encapsulated Dex formulations.

The *in vitro* Dex release data in Figure 2.2 show that approximately 60% of the encapsulated drug was released by 48h when measured at 25°C. Since Dex is susceptible to degradation (~6% in 7 days) at 37°C, the release kinetics of Dex-NPs was accurately determined at room temperature (121). Although, the drug release kinetics at 25°C does not reflect actual *in vivo* conditions at 37°C, reduced and steady levels of Dex induced GR phosphorylation in leukemic cells treated with Dex-NPs *in vitro* indicates sustained release capabilities of ECT2-NPs. Although direct measurement of Dex released from NPs within the cells was not performed, the lower levels of GR phosphorylation indicate that the effective intracellular dose of Dex may be lower in Dex-NP treated cells compared with free Dex treated cells. However, at 48h, cell death was not significantly different between the two treatments. Thus there was not a significant correlation between GR phosphorylation and cell death.

Leukemic cells treated with free NR revealed intense continuous intracellular staining (Figure 2.9) compared to distinct punctate staining observed in the NR-NP treated cells. This depicts that the fluorescence observed is primarily from the NR-NPs internalized by the leukemic cells and not due to

premature and undesirable NR release. This is further supported by the slow *in vitro* release of NR from ECT2-NPs (Figure 2.2).

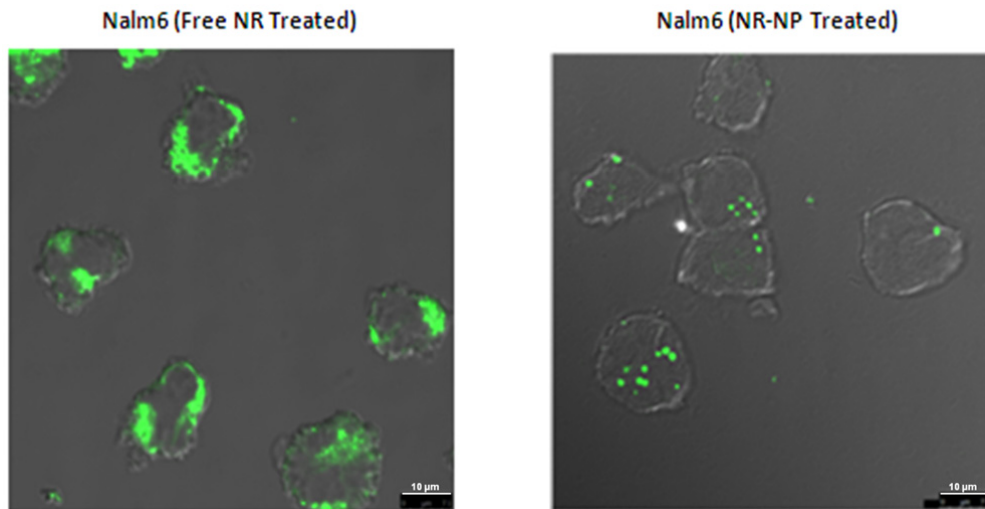


Figure 2.9. CLSM images of Nalm6 leukemic cells treated with free Nile-red (L) and NR-NP (R): Please note the cytoplasmic staining in cells treated with free Nile Red. The nuclear regions are excluded. Scale Bar: 10 μ m

Dex clearance rates in children with ALL are highly variable and dependent on co-administered drugs, age and treatment intensity (122). This variable clearance raises the need for repetitive drug dosing that can lead to overdosing and harmful side effects. The plasma profile and clearance rates of ECT2-NPs in this study do not correlate with the drug's half-life *in vivo*. The “DiR” dye is used to monitor the fate of the carriers and not the drug encapsulated within. The data could therefore, be used to indirectly gauge the fate of Dex-NPs alone.

Non-targeted NPs typically accumulate rapidly in the liver (first pass metabolism) and spleen, often preventing them from reaching target organs (123). The data here corroborate these prior studies, showing that liver and spleen are the major organs that accumulate the NPs used in this study. Although, the plasma

profile and clearance rates of the NPs do not directly correlate with Dex clearance rates, this may be an advantage in the treatment of ALL because leukemic blasts accumulate and proliferate in these tissues resulting in hepatosplenomegaly (a symptom in pediatric ALL). It takes more than two weeks for these NPs to be eliminated from these tissues, indicating that non-targeted Dex-NPs are potentially valuable as a novel chemotherapy for ALL. In addition, reduced NP accumulation in organs of active filtration such as lungs and kidneys indicate that encapsulated Dex may have a longer elimination half-life than Dex administered as the free active form.

ALL being a liquid tumor, passive targeting by enhanced permeability and retention (EPR) effect is not relevant. The absence of targeting ligands on Dex-NPs does not permit active targeting. This significantly limits the rate of leukemic cell uptake *in vivo* despite being in systemic circulation. The short half-life of Dex in ALL patients entails the daily administration of high doses of the drug in actual clinical settings. Encapsulating Dex within ECT2-NPs may have increased the drug's half-life marginally though not to an extent that could improve the outcome in terms of reducing the dosage frequency.

In this study, a dose of 5mg/kg was utilized to evaluate therapeutic efficacy. Although treatment with Dex-NPs could not cure the mice, it is noteworthy that NP encapsulation significantly enhanced the drug's efficacy delaying onset of disease symptoms and increasing survival time. Similar increases in efficacy of drug encapsulated in non-targeted liposomes or NPs have been noted for other cancers, (120, 124) but not in leukemia. ALL is treated at

various stages with a combination of at least six drugs including Dex. Such a regimen is necessary for attaining full remission of the cancer in patients with treatable disease. The fact that reduced dose of Dex alone has improved the quality and survival significantly than the control is the key discovery of this study and justifies the potential of this platform for further development.

2.5 Conclusion

The results indicate that Dex encapsulated in nanoparticles may enable the use of reduced doses of Dex to induce leukemia cell death and improve survival. The next step is to establish targeted drug delivery platforms with this novel system. The NP surface here can easily be modified to covalently link targeting moieties. Several targeting moieties directed against folate (125, 126), CD19 (127, 128), CD10 (129, 130), or transferrin receptors (131, 132) have been utilized for specific targeting of hematological malignancies. The next chapter in this dissertation describes the studies that tested the effectiveness of such targeted NPs to delivery chemotherapy specifically to ALL and reduce systemic toxicity while achieving prolonged survival in leukemic mice. Translation of this technology into the clinic could reduce treatment related side effects in children treated for cancer.

Chapter 3

CD19-TARGETED NANODELIVERY OF DOXORUBICIN ENHANCES THERAPEUTIC EFFICACY IN ACUTE LYMPHOBLASTIC LEUKEMIA

3.1 Introduction

Acute Lymphoblastic Leukemia or ALL, is the most prominent form of all pediatric cancers (1). Based on Leukemia and Lymphoma Society's Facts 2013, the disease accounted for one-third of cancer deaths in children and adolescents affected by blood cancers. ALL is characterized by massive proliferation of immature white blood cells (WBCs) or lymphoblastic cells in the blood and bone marrow; that subsequently infiltrates and cause enlargement of various sites such as the liver and spleen (hepatosplenomegaly), lymph nodes (lymphadenopathy) and the central nervous system (causing headaches, sixth-nerve palsy, edema and vomiting). The uncontrolled immature blast proliferation further restricts the development of mature blood cells including (a) red blood cells (RBCs), that are critical to transport oxygen and nutrients throughout the body; (b) platelets, which are essential to control excessive bleeding at sites of injury and (c) WBCs, that primarily constitute the body's defense mechanism against infections.

Existing treatment protocols in the clinic employ combinations of conventional chemotherapy, molecularly targeted therapies and immunotherapies, often in conjunction with radiation and hematopoietic stem cell transplantation. This achieves an overall five-year relative survival rates that exceed 90% in

children treated for ALL (1). Although effective in controlling the growth of rapidly dividing malignant cells, conventional chemotherapeutic drugs do not differentiate between a normal dividing healthy cell and a rapidly dividing cancerous cell. As a result, induction of treatment related side effects in more than 60% of pediatric cancer survivors has undermined the very significance of the 90% five-year relative survival rate achieved by combination therapies in pediatric leukemia (7).

To date, several nanoparticle-based drug delivery systems have been formulated and evaluated preclinically for cancer therapy (3, 4, 133). Some of these systems have advanced into clinical trials for adult cancer therapy. However, efforts to direct research, development and application of nanotherapeutic platforms in pediatric oncology is lagging (133). Liposomal vincristine sulfate (Marqibo[®]) is the first system to have entered into Phase I clinical trials for the treatment of pediatric ALL following its approval by the FDA to treat Philadelphia chromosome positive (Ph+) ALL in adults (62).

Targeted nanoparticles (NPs) hold tremendous potential to revolutionize the field of cancer detection and therapy (134). While enhanced permeability and retention (EPR) effect plays a critical role in localizing NPs at the tumor site in solid cancer therapy, conjugating targeting ligands to these particles further improves its diagnostic potential and antitumor activity (83, 135). However, in hematologic malignancies such as leukemia, the EPR effect is less relevant since the tumor is disseminated throughout the body. It is therefore critical to target NPs

directly to tumor cells in the blood and thus, improve its uptake and anti-tumor activity.

The CD19 antigen is a single chain, type 1 transmembrane glycoprotein with an extracellular domain composed of 280 amino acids. The amino acids are further organized into two C2-type (Ig)1-like domains separated by a smaller non-Ig-like domain that has potential disulfide bonds and N-linked carbohydrate addition sites (136, 137). CD19 is expressed in nearly all stages of B-cell development and also on the majority of acute B-ALL cells (137-139). It is generally absent in normal T-lymphocytes, NK cells, monocytes, and granulocytes and its expression is seldom lost during malignant transformation (140). Since it is not shed from the surface of malignant cells and is internalized after antibody (Ab) binding, CD19 has been used as a target antigen for development of antibody-based therapeutics for B-lymphoid malignancies (141-143). CD19-targeted DOX or vincristine (VCR)-encapsulated immunoliposomes have been used to treat B-cell lymphoma (144, 145). Recently, CD19-targeted blinatumomab (BLINCYTOTM, Amgen Inc.) has been approved by the FDA for the treatment of Philadelphia chromosome-negative relapsed or refractory B-cell precursor ALL (146).

In Chapter 2, it was shown that NPs derived from an amphiphilic block copolymer consisting of hydrophilic poly(ethylene glycol) (PEG) and hydrophobic poly(ϵ -caprolactone) (PCL) bearing pendent cyclic ketals were biocompatible *in vitro* and *in vivo*. Encapsulation of dexamethasone (a steroidal drug used for treating ALL) in these polymeric nanocarriers significantly extended survival and

reduced disease symptoms in human xenograft models of ALL. Encouraged by these results, a second generation of polymeric NPs was engineered and tested to deliver doxorubicin (DOX) specifically to leukemic cells. DOX belongs to the anthracycline class of drugs and is widely used for treating pediatric leukemia. The drug is primarily known to cause significant cardiomyopathy and congestive heart failure apart from other side effects including myelosuppression, nausea and vomiting, hair loss, diarrhea, mucositis, encephalopathy and hemorrhagic cystitis in children (9, 147). To target the ALL cells, the NP surface was modified to display antibodies (Abs) directed against CD19 (a B-lymphoblast cell surface antigen that shows enhanced expression on ALL cells with reduced expression on pluripotent stem cells).

The results in this chapter demonstrates that anti-CD19Ab-conjugated DOX-encapsulated NPs (CD19-DOX-NPs) can specifically target DOX into CD19-positive; CD19(+) B-ALL cells and induce apoptosis in a target specific manner *in vitro*. It is also shown that the CD19-DOX-NPs are rapidly internalized via clathrin-mediated endocytosis and impart target specific cytotoxicity at a lower concentration of the encapsulated drug compared to free DOX. Further, the study in this section depicted that CD19-DOX-NPs treated leukemic mice survived longer and manifested higher degree of agility compared to mice treated with free DOX. It is therefore suggested that targeted delivery of clinically used chemotherapeutics should improve or sustain current survival rates with reduced side effects in children treated for leukemia.

3.2 Experimental Section

3.2.1 Reagents, cell lines and mouse models:

All chemicals necessary for the synthesis of the amphiphilic block copolymers were purchased from Sigma-Aldrich (St. Louis, MO) and were used as received unless otherwise indicated. Palmitic acid N-hydroxysuccinimide ester and avidin from egg white were also obtained from Sigma-Aldrich (St. Louis, MO). Biotinylated mouse anti-human CD19Ab and biotinylated mouse IgG isotype control was obtained from eBioscience (San Diego, CA). Solvents were purchased as anhydrous grade and used without further purification. Doxorubicin Hydrochloride (DOX-HCL) for *in vitro* and *in vivo* studies was purchased from Tocris Biosciences (Minneapolis, MN). Nile red used as a fluorescent probe for cellular tracking of NPs and sucrose was purchased from Sigma-Aldrich. Nystatin was obtained from Thermo-Fisher Scientific (Waltham, MA) and amiloride-hydrochloride was purchased from MP Biomedicals (Santa Ana, CA). DilC18 (7) tricarbocyanine probe (DiR) for *in vivo* biodistribution studies was acquired from Life Technologies (Grand Island, NY). Human acute leukemia cell lines RS4;11 (ATCC® CRL-1873™, established from a patient with B-ALL at first relapse) and REH (ATCC® CRL-8286™, also established from a patient with B-ALL at first relapse) were purchased from the American Type Culture Collection (ATCC, Manassas, VA). Both RS4;11 and REH cells were maintained in Roswell Park Memorial Institute (RPMI) media (Life Technologies) supplemented with 10% fetal bovine serum (FBS), 2 mmol/L l-glutamine, 25 U/mL penicillin, and 25 µg/mL streptomycin. The cell lines were maintained at 37°C under a humidified

atmosphere of 95% air and 5% CO₂. BALB/c mice used for *in vivo* pharmacokinetic and organ biodistribution analysis, and immune-compromised NSG-B2m mice used to develop preclinical B-ALL mouse models for therapeutic efficacy studies were all purchased from Jacksonville Laboratories, U.S.A. Animal studies were approved by the Institutional Animal Care and Use Committee at the University of Delaware.

3.2.2 Preparation of DOX-loaded NPs with or without the targeting Ab:

3.2.2.1 Polymer synthesis:

The amphiphilic block copolymer was synthesized via a ring-opening copolymerization of ϵ -caprolactone (CL) and 1,4,8-trioxaspiro-[4,6]-9-undecanone (TSU) using α -hydroxy, ω -methoxy PEG as the initiator, following previously reported procedures (95). The resultant copolymer had a composition of EG₁₁₃CL₁₅₂TSU₂₅, a number-average molecular weight (Mn) of 40.6 kg/mol and a polydispersity index (PDI) of 1.57.

3.2.2.2 Synthesis of avidin-palmitic acid conjugates (avidin-PA):

Avidin at a concentration of 0.25 mg/ml was reacted with palmitic acid N-hydroxysuccinimide ester (NHS-PA, 0.54 mg/ml) in a solvent mixture of DI H₂O and dimethylformamide (DMF) (1:39, v/v). The reaction was conducted at 37°C for 4h. To remove excess fatty acid and hydrolyzed ester, the reactants were extensively dialyzed against DMF, followed by DI water using hydrated regenerated cellulose dialysis tubing with a molecular weight cutoff (MWCO) of 10KDa. Dry product was obtained after lyophilization.

3.2.2.3 Preparation of drug/dye-loaded NPs:

Prior to drug encapsulation, DOX-HCl was desalted to generate DOX following reported procedures (148). NPs were then formulated following a nanoprecipitation method (149). Briefly, an acetone/DMSO (1:1, v/v) solution of the block copolymer (10 mg/ml, 1 ml) was added dropwise to a stirred aqueous phase (5 ml DI water). The mixture was stirred at 900 rpm for 2h at ambient temperature to obtain blank NPs. DOX, NR or DiR dye-loaded NPs were similarly prepared using an acetone/DMSO (1:1, v/v) solution of the block copolymer (10 mg/ml, 1 ml) containing 2 mg/ml DOX, 0.1 mg/ml NR or 0.036 mg/ml DiR, respectively. The NP suspensions were subsequently centrifuged (4,000 rpm for 10min) and the supernatant was transferred to an Amicon regenerated cellulose centrifuge filter (MWCO=30KDa, EMD Millipore). Drug/dye-loaded NPs were collected after repeated ultracentrifugation (40,000 rpm) and PBS (pH 7.4) wash (three times).

3.2.2.4 Preparation of drug-loaded Ab-conjugated NPs:

Drug or dye-loaded NPs with immobilized avidin-PA were prepared following the procedure described in 3.2.2.3, with the addition of avidin-PA (0.125 mg/ml) in the stock polymer solution . The purified avidin-PA-NPs were re-suspended in PBS at a concentration of 10 mg/ml. Avidin-PA incorporation in the NPs was quantified by a bicinchoninic acid (BCA) assay following the manufacturer's protocols. The concentration of immobilized avidin-PA was derived from a series of standards at an avidin concentration of 6.25-100 µg/ml. NPs without avidin-PA was used as the control. Finally, biotinylated anti-

CD19Abs (20 μ l, 0.5 mg/ml) were added to avidin-PA-NP suspension (0.5 ml, 10 mg/ml) in PBS, and the mixture was incubated at 37°C for 2h. Free Abs were removed by ultracentrifugation as described above. The resultant CD19-targeting NPs (CD19-NPs) was resuspended in PBS at desired concentrations for *in vitro* and *in vivo* testing.

3.2.3 NP characterization:

3.2.3.1 Particle size and surface charge:

Various NP fomulations were analyzed by dynamic light scattering (DLS) using the Zetasizer nanoZS (Malvern Instruments, Westborough, MA) via. The mean diameter was computed from the scattered light intensity using the Malvern software package based on the theory of Brownian motion and Stokes-Einstein equation. Zeta potential of NPs was measured by electrophoretic light scattering.

3.2.3.2 Drug/dye loading and *in vitro* release:

Freshly prepared NPs were lyophilized and the dry weight was noted. The powder was then dissolved in DMSO (1 ml) and DOX/NR concentration was determined by fluorescence using a plate reader (DTX880 Multimode Detector, Beckman Coulter, Fullerton, CA) at 485nm/595nm and at 535nm/595nm for DOX and NR, respectively. The concentration of DiR was quantified using a UV-Vis spectrophotometer (Agilent Technologies, Santa Clara, CA) at 750 nm. The loading content (LC) was defined as the amount of drug/dye (μ g) loaded per milligram of NPs and the encapsulation efficiency (EE) was calculated as a percentage based on the amount of drug/dye encapsulated over that in feed. For

studying the *in vitro* release rates, freshly formulated NPs were incubated at 37°C in PBS under sink conditions for up to 7 days. The release medium was collected daily by removing NPs using centrifuge filters as described above and the NP pellet was re-dispersed in fresh PBS to continue the release study. Drug/dye concentration in the collected filtrate was analyzed as described above after freeze drying and subsequent dissolution in DMSO. The cumulative release was calculated by dividing the amount of drug or dye released each day with the total mass initially loaded. All measurements were carried out in triplicate, and the results were indicated as the mean ± SD.

3.2.3.3 Quantifying anti-CD19Abs on NPs:

Serial dilutions of free biotinylated anti-CD19Abs were prepared and resolved on 10% SDS-PAGE gels and transferred overnight onto nitrocellulose membranes (Bio-Rad) in 20% methanol, 25mM Tris, and 192mM glycine. After transfer, the membranes were blotted with mouse HRP-conjugated streptavidin to bind to biotin and visualized by incubating the membrane with Enhanced Chemiluminescence Plus reagent (GE Healthcare, Piscataway, NJ) followed by exposure to X-ray film (Amersham Biosciences, Piscataway, NJ). A calibration curve obtained from using free anti-CD19Abs was used to determine the level of anti-CD19Abs incorporated on the NPs.

3.2.4 Analyzing CD19 cellular levels:

3.2.4.1 Immunoblot:

To examine and compare the total levels of CD19, B-Cell ALL (B-ALL) cells (REH or RS4; 11) at a density of 3×10^6 cells/dish were collected, washed with cold PBS twice and resuspended in a lysis buffer (20mM Tris-HCl, pH 7.5; 150mM NaCl; 1mM EDTA; 1mM EGTA; 1mM β -Glycerol Phosphate; 1mM Sodium Vanadate; 1.25mM Sodium Pyrophosphate; 1% (w/v) Triton X-100) with a 1% protease inhibitor cocktail (100mM Phenylmethylsulfonyl Fluoride, 1:100; 15 mg/ml mixture of Antipain, Leupeptin, Pepstatin, 1:1000; Sigma-Aldrich. St Louis, MO) at 4°C for 30min. Cell lysates were then prepared by sonication and removal of insoluble material by centrifugation (12,000 rpm) at 4°C for 15min. The protein concentration in the lysates was determined using a protein assay kit (DC protein assay reagent, Bio-Rad, Hercules, CA, USA). Equal amounts of protein (100 μ g) were resolved on 10% SDS-PAGE gels and transferred overnight onto nitrocellulose membranes in 20% methanol, 25mM Tris, and 192mM glycine. After transfer, the membranes were blotted with a mouse monoclonal antibody against CD19 (1:1000, Cell Signaling, Danvers, MA) and visualized by HRP-conjugated secondary antibodies and Enhanced Chemiluminescence Plus reagent (GE Healthcare, Piscataway, NJ) followed by exposure to X-ray film (Amersham Biosciences, Piscataway, NJ). Subsequently, densitometric analysis of the blots was performed using Tina image analysis software to quantify CD19 levels.

3.2.4.2 Flow cytometry.

To quantify the cell surface levels of CD19, B-ALL cells (1.0×10^6) were stained with fluorescein isothiocyanate (FITC)-conjugated mouse anti-human CD19Ab (eBioscience) for 30min at 4°C. Cells were then washed three times with cold PBS and analyzed using a BD Acuri C6 Flow Cytometer® System. For each sample, FITC fluorescence emitted by approximately 10,000 cells was measured using the FL-1 detector (wavelength 530 nm). Data was analyzed using BD Accuri CFlow® software.

3.2.5 Cell uptake of non-targeted and targeted NPs:

3.2.5.1 Treatment with NPs, CD19-NPs and IgG-NPs:

B-ALL cells (REH or RS4; 11) were seeded at a density of 300, 000 cells/ml and incubated at 37°C for 1h in the presence or absence of Nile red ($543_{\text{Ex}}/650_{\text{Em}}$) encapsulated non-targeted NPs (NR-NPs) or anti-CD19Ab-conjugated NPs (CD19-NR-NPs) or an irrelevant isotype control IgG-conjugated NPs (IgG-NR-NPs) at a final concentration equivalent to $1\mu\text{M}$ of encapsulated DOX. When indicated, 100 μg of free rabbit anti-human CD19Abs (Cell Signaling) or free irrelevant isotype control IgG (EMD Millipore) was added to the cells at 4°C, 30min prior to incubating with the NPs. To visualize cellular uptake of NPs by CLSM, the treated cells were washed three times with cold PBS and mounted on Poly Prep Slides™ (Sigma Aldrich, St. Louis, USA), fixed with 2% paraformaldehyde solution and embedded in ProLong Antifade Kit® mounting medium (Life Technologies, Grand Island, NY) for fluorescent

immunocytochemistry. Image acquisition was performed by sequential scanning using a Leica TCS SP5 laser-scanning confocal microscope and subsequently processed by merging of the fluorescence channels using the software LSM (Leica Microsystems, Mannheim, Germany). The cell uptake levels of NR-NPs and CD19-NR-NPs in REH and RS4;11 B-ALL cells were quantified using the ImageJ analysis software (NIH, Bethesda, MD). Statistical significance of the values obtained were then determined by performing multiple t-tests using the Holm-Sidak method, with alpha=5.0%.

3.2.5.2 Treatment with endocytic inhibitors:

To examine the endocytic mode of uptake for CD19-NPs, RS4; 11 cells were seeded at a density of 300,000 cells/ml and pre-treated at 37°C for 30min with one of the following inhibitors: 0.1M hypertonic sucrose (an inhibitor of clathrin-mediated endocytosis) (150), 20 µg/ml Nystatin (an inhibitor of caveolae-mediated endocytosis) (151); and 8 µg/ml amiloride-hydrochloride (an inhibitor of macropinocytosis) (151). Subsequently, the cells were incubated with CD19-NR-NPs at a final concentration equivalent to 1µM of encapsulated DOX for 30min in cell culture media at 37°C, washed and processed for CLSM imaging to visualize uptake of NPs as explained previously. When indicated, RS4; 11 cells were co-treated with fluorescein isothiocyanate-conjugated transferrin (FITC-Tf, Life Technologies) and CD19-NR-NPs at 37°C and processed for further analysis by CLSM imaging.

3.2.6 Cytotoxicity evaluation of DOX formulations:

3.2.6.1 Evaluation of toxicity:

The toxicity of free DOX or CD19-DOX-NPs was tested and compared between B-ALL cell lines REH and RS4; 11. When indicated, 100 μ g of free anti-CD19Ab or free irrelevant isotype control IgG was added to the cells at 4°C, 30min prior to incubating with the DOX nanoformulations. The assays were performed in 96-well cell culture plates which were maintained at 37°C in 5% CO₂ atmosphere. The cells were seeded at an initial density of 30,000 cells per well and treated with free DOX or CD19-DOX-NPs at an equivalent dose of 100nM DOX for 1h. Following treatment, the cells were washed with PBS at least two times and left for further incubation up to 48h and 72h. At the end of each incubation period, cell viability was measured by Cell Titer-Blue® Viability Assay. The measurements were then expressed as the percentage of viable cells compared to the survival of untreated cells defined as the maximum cell viability.

3.2.6.2 Evaluation of apoptosis:

B-ALL RS4; 11 cells were plated in 10 cm dishes at a density of 3 x 10⁶ cells/dish and incubated with CD19-DOX-NPs at doses ranging from 1pM to 10 μ M of encapsulated DOX for 48h. Leukemia cells untreated or treated with 10 μ M DOX in free form were considered as negative and positive experimental controls respectively. The cell lysates were prepared and protein concentrations were estimated as described earlier. Equal amounts of protein (90 μ g) were resolved on 10% SDS-PAGE gels and transferred overnight onto nitrocellulose

membranes and blotted with a rabbit polyclonal against cleaved PARP(1:1000, Cell Signaling, Danvers, MA) and a mouse monoclonal antibody against actin (1:10000, Cell Signaling) as explained previously.

3.2.7 HPLC/MS/MS analysis of cell associated DOX (intracellular and cell surface bound) levels in targeted and non-targeted cells:

To determine the concentration levels of cell associated DOX (caDOX), B-ALL cells (REH or RS4;11) were seeded in 12 well plates at a density of 300,000 cells/ml and incubated in the presence of either free DOX or CD19-DOX-NPs at concentrations corresponding to 100nM, 1 μ M or 10 μ M of DOX equivalents at 37°C for 1h. Subsequently, the cells were lysed and centrifuged at 14,000 rpm. The supernatant was then subjected to acetonitrile extraction and quantitation of DOX was determined using HPLC/MS/MS. DOX was initially purified by chromatography on a Poroshell 120 EC-C18 column (2.7 μ m, 3.0 X 50 mm) at 50°C and eluted with a gradient from 0.1% formic acid to 100% methanol in 0.1% formic acid (1.0 – 3.0min) using an Agilent 1260 Infinity high-performance liquid chromatography (HPLC) system. Solvent flow rate was 0.4 mL/min and total run time per sample was 8min, including column equilibration. DOX was detected using an Agilent 6460 Triple Quad MS/MS equipped with an ESI source. MS conditions were: gas temperature 350°C and flow rate 10 L/min; sheath gas temperature 400°C, flow rate 12 L/min; nebulizer pressure 45 psi; capillary 3500 V and detector in positive ion mode. DOX primary ion was 544 and fragment ion 361 with fragmentor set at 120 V and collision energy 30 eV. A standard curve was created using pure DOX for quantitation of the drug in the supernatant.

3.2.8 *In vivo* pharmacokinetics and biodistribution:

To analyze plasma pharmacokinetics; female BALB/c mice (4-6 weeks of age; 3/group) were injected via the tail vein with a single dose of 100 µl of CD19-NPs (\approx 2.5 mg/kg DOX) loaded with a lipophilic “far-red” dye DiR (750_{Ex}/830_{Em}) resuspended in PBS (CD19-DiR-NPs). At 0.08, 0.25, 0.5, 1, 2, 6, 8 and 12h post NP injection, peripheral blood was collected from the mice by submandibular bleeding in heparinized tubes to prevent the blood from clotting. Blood was then centrifuged and CD19-DiR-NP fluorescence levels in the plasma were analyzed by using multi-label microplate reader (Plate Chameleon V, Hidex, Finland) to assess its plasma half-life. The NP levels were then estimated by comparing with standards prepared in plasma.

To investigate the organ biodistribution and clearance rates of CD19-NPs, female BALB/c mice (4-6 weeks of age; 3 per group) received intravenous injections of 100 µl of CD19-DiR-NPs (\approx 2.5 mg/kg DOX). Subsequently, liver, spleen, lung, heart, stomach, kidney and brain were dissected from euthanized mice 6h, 12h, 24h, 48h, 96h, 1week, 2weeks and a month post administration. The organs were then homogenized in tissue lysis buffer (20mM Tris-HCL, pH 7.5; 150mM Sodium Chloride; 1mM EDTA; 1mM EGTA; 1mM β -Glycerol Phosphate; 1mM Sodium Vanadate; 2.5mM Sodium Pyrophosphate; 1% (w/v) Triton X-100; 1% (w/v) IGEPAL; 0.5 % (w/v) Deoxycholate; 1 % (w/v) SDS) and 1% protease inhibitor cocktail (100mM Phenylmethylsulfonyl Fluoride, 1:100; 15 mg/ml mixture of Antipain, Leupeptin, Pepstatin, 1:1000; Sigma-Aldrich, St Louis, MO) at 4°C for 1h. The lysates were used to quantify the CD19-DiR-NP fluorescence levels in various organs using the multi-label microplate reader (Plate

Chameleon V, Hidex, Finland) and the NP levels were estimated by comparing with standards prepared in tissue lysis buffer. BALB/c mice treated with saline were included as controls for the experiment and to establish the measurement settings based on background fluorescence.

3.2.9 Measurement of agility and monitoring of survival:

RS4; 11 cells (5×10^6) were injected via the tail vein into female NSG-B2m mice (6 - 8 weeks old; 8 per group). Three days later, the mice were given intraperitoneal injections of saline, free DOX, IgG-DOX-NPs or CD19-DOX-NPs at dose equivalents of 2.5 mg/kg DOX, once a week. Simultaneously, the physical activity of mice was measured with a Low Profile Wireless Running Wheel (Med Associates Inc., St. Albans, VT, USA) every 7 days over the course of the treatment and data was analyzed with CHRONO software. The treatment efficacy was finally determined using Kaplan-Meier survival curves and the wheel running activity was recorded and plotted to determine agility. Animals were sacrificed when they depicted signs of morbidity, including hind-limb paralysis or excessive weight loss, according to the University of Delaware's IACUC guidelines.

3.2.10 Statistical Analysis:

All experiments were carried out in triplicates, and results are indicated as the mean \pm SD unless otherwise indicated. All graphs have been generated and analyzed using Prism nonlinear regression software (Graphpad Software). The survival data in efficacy studies are presented using Kaplan-Meier plots and the

data was analyzed using “Log-rank (Mantel–Cox) test”. A $p < 0.05$ was considered significant.

3.3 Results

3.3.1 NP formulation and characterization:

Particle size analysis by dynamic light scattering (DLS) (Table 3.1) showed that the DOX-NPs exhibited an intensity average size of 81 ± 4 nm and a volume average size of 62 ± 3 nm. Similarly, NR-NPs and DiR-NPs displayed the intensity average size of 80 ± 8 nm and 88 ± 1 nm, and the volume average size of 63 ± 2 nm and 73 ± 1 nm, respectively. The average sizes from intensity and volume were in agreement with each other and reflected the size distribution of major population of the NPs. Table 3.1 also reveals that the incorporation of anti-CD19Abs slightly increased the size of the particles. Moreover, all NPs exhibited a narrow size distribution as indicated by their polydispersity index. In addition, measurement of zeta potential values revealed that IgG conjugation to NPs significantly decreased the surface charge (-5mV for non-targeted vs -42mV for anti-CD19Ab-conjugated and -50mV for IgG-conjugated NPs).

Table 3.1 Summary of size, loading content and encapsulation efficiency of different types of NPs

Samples	By Intensity (nm)	By Volume (nm)	PDI	Loading Efficiency ($\mu\text{g}/\text{mg}$)	Encapsulation Efficiency (%)
Blank NPs	75 ± 1	65 ± 1	0.073	-	-
DOX-NPs	81 ± 4	62 ± 3	0.094	71.3 ± 4.7	42.8 ± 2.8
NR-NPs	80 ± 8	63 ± 2	0.106	3.4 ± 0.4	34.4 ± 4.0
DiR-NPs	83 ± 1	69 ± 1	0.133	3.1 ± 0.3	86.4 ± 8.4
Anti-CD19 Blank NPs	82 ± 1	68 ± 1	0.145	-	-
Anti-CD19 DOX-NPs	83 ± 1	69 ± 1	0.139	72.1 ± 6.4	45.4 ± 2.1
Anti-CD19 NR-NPs	88 ± 1	75 ± 3	0.068	3.5 ± 0.1	35.3 ± 1.0
Anti-CD19 DiR-NPs	88 ± 1	73 ± 1	0.137	3.2 ± 0.4	89.1 ± 11.1

Protein assays showed that an average of $8.2 \pm 1.2 \mu\text{g}$ of avidin was immobilized onto 1 mg of NPs. The targeting Abs were anchored on the avidin-PA-NPs through the strong binding between the biotinylated Ab and avidin. Quantification of the surface density of biotinylated anti-CD19Abs by immunoblot

analysis revealed approximately 120 ng (77×10^{10} molecules) of anti-CD19Ab per mg of NPs or approximately 3 Ab molecules/NP. (Figure 3.1 and Appendix B.1).

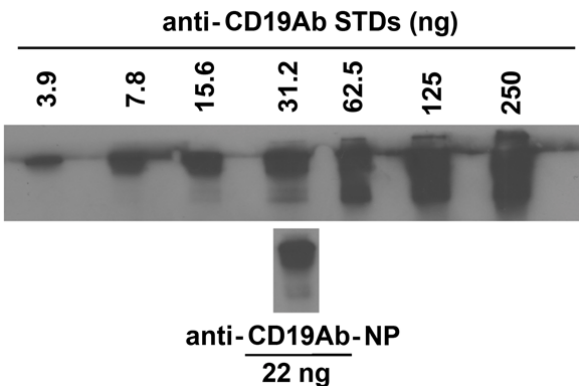


Figure 3.1. A representative immunoblot used to quantify biotinylated anti-CD19Ab levels on NPs.

3.3.2 Drug/dye loading and release:

DOX was efficiently entrapped in the polymeric NPs with a loading content and encapsulation efficiency of 71.3 ± 4.7 $\mu\text{g}/\text{mg}$ and 42.8 ± 2.8 % for non-targeted-NPs, and of 72.1 ± 6.4 $\mu\text{g}/\text{mg}$ and 45.4 ± 2.1 % for targeted-NPs, respectively (Table 3.1). *In vitro* release was evaluated by incubating targeted or non-targeted DOX-NPs in PBS under sink conditions at 37°C for up to 7 days. For non-targeted NPs, an average of 18.5 ± 2.7 wt% of DOX was released per day from day 0 to day 3, and a slower DOX release rate of 8.4 ± 4.8 wt% per day was obtained from day 3 to day 7. By day 7, a total of 88.9 ± 4.8 wt% of the initially loaded DOX was released. The release rate of DOX from targeted-NPs was estimated as 15.8 ± 2.2 wt% and 12.2 ± 2.7 wt% from day 0 to day 3 and day3 to day 7, respectively (Figure 3.2).

Separately, the loading content and encapsulation efficiency for NR in non-targeted NPs were quantified as 3.4 ± 0.4 $\mu\text{g}/\text{mg}$ and 34.4 ± 4.0 %, respectively; and for DiR loaded non-targeted NPs, those values were 3.1 ± 0.3 $\mu\text{g}/\text{mg}$ and 86.4 ± 8.4 %, respectively. The loading content and encapsulation efficiency of the dyes in targeted-NPs were similar to that in the non-targeted ones (Table 3.1). The release profiles revealed limited dye release (equal or less than 10 wt%) by day 7 from both the non-targeted and targeted NPs (Figure 3.2).

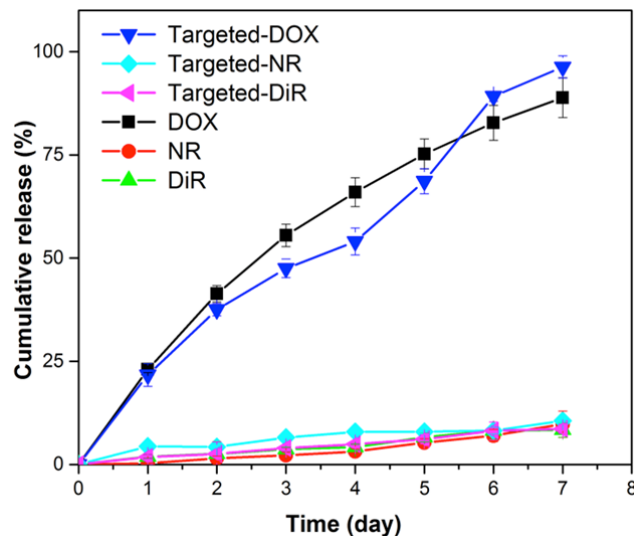


Figure 3.2. *In vitro* release profiles of: DOX (black - targeted; blue - non-targeted), NR (turquoise - targeted; red - non-targeted), and DiR (pink - targeted; bright green - non-targeted) from NPs in PBS (pH 7.4) at 37°C. Data shown are averages of three independent experiments.

This could be attributed to the strong hydrophobicity of the dyes (98, 99). The high retention of the hydrophobic fluorescent probes by NPs demonstrates the feasibility to use NR and DiR to track the location of NPs without undesirable dye leaking concerns.

3.3.3 CD19-specific targeting and uptake of anti-CD19Ab-conjugated NPs:

The ability of CD19-NPs to function as a targeted drug delivery system was examined by comparing uptake of particles by the cell lines REH and RS4;11, two B-ALL cell lines that express different levels of CD19. Immunoblot analysis revealed that RS4;11 cells express approximately 3 times as much CD19 protein than REH cells (Figures 3.3A and B). Flow cytometry confirmed enhanced cell surface expression of CD19 in RS4;11 cells (Figure 3.3C). These cell lines were then utilized to characterize the CD19-specific targeting of NPs.

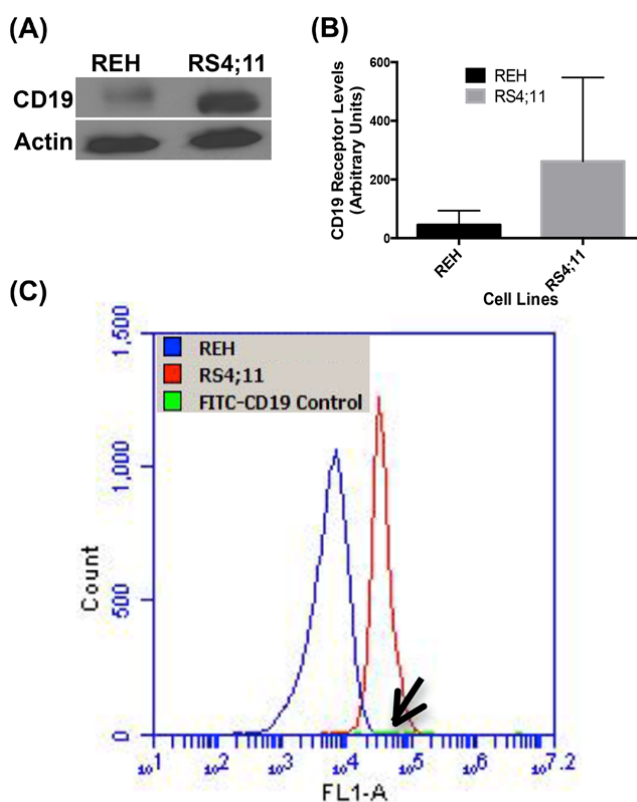


Figure 3.3. Quantification of CD19 total and surface expression levels in REH and RS4;11 B-ALL cells: (A and B) Immunoblot and quantification of the CD19 levels. (C) Flow cytometry analysis of surface levels of CD19 (Note FITC-(anti-CD19Ab) control, arrow).

Cell binding and uptake studies with REH and RS4;11 leukemia cells were performed using Nile red (NR) encapsulated NPs that were either non-targeted (NR-NPs) or conjugated with an irrelevant isotype control IgG (IgG-NR-NPs) or anti-CD19Abs (CD19-NR-NPs). CLSM imaging revealed that uptake levels of CD19-NR-NPs were more than 5-times in RS4;11 cells than in REH cells ($P=0.0076$, Figure 3.4A upper panels, and 3.4B, left bars). Interestingly, the uptake of NR-NPs in REH cell line was significantly higher than RS4;11 cells ($P=0.03$) indicating that CD19 targeting reduces the non-specific uptake. (Figure 3.4A lower panels and 3.4B right bars). No uptake was observed for IgG-NR-NPs (Figure 3.4C). This could be attributed to the highly negative zeta potential of IgG-conjugated NPs. These data show that the anti-CD19Ab-conjugated NPs were taken up by a CD19-dependent uptake mechanism.

3.3.4 Competition assays confirmed specific binding and uptake of anti-CD19Ab-conjugated NPs:

A competition assay was conducted to confirm the CD19-specific uptake of targeted NPs. RS4;11 cells were pre-incubated with excess of free anti-CD19Abs or free irrelevant isotype matched IgG for 30min at 4°C prior to treatment with CD19-NR-NPs. CLSM imaging showed that pre-treatment with free anti-CD19Abs reduced uptake of CD19-NR-NPs in RS4;11 cells but that pre-incubation with excess control IgG does not (Figure 3.4D, upper panels), confirming CD19-specific uptake of the targeted NPs. There was no background fluorescence either in free anti-CD19Ab or irrelevant IgG treated cells (Figure 3.4D, lower panels).

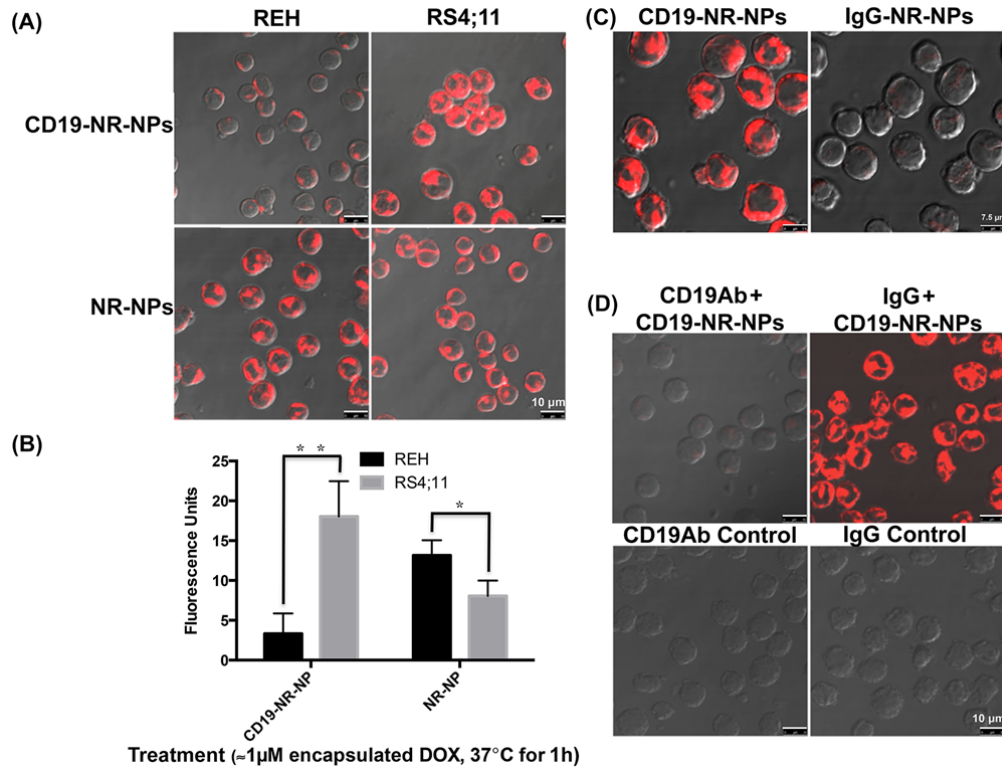


Figure 3.4. CD19 specific targeting and uptake of anti-CD19Ab conjugated NPs: (A) CLSM analysis to compare uptake of CD19-NR-NPs and NR-NPs (final concentration $\approx 1\mu\text{M}$ of encapsulated DOX) in REH and RS4;11 cells for 1h at 37°C . The uptake pattern was similar at 5min. Note that even after 1h exposure, REH cells shows minimal uptake. Scale bar, 10 μm . (B) Quantification of cell uptake levels of CD19-NR-NPs and NR-NPs in REH and RS4;11 cells. (C) CLSM analysis to compare uptake of CD19-NR-NPs with isotype matched non-specific uptake of IgG-NR-NPs (final concentration $\approx 1\mu\text{M}$ of encapsulated DOX) in RS4;11 cells for 1h at 37°C . Scale bar, 7.5 μm . (D). CLSM analysis to confirm CD19 dependent uptake of CD19-NR-NPs (final concentration $\approx 1\mu\text{M}$ of encapsulated DOX) in RS4;11 cells for 1h at 37°C . Scale bar, 10 μm .

3.3.5 Analysis of endocytic mechanism for anti-CD19Ab-conjugated NPs:

To investigate the mechanism of uptake of CD19-NPs in CD19(+) RS4;11 cells, the effect of various endocytic pathway inhibitors was analyzed. Compared to Nystatin (caveolae-mediated endocytic inhibitor, (151) or A-Hcl (a

macropinocytosis inhibitor, (151), sucrose (clathrin-mediated endocytic inhibitor) (150), inhibited uptake of CD19-NR-NP (Figure 3.5A). In addition, FITC-Tf (a well-established marker for clathrin-mediated endocytosis), (152), colocalized with CD19-NR-NPs (Figure 3.5B), demonstrating that anti-CD19Ab-conjugated NPs are internalized primarily into endosomes via clathrin-dependent endocytosis.

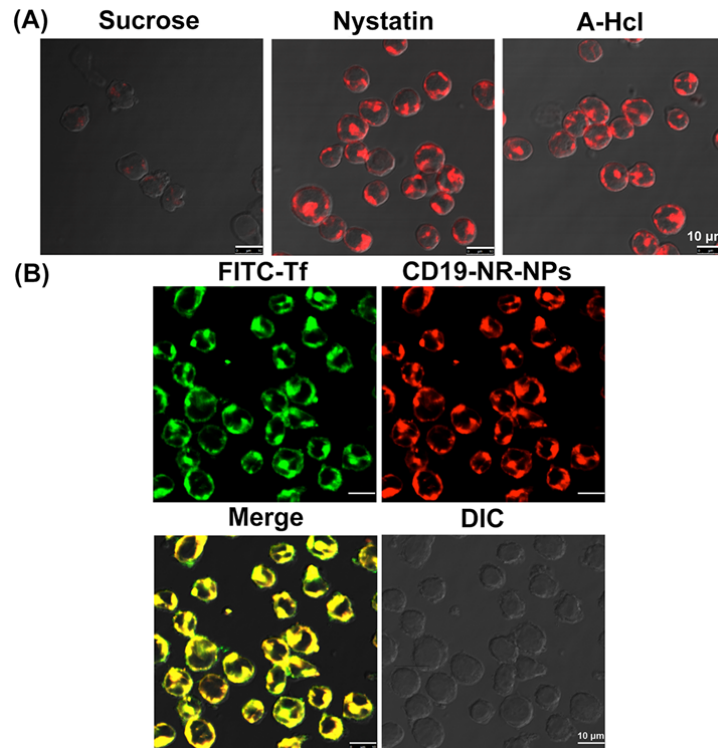


Figure 3.5. Analysis of endocytic mechanism for anti-CD19Ab conjugated NPs: (A) Inhibiting clathrin-mediated uptake of CD19-NR-NPs (final concentration $\approx 1\mu\text{M}$ of encapsulated DOX) in RS4;11 cells for 30 min at 37°C . Scale bar, 10 μm . (B) Colocalization of FITC-transferrin and CD19-NR-NPs in RS4;11 cells. Scale bar, 10 μm .

3.3.6 CD19-mediated induction of apoptosis in leukemia cells:

After confirming CD19-mediated internalization of NPs, we investigated whether DOX loaded targeted NPs induce CD19-dependent cytotoxicity. For this purpose, cells were incubated with free DOX or CD19-DOX-NPs for 1h, washed to remove the excess drug present in the media and incubated for an additional 72h in drug free medium. REH cells were more sensitive to free DOX than RS4;11 cells. In contrast, the latter cells were even more sensitive to CD19-DOX-NPs while 95% REH cells remained viable when treated with the targeted NPs (Figure 3.6A).

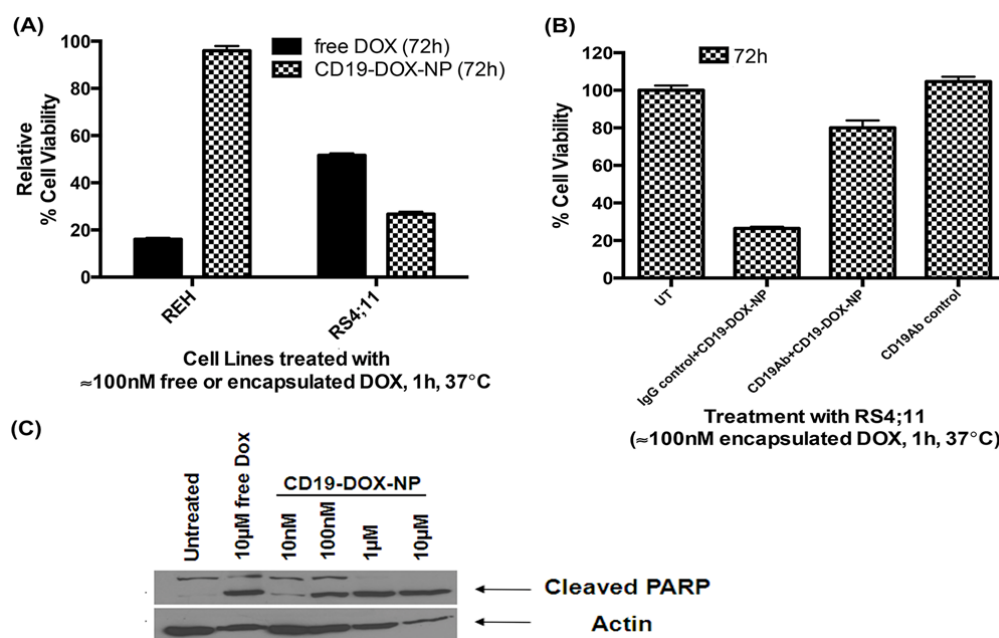


Figure 3.6. CD19-mediated induction of apoptosis in leukemia cells: (A) Comparison of toxicity induced by free DOX, and CD19-DOX-NPs ($\approx 100\text{nM}$ DOX) in REH and RS4;11 cells. (B) Competition assay to confirm CD19-receptor dependent induction of toxicity by CD19-DOX-NPs ($\approx 100\text{nM}$ DOX) in RS4;11 cells. (Data indicated as mean \pm SEM). (C) Dose-dependent cleaved PARP levels due to treatment of CD19-DOX-NPs with RS4;11 cells (48h).

To confirm that selective toxicity is induced via the CD19-mediated uptake of CD19-DOX-NPs, competition experiments were performed by pre-incubating RS4;11 cells with excess of free irrelevant isotype matched IgG or free anti-CD19Abs for 30min at 4°C prior to treatment with CD19-DOX-NPs. Pretreatment with control IgG had not significant effect on toxicity of the CD19-DOX-NPs, but pretreatment with free anti-CD19Ab caused a 54% increase in cell viability (Figure 3.6B). It is therefore possible to conclude that induction of selective toxicity is mediated via the CD19. Furthermore, CD19-DOX-NPs induced dose-dependent cleavage of PARP (Figure 3.6C), in RS4;11 cells indicating apoptotic cell death. Taken together, the results validate that CD19-NPs can specifically deliver DOX and induce cytotoxicity in cells that express high levels of CD19.

3.3.7 CD19 targeting increases the cell-associated DOX (intracellular and cell surface bound) levels in RS4;11 cells:

Treatment with DOX (1 and 10 μ M) reduced viability in RS4;11 and REH irrespective of the method of delivery (Figures 3.7 and 3.8). However, CD19-DOX-NPs (\approx 100nM DOX) reduced the viability of RS4;11 but not REH cells (Figure 3.6A). Reduced uptake of CD19-targeted NPs in REH cells should reduce levels of cell associated DOX (caDOX) and as a consequence have a reduced effect on viability of these cells. To test this possibility, REH and RS4;11 cell lines were treated with increasing doses of free DOX and CD19-DOX-NPs (\approx 100nM, 1 μ M, 10 μ M DOX) and quantified caDOX levels using HPLC/MS/MS (Figure 3.9A).

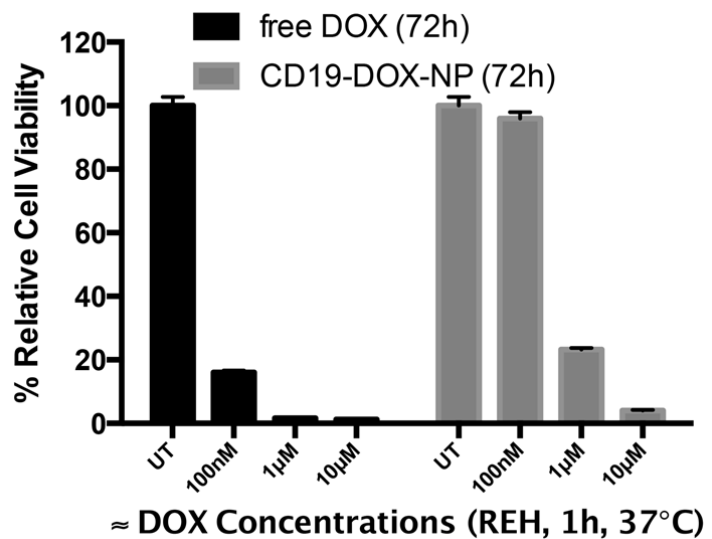


Figure 3.7. Treatment of REH cells with free DOX or CD19-DOX-NPs (\approx 100nM, 1 μ M or 10 μ M DOX) for 1h at 37°C. CD19-DOX-NPs did not affect the cell viability at 100nM DOX, but reduced the viability at higher concentrations of 1 and 10 μ M DOX.

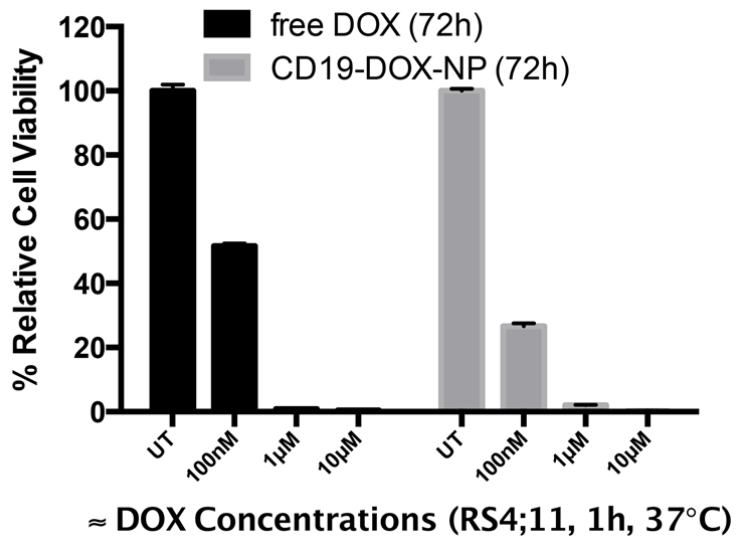


Figure 3.8. Treatment of RS4;11 cells with free DOX or CD19-DOX-NPs (\approx 100nM, 1 μ M or 10 μ M DOX) for 1h at 37°C. CD19-DOX-NPs reduced the cell viability at all concentrations of DOX.

The caDOX levels in free DOX treated REH and RS4;11 cells were similar (Figure 3.9B). By contrast, in CD19-DOX-NPs treated cells, the caDOX levels in RS4;11 cells was 4-10 times higher than in REH cells (Figure 3.9C). These results indicate that specific targeting of NPs via CD19 results in elevation of caDOX to levels that can cause loss of viability in RS4;11 cells. It is also noteworthy that at the same doses of DOX, caDOX levels in RS4;11 cells were not very different on treatment with targeted NPs compared to free DOX (Figure 3.10). However, the caDOX levels in free DOX treated REH cells are an order of magnitude higher than the targeted NPs treated cells (Figure 3.11).

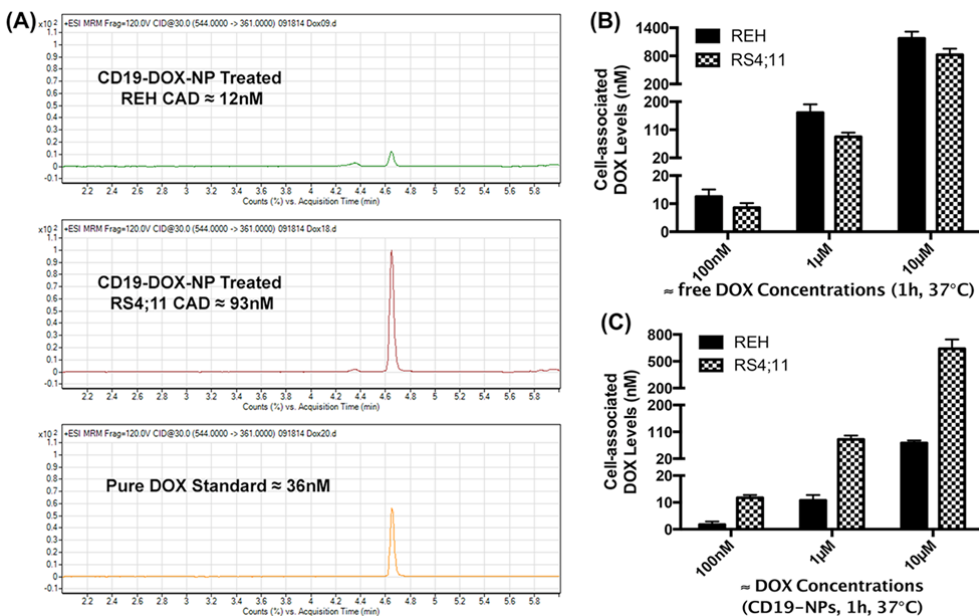


Figure 3.9. CD19-targeting increases the cell associated DOX (intracellular and cell surface bound, caDOX) levels in RS4;11 cells: (A) HPLC/MS/MS representative quantitation of caDOX levels in REH and RS4;11 cells treated with CD19-DOX-NPs ($\approx 1\mu\text{M}$ DOX, for 1h at 37°C). (B) REH and RS4;11 caDOX levels on treatment with free DOX for 1h at 37°C . (C) REH and RS4;11 caDOX levels on treatment with CD19-DOX-NPs for 1h at 37°C .

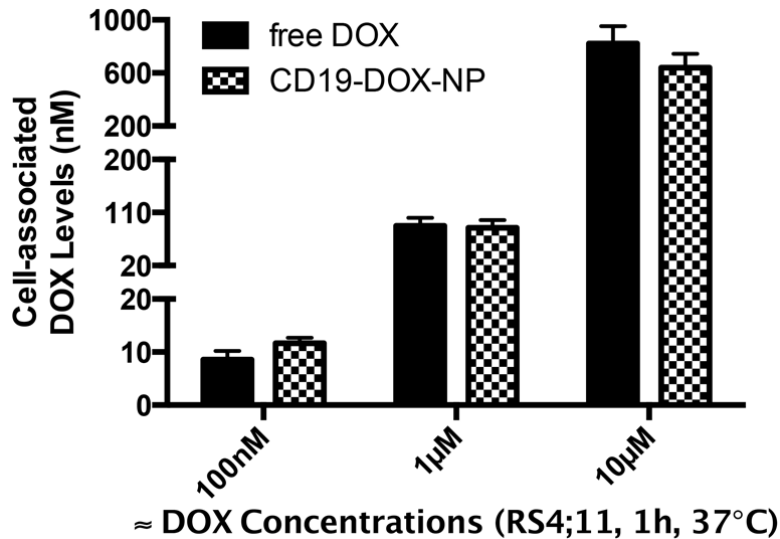


Figure 3.10. CD19-targeting achieves similar cell associated DOX (intracellular and cell surface bound, caDOX) levels in RS4;11 cells: RS4;11 caDOX levels on treatment with free DOX or CD19-DOX-NPs (\approx 100nM, 1 μ M or 10 μ M DOX) for 1h at 37°C.

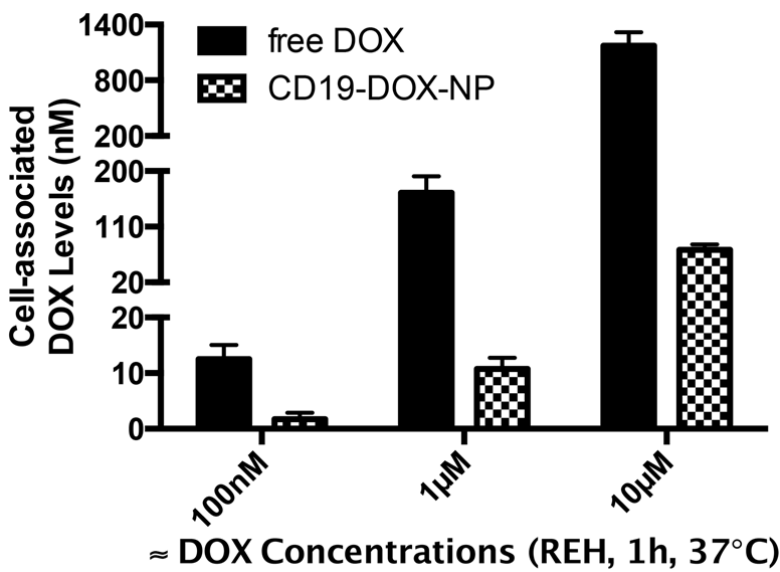


Figure 3.11. CD19-targeting reduces the cell associated DOX (intracellular and cell surface bound, caDOX) levels in REH cells: REH caDOX levels on treatment with free DOX or CD19-DOX-NPs (\approx 100nM, 1 μ M or 10 μ M DOX) for 1h at 37°C.

3.3.8 Plasma levels and biodistribution of anti-CD19Ab-conjugated NPs in mice:

In order to evaluate plasma levels of CD19-DiR-NPs, peripheral blood samples drawn from mice at various time points were assessed for “DiR” fluorescence levels. Soon after the tail vein injection of NPs, there was an initial spike in the plasma at 5min, which then dropped and sustained in circulation for approximately 8h only to further drop at 12h and 24h. (Figure 3.12A).

To assess tissue distribution levels, BALB/c mice injected via the tail vein with CD19-DiR-NPs (2.5mg/kg DOX) were euthanized at different time points to harvest liver, spleen, heart, lung, kidney and brain. Six hours after treatment, CD19-DiR-NP fluorescence was primarily detected in liver and spleen with lower levels in kidney, lung and heart. Levels increased at 12h and then slowly declined over the next 4 weeks (Figure 3.12B).

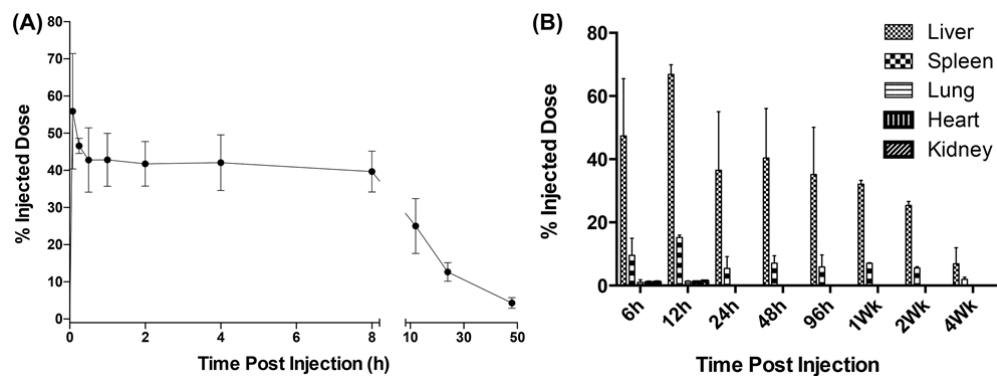
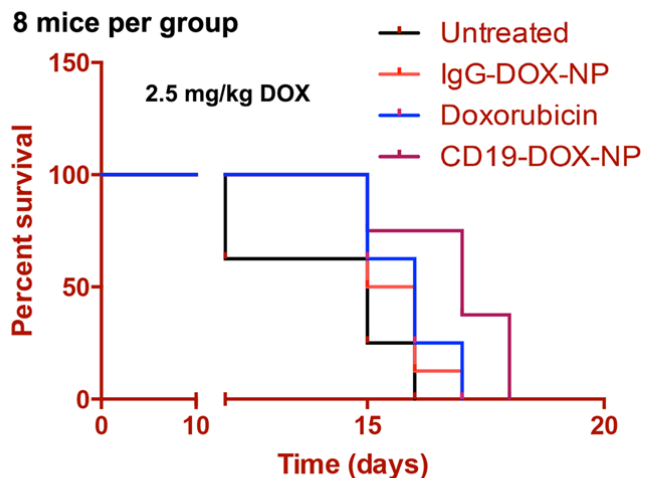


Figure 3.12. Plasma levels and biodistribution of anti-CD19Ab conjugated NPs in mice. (A) Plasma distribution of CD19-DiR-NPs in BALB/c mice. (B) Biodistribution and clearance of CD19-DiR-NPs in mice.

3.3.9 CD19-DOX-NPs Enhance Therapeutic Efficacy in a Pre-clinical Mouse Model of ALL:

To test the *in vivo* efficacy of CD19-DOX-NPs, an ALL human xenograft model, developed in NSG-B2m mice, received intraperitoneal injections at 2.5 mg/kg DOX once a week. The mice were randomized into four groups (8/group) to receive saline, free DOX, IgG-DOX-NPs, or CD19-DOX-NPs. Kaplan-Meier survival curves showed that mice that received CD19-DOX-NPs survived significantly longer than those treated with saline ($P = 0.0021$) or the group treated with free DOX ($P = 0.0369$) or IgG-DOX-NPs ($P = 0.0163$) (Figure 3.13).



"Log-rank (Mantel-Cox) Test"

P value = 0.0369 between DOX and CD19-DOX-NP,
 P value = 0.0163 between IgG-DOX-NP and CD19-DOX-NP,
 P value = 0.1006 between Untreated and IgG-DOX-NP,
 P value = 0.0404 between Untreated and DOX,
 P value = 0.0021 between Untreated and CD19-DOX-NP

Figure 3.13. CD19-DOX-NPs enhance therapeutic efficacy and prolongs survival in pre-clinical leukemia mouse models. Efficacy of CD19-DOX-NPs in xenograft model of ALL. (Survival rate is presented in a Kaplan-Meier plot). CD19-DOX-NPs (\approx 2.5 mg/kg DOX) significantly prolonged survival in comparison with groups treated with saline, IgG-DOX-NPs and free DOX (\approx 2.5 mg/kg DOX). This highlights the therapeutic efficacy of CD19-DOX-NP formulations *in vivo*.

During the survival study, the agility of different groups of treated mice were also monitored using a computerized low profile wireless running wheel. Interestingly, the group that received CD19-DOX-NPs manifested increased agility (an indirect measure of the degree of sickness) in comparison with the other groups during the treatment (Figure 3.14).

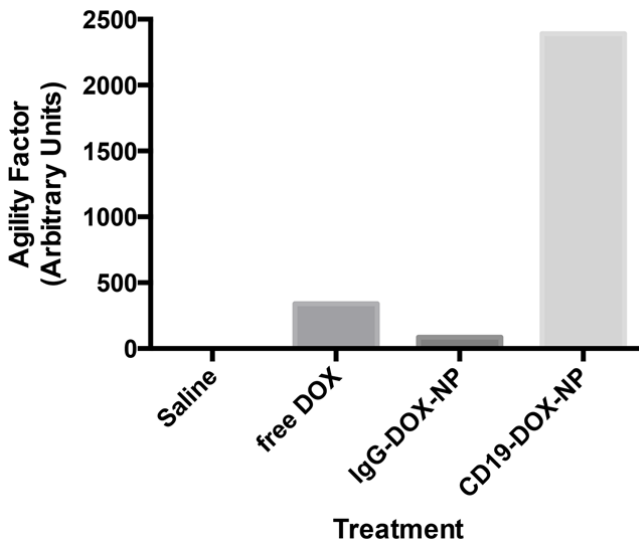


Figure 3.14. CD19-DOX-NPs maintained high agility factor in leukemic mice: Agility Factor (normalized to saline) = no. of wheel rotations on day 15 ÷ no. of wheel rotations on day 1. CD19-DOX-NPs (≈ 2.5 mg/kg DOX) maintained a high agility factor in comparison with groups treated with saline, IgG-DOX-NPs and free DOX (≈ 2.5 mg/kg DOX). This indicates reduced apparent systemic toxicity in leukemic mice treated with CD19-DOX-NPs.

3.4 Discussion

Nanoparticle (NP) based targeted drug delivery has a promising future in medicine due to its multiple applications in cancer treatment: it can improve the half-life of drugs, reduce dosage, improve drug solubility, reduce immunogenicity and minimize non-specific exposure of toxic drugs. While many of these applications have advanced for solid tumors, targeted delivery approaches are minimally developed for blood cancers especially in childhood leukemia. In this study, amphilic block copolymer NPs with anti-CD19Abs (CD19-NPs) as a targeting moiety were utilized to deliver DOX specifically to ALL cells. It is demonstrated that the targeting of DOX to ALL cells and its induction of cytotoxicity is mediated in a CD19-dependent manner. It is also shown that CD19-

NPs were internalized rapidly in a clathrin-dependent manner resulting in elevated levels of DOX only in targeted cells. The results further show that CD19-DOX-NPs treated leukemic mice survived longer and manifested higher degree of agility indicating reduced apparent systemic toxicity compared to mice treated with free DOX. This is the first time CD19-targeted polymeric NPs have been utilized in preclinical studies to show advantages over conventional chemotherapy in childhood acute leukemia. Based on these observations, it could be suggested that targeted drug delivery for liquid tumors such as ALL may be advantageous due to the ease of access to tumor cells, unlike solid tumors where targeting is complex on account of multiple physical barriers that NPs have to overcome (153).

In Chapter 2, it was shown that NPs formulated from amphiphilic block copolymers consisting of hydrophilic poly(ethylene glycol) (PEG) and hydrophobic polyester bearing pendent cyclic ketal groups efficiently encapsulated dexamethasone which is comparable to values other platforms have achieved (96, 97). The incorporation of pendent cyclic ketal groups on the hydrophobic portion on the polymer backbone increased the chain flexibility while decreasing polymer crystallinity which improved the drug loading capacity and its release profile. To immobilize the targeting moiety, avidin was chemically modified with a fatty acid (i.e. palmitic acid), and then incorporated onto the surface of NPs during the nanoprecipitation process. The palmitic acid preferentially partitions within the hydrophobic core of NPs, and the hydrophilic avidin head group is displayed on the particle surface along with the mPEG segments. Biotinylated Abs were then linked to the NP surface via the anchored avidin. A similar approach has been

reported previously with regards to incorporating avidin-fatty acid conjugates onto poly (lactic-co-glycolic acid) (PLGA) microspheres (154). It is further demonstrated that the fatty acid modified avidin can be efficiently anchored onto the surface of NPs, exhibiting an average surface modification efficiency of 8.2 µg avidin per mg of NPs. Subsequently, biotinylated anti-CD19Abs were linked onto the surface of the avidin-PA-NPs. An encapsulation efficiency of about 45% was achieved for DOX, irrespective of the presence or absence of avidin in NPs, indicating that addition of avidin does not compromise the encapsulation efficiency of DOX. In addition, the *in vitro* release profiles revealed that incorporation of avidin did not affect the release kinetics of DOX from the NPs.

One of the most important characterization studies of targeted NPs is validation of target specificity. Multiple approaches were utilized to confirm the specific targeting of CD19-targeted NPs: 1. RS4;11 cells that have higher expression levels of CD19 than REH cells showed more rapid uptake of CD19-NPs. 2. Uptake of IgG-NPs by RS4;11 cells was much lower than uptake of CD19-NPs. 3. Pre-incubation of RS4;11 cells with free anti-CD19Abs almost completely blocked the uptake of CD19-NPs. 4. Viability of RS4;11 cells was significantly reduced when treated with CD19-NPs containing 100nM of encapsulated DOX, but REH cells were unaffected. 5. Free anti-CD19Abs significantly blocked the toxicity of CD19-DOX-NPs in RS4;11 cells. 6. caDOX levels in RS4; 11 cells treated with CD19-DOX-NPs at 100nM of encapsulated DOX was 4-fold higher than in REH cells. Taken together, these results demonstrate that DOX is delivered in a CD19-dependent manner into CD19(+) leukemia cells.

Free hydrophobic drugs enter the cells via diffusion across the plasma membrane. By contrast, NP mediated drug delivery utilizes the cellular internalization machinery to deliver drugs into the cells. Internalization mechanisms include macropinocytosis, caveolae, and clathrin-dependent endocytosis (155). The results in this study show that CD19-NPs are internalized into endosomes of RS4;11 cells by a clathrin-dependent mechanism, demonstrated by inhibition of uptake by sucrose and co-localization with FITC-transferrin – a clathrin-dependent endocytic marker. Clathrin-dependent uptake results in rapid drug accumulation within the cells due to increased uptake of NPs. The number of NPs internalized within RS4;11 cells are 6 times more than the number of particles internalized within REH cells (Appendix B.2). Determination of the caDOX levels by HPLC/MS/MS indicated how much DOX is needed to induce cytotoxicity. caDOX levels in free DOX and CD19-DOX-NPs treated RS4;11 cells were comparable (Figure 3.10). However, caDOX levels in REH cells treated with free DOX were more than 6-fold higher than the CD19-DOX-NPs treated cells (Figure 3.11). These results show that delivery of DOX into cells expressing high levels of CD19 by endocytosis of targeted NPs is as efficient as free DOX and that the targeted NPs enhance selectivity for targeting of DOX to such cells.

Previously, in Chapter 2, the plasma levels of 110 nm diameter ECT2-NPs were stable for up to 2h compared to the 8h stability seen in this section for the smaller 80 nm diameter CD19-NPs. This is consistent with literature data showing better plasma profiles for smaller particles (134, 156, 157). *In vivo* studies demonstrated that survival of mice treated with CD19-DOX-NPs was significantly

better than untreated mice ($P = 0.0021$), free DOX treated mice ($P = 0.0369$) and IgG-DOX-NP treated mice ($P = 0.0163$).

The control mice in this study lived 15 days compared to the 27 days in the previous study in Chapter 1. We attribute this to the injected cells going through an exponential growth phase which could have led to the tumor's accelerated growth *in vivo*. In this severe model of ALL, therapeutic efficacy of all three treatments was limited, but increased agility in leukemic mice treated with CD19-DOX-NPs does provide proof-of-concept that such drug formulations can be effective against ALL and reduce systemic toxicity usually caused by the non-specific exposure to DOX. The *in vitro* data indicated that drug delivery of targeted NPs would be more specific than free DOX for leukemia cells than cells that do not express high levels of CD19. Consequently, the targeted NPs would be expected to be less toxic to other cells in animals. A larger toxicity study however, is required to determine whether the targeted NPs are safer than free DOX.

3.5 Conclusion

Results of this study demonstrate the potential for targeted NPs to selectively deliver drugs that can be effective against ALL. These encouraging results should lead to future studies that examine increased safety profiles of these drug formulations, particularly in relation to non-specific effects on other organs and tissues. Non-specific effects are of particular concern for pediatric ALL where non-targeted cytotoxic drugs can cause life-long problems for treated patients.

Chapter 4

CONCLUSIONS AND FUTURE WORK

4.1 Conclusions

The overall goal of this dissertation work is to engineer and advance preclinically a novel polymeric based nanotherapeutic approach that can target and treat pediatric acute lymphoblastic leukemia (ALL) with increased therapeutic efficacy and minimal treatment-related toxicity.

In the first part of this dissertation, amphiphilic block copolymers (number-average molecular weight, Mn of 64.2 kDa) consisting of hydrophilic polyether (polyethylene glycol, PEG) and hydrophobic polyester (poly (ϵ -caprolactone), PCL) bearing pendant cyclic ketals were synthesized by multi-step chemical transformations. Polymeric nanoparticles (NPs) with an average diameter of 110 nm were assembled from these block copolymers to form a core-shell architecture comprising a segregated PCL core for payload encapsulation and a sterically stabilized PEG shell for conjugating leukemia cell-specific targeting moieties such as CD19 as demonstrated in this study. The drug (dexamethasone, Dex) or fluorescent-dyes (Nile-red, NR; DilC18(7) tricarbocyanine probe, DiR) were encapsulated within these NPs by a nanoprecipitation method. Dynamic light scattering analysis revealed a narrow size distribution for all nanoformulations. The blank-NPs were non-toxic to cultured cells, non-hemolytic with human blood and safe to be administered to mice. Further, it was established that administering

Dex as a nanodrug significantly improved survival and dramatically reduced disease symptoms in leukemic mice at one-third the dose used for the drug in its conventional form.

Subsequently, an advanced generation of targeted nanocarriers based on (doxorubicin:DOX, NR and DiR) with an average diameter of 80 nm were formulated from similar PEG-PECL block copolymers (Mn of 39 kDa) bearing pendant cyclic ketals and validated for specific delivery and induction of cytotoxicity in leukemia therapy. The drug doxorubicin was used in this section due to its greater potency than dexamethasone. Targeting ligands against CD19 receptors that are expressed explicitly on B-cell leukemia cells and are absent on hematopoietic stem cells were conjugated by incorporating fatty acid modified avidin on the outer shell of NPs. Biotinylated antibodies targeting CD19 or control biotinylated IgGs were immobilized on NPs (CD19-NPs or IgG-NPs) by utilizing these fatty acid-avidin conjugates. Multiple approaches such as competition assays, inhibitor studies, and HPLC/MS/MS were utilized to validate target specific drug delivery and induction of cytotoxicity in leukemia cells by CD19-DOX-NPs. The CD19-targeted NPs delivered DOX specifically to CD19(+) leukemic cells and induced cytotoxicity in a receptor-dependent manner via clathrin-mediated endocytosis. Further, the CD19-targeted NPs achieved elevated levels of cellular DOX in CD19(+) leukemic cells in contrast to non-targeted CD19(-) cells. In a pre-clinical model of leukemia, the CD19- targeted NPs significantly improved the survival and the quality of life indicating reduced apparent systemic toxicity. In this dissertation, we successfully demonstrate the efficacy of polymeric

nanoparticles to achieve specific delivery of conventional chemotherapy in treating childhood acute leukemia. The nanoformulations developed in this study should act as a platform for further development and advance drug delivery systems that enhance drug efficacy and reduce treatment-related toxicity in pediatric oncology.

4.2 Future Work***

Advances in nanotechnology for drug delivery have resulted in pharmaceutical formulations that effectively combat adult cancers. As outlined in Tables 1.2 and 1.3 in Chapter 1, the clinical impact of nanotherapeutics in adults is evident. Though nanoformulations for treating adult leukemia have evolved; minimal research has been performed to develop innovative therapeutic strategies for pediatric leukemia. Pediatric nanomedicine is still in its infancy and well-designed pre-clinical and clinical trials are essential to advance the development of novel systems that treat any form of childhood malignancy.

This dissertation work describes the proof of principle for engineering and preclinical development of NP-based targeted drug delivery system to treat ALL in children. The polymeric NPs can be used to achieve efficient encapsulation and extended release of chemotherapeutic agents such as Dex and DOX. Incorporation of targeting moieties such as anti-CD19Ab onto the NP surface can lead to specific and accelerated uptake of particles in CD19(+) leukemic cells. This could result in enhanced therapeutic efficacy and reduced systemic toxicity in children treated for

***Reprinted (adapted) with permission from
(<http://onlinelibrary.wiley.com/doi/10.1038/clpt.2013.174/abstract>), *Clinical Pharmacology & Therapeutics*, 2014, 95 (2), pp 168–78). © 2014 American Society for Clinical Pharmacology and Therapeutics

leukemia. However, there are limitations associated with the current study and potential areas to be explored while advancing this technology into future are described below.

4.2.1 Nanomaterials Design and Characterization for ‘ALL’ Therapy

4.2.1.1 Size and Shape of Nanocarriers:

A distinct difference in the plasma half-life and time for organ clearance of NPs was observed in this study. It is well known that size and shape of NPs significantly affects the organ biodistribution pattern and plasma half-life of drug carriers (158-162). It would be vital to ensure that NPs circulate in the blood so long as to eliminate leukemic blasts in circulation and target those that reside in specialized sites such as the bone marrow, the CNS and the testicular region without harming normal lymphocytes or hematopoietic stem cells. A detailed study focusing on size and shape of nanocarriers and their preferred site-based accumulation in leukemic preclinical models should be performed in order to gain insights into the effect of these factors in ALL therapy. The EPR effect appears to benefit NPs based-drug delivery for solid tumors (160). However, for liquid tumors such as leukemia, the EPR effect is irrelevant. Distinct mechanisms might be involved in targeting tumors via EPR and non-EPR mechanisms. Ligand based targeting of leukemic cells may be advantageous for treatment of childhood leukemia. Future studies in this direction should allow the development of novel therapeutic applications for children and possibly for adults with leukemia.

4.2.1.2 Blood Half-life of Nanocarriers

It is well known that longer half-lives of drug delivery systems are beneficial for solid tumor treatment. This attributes to the multiple barriers NPs have to overcome to reach the tumor site (82). Drug-encapsulated NPs with shorter half-lives are rapidly eliminated from systemic circulation, diminishing the efficacy. Intravenous treatment of hematological malignancies ensures instant contact of nanocarriers with malignant cells in the blood and delivers drugs directly to the target. However, NPs with longer half-lives might be necessary to target leukemic cells in the bone marrow, CNS and testicles. Thus NPs with differential half-lives could be beneficial to treat ALL. Future studies focused on NPs with differential half-lives are necessary to maximize the efficacy of nanotherapeutics for treatment of ALL.

4.2.1.3 Active Targeting of Nanocarriers to Leukemic Cells

Active targeting of nanocarriers involve inclusion of ligands, antibodies or other aptamers that bind to a specific receptor or other binding partner on the target cell-membrane to facilitate cell uptake. Although the targeting moieties are expressed on the leukemic cell-surface in most ALL patients, there may be individual variations in the expression pattern of these receptors or membrane proteins that favor one of the moieties for a sub-set of patients. The expression pattern of the antigens may be influenced by the tumor-cell lineage and the stage of differentiation. Hence, it is essential to screen patients for the expression of targeting moieties by the leukemic cells and ensure the selection of an appropriate targeted nanocarrier for drug delivery by screening NP libraries (163). This will

form the foundation for a new clinical approach of “personalized nanotherapeutics” designed to enhance success of targeting and provide an effective treatment.

4.2.1.4 Drug Release Kinetics of Nanocarriers:

ALL is a rapidly progressing disease and drugs are instantly required to initiate its pharmacological activity to control leukemic cell proliferation. However, drug release outside the cells due to “burst-release” of encapsulated drugs may result in non-specific toxic effects on normal proliferating cells in children. Therefore, NPs with targeting ligands and pH-responsive traits that facilitate rapid uptake and instant delivery of drugs inside the leukemic cell are highly desirable. Although costly and time-consuming, systematic approaches to develop such NPs are worthwhile due to its enormous potential to reduce treatment-related side effects in children.

4.2.1.5 Mathematical Modeling:

Physiologically based pharmacokinetic (PBPK) modeling could aid the decision-making process to choose the appropriate size and shape of NPs while accounting for organ biodistribution and plasma retention times for ALL therapy. Such studies could help accounting for the total amount of NPs administered and the levels accumulated in various organs (164). Extrapolation of such studies from mice to human should further help to predict potential side effects of any particular formulations which would enable physicians to design an optimal treatment regimen with increased therapeutic efficacy and minimal toxicity.

4.2.1.6 Combinatorial Treatment Studies:

Current therapies to combat ALL require the use of multiple drugs given in combination. In this study, one or two low-level doses of a single drug was used to demonstrate efficacy in leukemic mice. It is also important to note that although controlled release was not sufficient to combat the rapidly progressing disease, the low dose of available drug reduced apparent systemic toxicity in mice treated with drug-encapsulated NPs. On this account, it may be ideal to further explore the utility of administering multiple drugs encapsulated within such controlled-release platforms or investigate the ability of nanodrugs with rapid drug-release kinetics to overcome the exponential rate at which this disease progresses.

4.3 Nanomedicine for Pediatric Leukemia – A Final Perspective

Results from Phase IIb clinical trials of CPX-351 - a liposomal system comprising of drugs used in childhood cancer treatments (Cytarabine and Daunorubicin) - revealed high response rates and reduction in 60-day mortality in adults receiving standard therapy for secondary acute myeloid leukemia (165). Encouragingly, liposomal vincristine sulfate (Marqibo®) has entered into Phase 1 clinical trials for pediatric ALL therapy (64). Marqibo® was recently approved by the FDA for treating a rare form of adult cancer (Ph- ALL) (62).

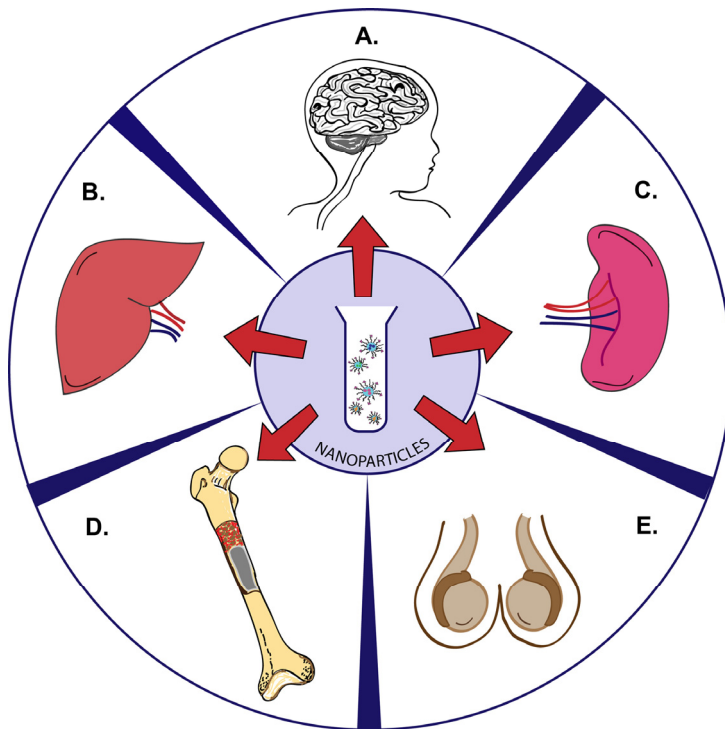


Figure 4.1. Nanoparticle design (size, shape and blood-half-life) requirements to target sites of leukemia-cell proliferation. (a and e) for brain and testicular region (b and c) for liver and spleen (d) for bone marrow.

Hematologic malignancies such as ALL enable extensive characterization of nanocarriers because of the ease of access to leukemic cells in the peripheral blood. Measurement of the percentage of leukemic cells in the blood is relatively simple; enabling rapid development of nanocarriers. These nanocarriers can be further optimized to target leukemic cells in more privileged locations such as the bone marrow, testicles or the CNS (Figure 4.1). Availability of nanocarriers that targets leukemia in the blood, bone marrow, testes and the CNS simultaneously as a single formulation should facilitate treatment of ALL in with minimal side effects (Figures 1.2 - Chapter 1 and 4.1). Achieving this goal requires systematic

approaches combined with long-term efforts and commitments by interdisciplinary biomedical researchers and clinicians.

A weekly dose regimen of a single drug was administered while evaluating the therapeutic efficacy of targeted nanodrugs in this study. The cost of mice, polymers and reagents (drugs and biotinylated antibodies) severely limited our ability to perform combinatorial treatment studies to validate targeted nanotherapy for ALL. Future studies performed in partnership with pharmaceutical companies should provide access to a larger budget. This should permit frequent dosing and testing of combinations of nanodrugs in ALL and could result in a stronger therapeutic effect that will reinforce the findings in this study. The targeted approach to therapy should limit long-term toxic side effects and enhance treatment efficacy by permitting increased doses of drugs to reach leukemic cells. Development of pediatric nanomedicine will bring us closer to the goal of eradicating childhood cancer.

REFERENCES

1. Facts 2012 - The Leukemia & Lymphoma Society. The Leukemia & Lymphoma Society Contract No.: December 3.
2. Mody R, Li S, Dover DC, Sallan S, Leisenring W, Oeffinger KC, et al. Twenty-five-year follow-up among survivors of childhood acute lymphoblastic leukemia: a report from the Childhood Cancer Survivor Study. *Blood*. 2008;111(12):5515-23.
3. Davis ME, Chen ZG, Shin DM. Nanoparticle therapeutics: an emerging treatment modality for cancer. *Nat Rev Drug Discov*. 2008;7(9):771-82.
4. Kamaly N, Xiao Z, Valencia PM, Radovic-Moreno AF, Farokhzad OC. Targeted polymeric therapeutic nanoparticles: design, development and clinical translation. *Chem Soc Rev*. 2012;41(7):2971-3010.
5. Henderson ES, Samaha RJ. Evidence that drugs in multiple combinations have materially advanced the treatment of human malignancies *Cancer Res*. 1969;29:2272-80.
6. DeVita VT. Principles of chemotherapy. In: DeVita VT HS, Rosenberg S, editor. *Principles and practice of oncology*. 3rd ed. Philadelphia, PA: JB Lippincott; 1989.
7. Stuart FA, Segal TY, Keady S. Adverse psychological effects of corticosteroids in children and adolescents. *Arch Dis Child*. 2005;90(5):500-6.
8. Von Hoff DD, Rozencweig M, Layard M, Slavik M, Muggia FM. Daunomycin-induced cardiotoxicity in children and adults. A review of 110 cases. *Am J Med*. 1977;62(2):200-8.
9. Lipshultz SE, Colan SD, Gelber RD, Perez-Atayde AR, Sallan SE, Sanders SP. Late cardiac effects of doxorubicin therapy for acute lymphoblastic leukemia in childhood. *N Engl J Med*. 1991;324(12):808-15.
10. Sandler SG, Tobin W, Henderson ES. Vincristine-induced neuropathy. A clinical study of fifty leukemic patients. *Neurology*. 1969;19(4):367-74.

11. Moe PJ, Holen A. High-dose methotrexate in childhood all. *Pediatr Hematol Oncol*. 2000;17(8):615-22.
12. Cheson BD. Infectious and immunosuppressive complications of purine analog therapy. *Journal of clinical oncology : official journal of the American Society of Clinical Oncology*. 1995;13(9):2431-48.
13. Baker WJ, Royer GL, Jr., Weiss RB. Cytarabine and neurologic toxicity. *Journal of clinical oncology : official journal of the American Society of Clinical Oncology*. 1991;9(4):679-93.
14. Thomas DA, Faderl S, Cortes J, O'Brien S, Giles FJ, Kornblau SM, et al. Treatment of Philadelphia chromosome-positive acute lymphocytic leukemia with hyper-CVAD and imatinib mesylate. *Blood*. 2004;103(12):4396-407.
15. Muller HJ, Boos J. Use of L-asparaginase in childhood ALL. *Crit Rev Oncol Hematol*. 1998;28(2):97-113.
16. Kellie SJ, Crist WM, Pui CH, Crone ME, Fairclough DL, Rodman JH, et al. Hypersensitivity reactions to epipodophyllotoxins in children with acute lymphoblastic leukemia. *Cancer*. 1991;67(4):1070-5.
17. Bradshaw DM, Arceci RJ. Clinical relevance of transmembrane drug efflux as a mechanism of multidrug resistance. *Journal of clinical oncology : official journal of the American Society of Clinical Oncology*. 1998;16(11):3674-90.
18. Arceci RJ. Can multidrug resistance mechanisms be modified? *Br J Haematol*. 2000;110(2):285-91.
19. Bixby D, Talpaz M. Mechanisms of resistance to tyrosine kinase inhibitors in chronic myeloid leukemia and recent therapeutic strategies to overcome resistance. *Hematology Am Soc Hematol Educ Program*. 2009:461-76.
20. Lee S, Kim YJ, Min CK, Kim HJ, Eom KS, Kim DW, et al. The effect of first-line imatinib interim therapy on the outcome of allogeneic stem cell transplantation in adults with newly diagnosed Philadelphia chromosome-positive acute lymphoblastic leukemia. *Blood*. 2005;105(9):3449-57.
21. Keating MJ, Cazin B, Coutre S, Birhiray R, Kovacsics T, Langer W, et al. Campath-1H treatment of T-cell prolymphocytic leukemia in patients for whom at least one prior chemotherapy regimen has failed. *Journal of clinical oncology : official journal of the American Society of Clinical Oncology*. 2002;20(1):205-13.

22. Lundin J, Hagberg H, Repp R, Cavallin-Stahl E, Freden S, Juliusson G, et al. Phase 2 study of alemtuzumab (anti-CD52 monoclonal antibody) in patients with advanced mycosis fungoides/Sezary syndrome. *Blood*. 2003;101(11):4267-72.
23. Keating MJ, Flinn I, Jain V, Binet JL, Hillmen P, Byrd J, et al. Therapeutic role of alemtuzumab (Campath-1H) in patients who have failed fludarabine: results of a large international study. *Blood*. 2002;99(10):3554-61.
24. Rai KR, Freter CE, Mercier RJ, Cooper MR, Mitchell BS, Stadtmauer EA, et al. Alemtuzumab in previously treated chronic lymphocytic leukemia patients who also had received fludarabine. *Journal of clinical oncology : official journal of the American Society of Clinical Oncology*. 2002;20(18):3891-7.
25. Angiolillo AL, Yu AL, Reaman G, Ingle AM, Secola R, Adamson PC. A phase II study of Campath-1H in children with relapsed or refractory acute lymphoblastic leukemia: a Children's Oncology Group report. *Pediatr Blood Cancer*. 2009;53(6):978-83.
26. Raetz EA, Borowitz MJ, Devidas M, Linda SB, Hunger SP, Winick NJ, et al. Reinduction platform for children with first marrow relapse of acute lymphoblastic Leukemia: A Children's Oncology Group Study[corrected]. *Journal of clinical oncology : official journal of the American Society of Clinical Oncology*. 2008;26(24):3971-8.
27. Raetz EA, Cairo MS, Borowitz MJ, Xiaomin Lu P, Devidas M, Reid JM, et al. Reinduction chemoimmunotherapy with epratuzumab in relapsed Acute lymphoblastic leukemia (ALL) in children, adolescents and young adults: results from children's oncology group (COG) study ADVL04P2. . 53rd ASH Annual Meeting and Exposition; December 12, 2011; San Diego, CA: Amer Soc of Hematol; 2011.
28. Jeha S, Behm F, Pei D, Sandlund JT, Ribeiro RC, Razzouk BI, et al. Prognostic significance of CD20 expression in childhood B-cell precursor acute lymphoblastic leukemia. *Blood*. 2006;108(10):3302-4.
29. Smith MA. Update on developmental therapeutics for acute lymphoblastic leukemia. *Curr Hematol Malig Rep*. 2009;4(3):175-82.
30. Belgaumi AF, Al-Bakrah M, Al-Mahr M, Al-Jefri A, Al-Musa A, Saleh M, et al. Dexamethasone-associated toxicity during induction chemotherapy for childhood acute lymphoblastic leukemia is augmented by concurrent use of daunomycin. *Cancer*. 2003;97(11):2898-903.

31. Kremer LC, van Dalen EC, Offringa M, Ottenkamp J, Voute PA. Anthracycline-induced clinical heart failure in a cohort of 607 children: long-term follow-up study. *Journal of clinical oncology : official journal of the American Society of Clinical Oncology*. 2001;19(1):191-6.
32. Giona F, Testi AM, Amadori S, Meloni G, Carotenuto M, Resegotti L, et al. Idarubicin and high-dose cytarabine in the treatment of refractory and relapsed acute lymphoblastic leukemia. *Ann Oncol*. 1990;1(1):51-5.
33. Klastersky J. Side effects of ifosfamide. *Oncology*. 2003;65 Suppl 2:7-10.
34. Brugieres L, Hartmann O, Travagli JP, Benhamou E, Pico JL, Valteau D, et al. Hemorrhagic cystitis following high-dose chemotherapy and bone marrow transplantation in children with malignancies: incidence, clinical course, and outcome. *Journal of clinical oncology : official journal of the American Society of Clinical Oncology*. 1989;7(2):194-9.
35. Vogelzang NJ. Nephrotoxicity from chemotherapy: prevention and management. *Oncology (Williston Park)*. 1991;5(10):97-102, 5; disc 5, 9-11.
36. Casey EB, Jellife AM, Le Quesne PM, Millett YL. Vincristine neuropathy. Clinical and electrophysiological observations. *Brain*. 1973;96(1):69-86.
37. Gokbuget N, Hoelzer D. Vindesine in the treatment of leukaemia. *Leuk Lymphoma*. 1997;26(5-6):497-506.
38. Dollery CT. *Praziquantel*. Therapeutic Drugs. 2nd ed. Edinburgh: Churchill Livingstone; 1999. p. M184-P8.
39. Chessells JM, Cox TC, Kendall B, Cavanagh NP, Jannoun L, Richards S. Neurotoxicity in lymphoblastic leukaemia: comparison of oral and intramuscular methotrexate and two doses of radiation. *Arch Dis Child*. 1990;65(4):416-22.
40. Dibenedetto SP, Guardabasso V, Ragusa R, Di Cataldo A, Miraglia V, D'Amico S, et al. 6-Mercaptopurine cumulative dose: a critical factor of maintenance therapy in average risk childhood acute lymphoblastic leukemia. *Pediatr Hematol Oncol*. 1994;11(3):251-8.
41. Relling MV, Hancock ML, Rivera GK, Sandlund JT, Ribeiro RC, Krynetski EY, et al. Mercaptopurine therapy intolerance and heterozygosity at the thiopurine S-methyltransferase gene locus. *J Natl Cancer Inst*. 1999;91(23):2001-8.

42. Stoneham S, Lennard L, Coen P, Lilleyman J, Saha V. Veno-occlusive disease in patients receiving thiopurines during maintenance therapy for childhood acute lymphoblastic leukaemia. *Br J Haematol.* 2003;123(1):100-2.
43. Chun HG, Leyland-Jones BR, Caryk SM, Hoth DF. Central nervous system toxicity of fludarabine phosphate. *Cancer Treat Rep.* 1986;70(10):1225-8.
44. Kantarjian HM, Gandhi V, Kozuch P, Faderl S, Giles F, Cortes J, et al. Phase I clinical and pharmacology study of clofarabine in patients with solid and hematologic cancers. *Journal of clinical oncology : official journal of the American Society of Clinical Oncology.* 2003;21(6):1167-73.
45. Blanke CD, Rankin C, Demetri GD, Ryan CW, von Mehren M, Benjamin RS, et al. Phase III randomized, intergroup trial assessing imatinib mesylate at two dose levels in patients with unresectable or metastatic gastrointestinal stromal tumors expressing the kit receptor tyrosine kinase: S0033. *Journal of clinical oncology : official journal of the American Society of Clinical Oncology.* 2008;26(4):626-32.
46. Quintas-Cardama A, Cortes J. Nilotinib: a phenylamino-pyrimidine derivative with activity against BCR-ABL, KIT and PDGFR kinases. *Future Oncol.* 2008;4(5):611-21.
47. Physicians' Desk Reference (PDR). 63rd ed. Florence, KY: Thompson Healthcare; 2009.
48. Redaelli S, Piazza R, Rostagno R, Magistroni V, Perini P, Marega M, et al. Activity of bosutinib, dasatinib, and nilotinib against 18 imatinib-resistant BCR/ABL mutants. *Journal of clinical oncology : official journal of the American Society of Clinical Oncology.* 2009;27(3):469-71.
49. Aguilera DG, Tsimberidou AM. Dasatinib in chronic myeloid leukemia: a review. *Ther Clin Risk Manag.* 2009;5(2):281-9.
50. Breccia M, Alimena G. Nilotinib therapy in chronic myelogenous leukemia: the strength of high selectivity on BCR/ABL. *Curr Drug Targets.* 2009;10(6):530-6.
51. Cortes JE, Jones D, O'Brien S, Jabbour E, Ravandi F, Koller C, et al. Results of dasatinib therapy in patients with early chronic-phase chronic myeloid leukemia. *Journal of clinical oncology : official journal of the American Society of Clinical Oncology.* 2010;28(3):398-404.
52. Furman WL, Stewart CF, Kirstein M, Kepner JL, Bernstein ML, Kung F, et al. Protracted intermittent schedule of topotecan in children with refractory

- acute leukemia: a pediatric oncology group study. *Journal of clinical oncology : official journal of the American Society of Clinical Oncology*. 2002;20(6):1617-24.
53. Christie D, Battin M, Leiper AD, Chessells J, Vargha-Khadem F, Neville BG. Neuropsychological and neurological outcome after relapse of lymphoblastic leukaemia. *Arch Dis Child*. 1994;70(4):275-80.
 54. Pui CH, Cheng C, Leung W, Rai SN, Rivera GK, Sandlund JT, et al. Extended follow-up of long-term survivors of childhood acute lymphoblastic leukemia. *N Engl J Med*. 2003;349(7):640-9.
 55. Nanotechnology 101: United States National Nanotechnology Initiative; 2012 [cited 2012 December 3, 2012]. Available from: <http://www.nano.gov/>.
 56. Forssen EA, Ross ME. Daunoxome® Treatment of Solid Tumors: Preclinical and Clinical Investigations. *J of Liposome Res*. 1994;4(1):481-512.
 57. Mross K, Niemann B, Massing U, Drevs J, Unger C, Bhamra R, et al. Pharmacokinetics of liposomal doxorubicin (TLC-D99; Myocet) in patients with solid tumors: an open-label, single-dose study. *Cancer Chemother Pharmacol*. 2004;54(6):514-24.
 58. Feldman EJ, Kolitz JE, Trang JM, Liboiron BD, Swenson CE, Chiarella MT, et al. Pharmacokinetics of CPX-351; a nano-scale liposomal fixed molar ratio formulation of cytarabine:daunorubicin, in patients with advanced leukemia. *Leuk Res*. 2012;36(10):1283-9.
 59. O'Brien ME, Wigler N, Inbar M, Rosso R, Grischke E, Santoro A, et al. Reduced cardiotoxicity and comparable efficacy in a phase III trial of pegylated liposomal doxorubicin HCl (CAELYX/Doxil) versus conventional doxorubicin for first-line treatment of metastatic breast cancer. *Ann Oncol*. 2004;15(3):440-9.
 60. Valle JW, Armstrong A, Newman C, Alakhov V, Pietrzynski G, Brewer J, et al. A phase 2 study of SP1049C, doxorubicin in P-glycoprotein-targeting pluronic, in patients with advanced adenocarcinoma of the esophagus and gastroesophageal junction. *Invest New Drugs*. 2011;29(5):1029-37.
 61. Matsumura Y, Hamaguchi T, Ura T, Muro K, Yamada Y, Shimada Y, et al. Phase I clinical trial and pharmacokinetic evaluation of NK911, a micelle-encapsulated doxorubicin. *Br J Cancer*. 2004;91(10):1775-81.
 62. FDA approves Marqibo to treat rare type of leukemia (accessed on April 30, 2013) [cited 2013 April 30]. Available from:

<http://www.fda.gov/NewsEvents/Newsroom/PressAnnouncements/ucm315027.htm>

63. Fasol U, Frost A, Buchert M, Arends J, Fiedler U, Scharr D, et al. Vascular and pharmacokinetic effects of EndoTAG-1 in patients with advanced cancer and liver metastasis. *Ann Oncol.* 2012;23(4):1030-6.
64. ClinicalTrials.gov, National Library of Medicine [Internet]. accessed on December 3, 2012. Available from: <http://www.clinicaltrials.gov>.
65. Montana M, Ducros C, Verhaeghe P, Terme T, Vanelle P, Rathelot P. Albumin-bound paclitaxel: the benefit of this new formulation in the treatment of various cancers. *J Chemother.* 2011;23(2):59-66.
66. Lee KS, Chung HC, Im SA, Park YH, Kim CS, Kim SB, et al. Multicenter phase II trial of Genexol-PM, a Cremophor-free, polymeric micelle formulation of paclitaxel, in patients with metastatic breast cancer. *Breast Cancer Res Treat.* 2008;108(2):241-50.
67. Lee JL, Ahn JH, Park SH, Lim HY, Kwon JH, Ahn S, et al. Phase II study of a cremophor-free, polymeric micelle formulation of paclitaxel for patients with advanced urothelial cancer previously treated with gemcitabine and platinum. *Invest New Drugs.* 2011;30(5):1984-90.
68. Kato K, Chin K, Yoshikawa T, Yamaguchi K, Tsuji Y, Esaki T, et al. Phase II study of NK105, a paclitaxel-incorporating micellar nanoparticle, for previously treated advanced or recurrent gastric cancer. *Invest New Drugs.* 2012;30(4):1621-7.
69. Galic VL, Wright JD, Lewin SN, Herzog TJ. Paclitaxel poliglumex for ovarian cancer. *Expert Opin Investig Drugs.* 2011;20(6):813-21.
70. Dark GG, Calvert AH, Grimshaw R, Poole C, Swenerton K, Kaye S, et al. Randomized trial of two intravenous schedules of the topoisomerase I inhibitor liposomal lurtotecan in women with relapsed epithelial ovarian cancer: a trial of the national cancer institute of Canada clinical trials group. *Journal of clinical oncology : official journal of the American Society of Clinical Oncology.* 2005;23(9):1859-66.
71. Zamboni WC, Ramalingam S, Friedland DM, Edwards RP, Stoller RG, Strychor S, et al. Phase I and pharmacokinetic study of pegylated liposomal CKD-602 in patients with advanced malignancies. *Clinical cancer research : an official journal of the American Association for Cancer Research.* 2009;15(4):1466-72.

72. Weiss GJ, Chao J, Neidhart JD, Ramanathan RK, Bassett D, Neidhart JA, et al. First-in-human phase 1/2a trial of CRLX101, a cyclodextrin-containing polymer-camptothecin nanopharmaceutical in patients with advanced solid tumor malignancies. *Invest New Drugs*. 2013.
73. Hamaguchi T, Doi T, Eguchi-Nakajima T, Kato K, Yamada Y, Shimada Y, et al. Phase I study of NK012, a novel SN-38-incorporating micellar nanoparticle, in adult patients with solid tumors. *Clinical cancer research : an official journal of the American Association for Cancer Research*. 2010;16(20):5058-66.
74. Plummer R, Wilson RH, Calvert H, Boddy AV, Griffin M, Sludden J, et al. A Phase I clinical study of cisplatin-incorporated polymeric micelles (NC-6004) in patients with solid tumours. *Br J Cancer*. 2011;104(4):593-8.
75. Ishida T, Ichihara M, Wang X, Yamamoto K, Kimura J, Majima E, et al. Injection of PEGylated liposomes in rats elicits PEG-specific IgM, which is responsible for rapid elimination of a second dose of PEGylated liposomes. *Journal of controlled release : official journal of the Controlled Release Society*. 2006;112(1):15-25.
76. Koide H, Asai T, Hatanaka K, Urakami T, Ishii T, Kenjo E, et al. Particle size-dependent triggering of accelerated blood clearance phenomenon. *International journal of pharmaceutics*. 2008;362(1-2):197-200.
77. Lu W, Wan J, She Z, Jiang X. Brain delivery property and accelerated blood clearance of cationic albumin conjugated pegylated nanoparticle. *Journal of controlled release : official journal of the Controlled Release Society*. 2007;118(1):38-53.
78. Tagami T, Uehara Y, Moriyoshi N, Ishida T, Kiwada H. Anti-PEG IgM production by siRNA encapsulated in a PEGylated lipid nanocarrier is dependent on the sequence of the siRNA. *Journal of controlled release : official journal of the Controlled Release Society*. 2011;151(2):149-54.
79. Kaminskas LM, McLeod VM, Porter CJ, Boyd BJ. Differences in colloidal structure of PEGylated nanomaterials dictate the likelihood of accelerated blood clearance. *Journal of pharmaceutical sciences*. 2011;100(11):5069-77.
80. Huang X, Brazel CS. On the importance and mechanisms of burst release in matrix-controlled drug delivery systems. *Journal of controlled release : official journal of the Controlled Release Society*. 2001;73(2-3):121-36.
81. Maeda H. Tumor-selective delivery of macromolecular drugs via the EPR effect: background and future prospects. *Bioconjugate chemistry*. 2010;21(5):797-802.

82. Chrastina A, Massey KA, Schnitzer JE. Overcoming in vivo barriers to targeted nanodelivery. Wiley Interdiscip Rev Nanomed Nanobiotechnol. 2011;3(4):421-37.
83. Bartlett DW, Su H, Hildebrandt IJ, Weber WA, Davis ME. Impact of tumor-specific targeting on the biodistribution and efficacy of siRNA nanoparticles measured by multimodality in vivo imaging. Proceedings of the National Academy of Sciences of the United States of America. 2007;104(39):15549-54.
84. He H, Chen S, Zhou J, Dou Y, Song L, Che L, et al. Cyclodextrin-derived pH-responsive nanoparticles for delivery of paclitaxel. Biomaterials. 2013;34(21):5344-58.
85. Matsumura Y, Gotoh M, Muro K, Yamada Y, Shirao K, Shimada Y, et al. Phase I and pharmacokinetic study of MCC-465, a doxorubicin (DXR) encapsulated in PEG immunoliposome, in patients with metastatic stomach cancer. Ann Oncol. 2004;15(3):517-25.
86. Sankhala KK, Mita AC, Adinin R, Wood L, Beeram M, Bullock S, et al. A phase I pharmacokinetic (PK) study of MBP-426, a novel liposome encapsulated oxaliplatin. 2009 ASCO Annual Meeting; Orlando, Florida: J Clin Oncol; 2009. p. 15s.
87. Nemunaitis J, Senzer N, Bedell C, Nunan R, Sleer L, Chang E. A phase I study of escalating doses of SGT-53 for intravenous infusion of patients with advanced solid tumors. Mol Ther. 2009;17:S226.
88. Hrkach J, Von Hoff D, Mukkaram Ali M, Andrianova E, Auer J, Campbell T, et al. Preclinical development and clinical translation of a PSMA-targeted docetaxel nanoparticle with a differentiated pharmacological profile. Sci Transl Med. 2012;4(128):128ra39.
89. Davis ME. The first targeted delivery of siRNA in humans via a self-assembling, cyclodextrin polymer-based nanoparticle: from concept to clinic. Molecular pharmaceutics. 2009;6(3):659-68.
90. National Cancer Institute - The Childhood Cancer Survivor Study: An Overview. 2012 June 06, 2012. Report No.
91. Hunger SP, Lu X, Devidas M, Camitta BM, Gaynon PS, Winick NJ, et al. Improved survival for children and adolescents with acute lymphoblastic leukemia between 1990 and 2005: a report from the children's oncology group. Journal of clinical oncology : official journal of the American Society of Clinical Oncology. 2012;30(14):1663-9.

92. U.S. National Library of Medicine (PubMed Health) [Internet]. (accessed on December 30, 2014). Available from: <http://www.ncbi.nlm.nih.gov/pubmedhealth/PMHT0000542/>
93. Hyman CB, Sturgeon P. Prednisone therapy of acute lymphatic leukemia in children. *Cancer.* 1956;9(5):965-70.
94. Gaynon PS, Carrel AL. Glucocorticosteroid therapy in childhood acute lymphoblastic leukemia. *Advances in experimental medicine and biology.* 1999;457:593-605.
95. Wang X, Gurski LA, Zhong S, Xu X, Pochan DJ, Farach-Carson MC, et al. Amphiphilic Block Co-polyesters Bearing Pendant Cyclic Ketal Groups as Nanocarriers for Controlled Release of Camptothecin. *J Biomater Sci Polym Ed.* 2010;22(10):1275– 98.
96. Yoo HS, Park TG. Biodegradable polymeric micelles composed of doxorubicin conjugated PLGA-PEG block copolymer. *Journal of controlled release : official journal of the Controlled Release Society.* 2001;70(1-2):63-70.
97. Shuai X, Merdan T, Schaper AK, Xi F, Kissel T. Core-cross-linked polymeric micelles as paclitaxel carriers. *Bioconjugate chemistry.* 2004;15(3):441-8.
98. Garcia-Garcia E, Andrieux K, Gil S, Kim HR, Le Doan T, Desmaele D, et al. A methodology to study intracellular distribution of nanoparticles in brain endothelial cells. *International journal of pharmaceutics.* 2005;298(2):310-4.
99. Bilensoy E, Sarisozen C, Esendagli G, Dogan AL, Aktas Y, Sen M, et al. Intravesical cationic nanoparticles of chitosan and polycaprolactone for the delivery of Mitomycin C to bladder tumors. *International journal of pharmaceutics.* 2009;371(1-2):170-6.
100. Laane E, Panaretakis T, Pokrovskaja K, Buentke E, Corcoran M, Soderhall S, et al. Dexamethasone-induced apoptosis in acute lymphoblastic leukemia involves differential regulation of Bcl-2 family members. *Haematologica.* 2007;92(11):1460-9.
101. Yim EK, Lee MJ, Lee KH, Um SJ, Park JS. Antiproliferative and antiviral mechanisms of ursolic acid and dexamethasone in cervical carcinoma cell lines. *International journal of gynecological cancer : official journal of the International Gynecological Cancer Society.* 2006;16(6):2023-31.
102. Zhang JP, Wong CK, Lam CW. Role of caspases in dexamethasone-induced apoptosis and activation of c-Jun NH₂-terminal kinase and p38

- mitogen-activated protein kinase in human eosinophils. Clinical and experimental immunology. 2000;122(1):20-7.
103. Planey SL, Litwack G. Glucocorticoid-induced apoptosis in lymphocytes. Biochemical and biophysical research communications. 2000;279(2):307-12.
 104. Liem NL, Papa RA, Milross CG, Schmid MA, Tajbakhsh M, Choi S, et al. Characterization of childhood acute lymphoblastic leukemia xenograft models for the preclinical evaluation of new therapies. Blood. 2004;103(10):3905-14.
 105. Lal D, Park JA, Demock K, Marinaro J, Perez AM, Lin MH, et al. Afibbercept exerts antivascular effects and enhances levels of anthracycline chemotherapy in vivo in human acute myeloid leukemia models. Molecular cancer therapeutics. 2010;9(10):2737-51.
 106. Lock RB, Liem N, Farnsworth ML, Milross CG, Xue C, Tajbakhsh M, et al. The nonobese diabetic/severe combined immunodeficient (NOD/SCID) mouse model of childhood acute lymphoblastic leukemia reveals intrinsic differences in biologic characteristics at diagnosis and relapse. Blood. 2002;99(11):4100-8.
 107. van Kooten C, Stax AS, Wolzman AM, Gelderman KA. Handbook of experimental pharmacology "dendritic cells": the use of dexamethasone in the induction of tolerogenic DCs. Handbook of experimental pharmacology. 2009(188):233-49.
 108. Chen Y, Song S, Yan Z, Fenniri H, Webster TJ. Self-assembled rosette nanotubes encapsulate and slowly release dexamethasone. International journal of nanomedicine. 2011;6:1035-44.
 109. Fialho SL, Behar-Cohen F, Silva-Cunha A. Dexamethasone-loaded poly(epsilon-caprolactone) intravitreal implants: a pilot study. European journal of pharmaceuticals and biopharmaceutics : official journal of Arbeitsgemeinschaft fur Pharmazeutische Verfahrenstechnik eV. 2008;68(3):637-46.
 110. Zhang L, Li Y, Zhang C, Wang Y, Song C. Pharmacokinetics and tolerance study of intravitreal injection of dexamethasone-loaded nanoparticles in rabbits. International journal of nanomedicine. 2009;4:175-83.
 111. Liu X, Huang Y, Hanet C, Vandormael M, Legrand V, Dens J, et al. Study of antirestenosis with the BiodivYsio dexamethasone-eluting stent (STRIDE): a first-in-human multicenter pilot trial. Catheterization and

cardiovascular interventions : official journal of the Society for Cardiac Angiography & Interventions. 2003;60(2):172-8; discussion 9.

112. Hoffmann R, Langenberg R, Radke P, Franke A, Blindt R, Ortlepp J, et al. Evaluation of a high-dose dexamethasone-eluting stent. *The American journal of cardiology*. 2004;94(2):193-5.
113. Dhar S, Kolishetti N, Lippard SJ, Farokhzad OC. Targeted delivery of a cisplatin prodrug for safer and more effective prostate cancer therapy in vivo. *Proceedings of the National Academy of Sciences of the United States of America*. 2011;108(5):1850-5.
114. Wang X, Li J, Wang Y, Koenig L, Gjyrezi A, Giannakakou P, et al. A folate receptor-targeting nanoparticle minimizes drug resistance in a human cancer model. *ACS nano*. 2011;5(8):6184-94.
115. Aliabadi HM, Lavasanifar A. Polymeric micelles for drug delivery. *Expert opinion on drug delivery*. 2006;3(1):139-62.
116. Mohanty C, Acharya S, Mohanty AK, Dilnawaz F, Sahoo SK. Curcumin-encapsulated MePEG/PCL diblock copolymeric micelles: a novel controlled delivery vehicle for cancer therapy. *Nanomedicine*. 2010;5(3):433-49.
117. Mikhail AS, Allen C. Poly(ethylene glycol)-b-poly(epsilon-caprolactone) micelles containing chemically conjugated and physically entrapped docetaxel: synthesis, characterization, and the influence of the drug on micelle morphology. *Biomacromolecules*. 2010;11(5):1273-80.
118. Aliabadi HM, Mahmud A, Sharifabadi AD, Lavasanifar A. Micelles of methoxy poly(ethylene oxide)-b-poly(epsilon-caprolactone) as vehicles for the solubilization and controlled delivery of cyclosporine A. *Journal of controlled release : official journal of the Controlled Release Society*. 2005;104(2):301-11.
119. Panyam J, Williams D, Dash A, Leslie-Pelecky D, Labhasetwar V. Solid-state solubility influences encapsulation and release of hydrophobic drugs from PLGA/PLA nanoparticles. *Journal of pharmaceutical sciences*. 2004;93(7):1804-14.
120. Chen WC, Completo GC, Sigal DS, Crocker PR, Saven A, Paulson JC. In vivo targeting of B-cell lymphoma with glycan ligands of CD22. *Blood*. 2010;115(23):4778-86.
121. Hickey T, Kreutzer D, Burgess DJ, Moussy F. Dexamethasone/PLGA microspheres for continuous delivery of an anti-inflammatory drug for implantable medical devices. *Biomaterials*. 2002;23(7):1649-56.

122. Yang L, Panetta JC, Cai X, Yang W, Pei D, Cheng C, et al. Asparaginase may influence dexamethasone pharmacokinetics in acute lymphoblastic leukemia. *Journal of clinical oncology : official journal of the American Society of Clinical Oncology*. 2008;26(12):1932-9.
123. Alexis F, Pridgen E, Molnar LK, Farokhzad OC. Factors affecting the clearance and biodistribution of polymeric nanoparticles. *Molecular pharmaceutics*. 2008;5(4):505-15.
124. Zhan C, Gu B, Xie C, Li J, Liu Y, Lu W. Cyclic RGD conjugated poly(ethylene glycol)-co-poly(lactic acid) micelle enhances paclitaxel anti-glioblastoma effect. *Journal of controlled release : official journal of the Controlled Release Society*. 2010;143(1):136-42.
125. Pan XQ, Zheng X, Shi G, Wang H, Ratnam M, Lee RJ. Strategy for the treatment of acute myelogenous leukemia based on folate receptor beta-targeted liposomal doxorubicin combined with receptor induction using all-trans retinoic acid. *Blood*. 2002;100(2):594-602.
126. Chen H, Ahn R, Van den Bossche J, Thompson DH, O'Halloran TV. Folate-mediated intracellular drug delivery increases the anticancer efficacy of nanoparticulate formulation of arsenic trioxide. *Molecular cancer therapeutics*. 2009;8(7):1955-63.
127. Harata M, Soda Y, Tani K, Ooi J, Takizawa T, Chen M, et al. CD19-targeting liposomes containing imatinib efficiently kill Philadelphia chromosome-positive acute lymphoblastic leukemia cells. *Blood*. 2004;104(5):1442-9.
128. Zhang J, Tang Y, Li S, Liao C, Guo X. Targeting of the B-lineage leukemia stem cells and their progeny with norcantharidin encapsulated liposomes modified with a novel CD19 monoclonal antibody 2E8 in vitro. *Journal of drug targeting*. 2010;18(9):675-87.
129. Yoon TJ, Yu KN, Kim E, Kim JS, Kim BG, Yun SH, et al. Specific targeting, cell sorting, and bioimaging with smart magnetic silica core-shell nanomaterials. *Small*. 2006;2(2):209-15.
130. Lapotko DO, Lukianova E, Oraevsky AA. Selective laser nano-thermolysis of human leukemia cells with microbubbles generated around clusters of gold nanoparticles. *Lasers in surgery and medicine*. 2006;38(6):631-42.
131. Qian ZM, Li H, Sun H, Ho K. Targeted drug delivery via the transferrin receptor-mediated endocytosis pathway. *Pharmacological reviews*. 2002;54(4):561-87.

132. Yang X, Koh CG, Liu S, Pan X, Santhanam R, Yu B, et al. Transferrin receptor-targeted lipid nanoparticles for delivery of an antisense oligodeoxyribonucleotide against Bcl-2. *Molecular pharmaceutics*. 2009;6(1):221-30.
133. Krishnan V, Rajasekaran AK. Clinical Nanomedicine: a solution to the chemotherapy conundrum in pediatric leukemia therapy. *Clin Pharmacol Ther*. 2013.
134. Peer D, Karp JM, Hong S, Farokhzad OC, Margalit R, Langer R. Nanocarriers as an emerging platform for cancer therapy. *Nat Nanotechnol*. 2007;2(12):751-60.
135. Kirpotin DB, Drummond DC, Shao Y, Shalaby MR, Hong K, Nielsen UB, et al. Antibody targeting of long-circulating lipidic nanoparticles does not increase tumor localization but does increase internalization in animal models. *Cancer Res*. 2006;66(13):6732-40.
136. Tedder TF, Isaacs CM. Isolation of cDNAs encoding the CD19 antigen of human and mouse B lymphocytes. A new member of the immunoglobulin superfamily. *Journal of immunology*. 1989;143(2):712-7.
137. Tedder TF. CD19: a promising B cell target for rheumatoid arthritis. *Nature reviews Rheumatology*. 2009;5(10):572-7.
138. Uckun FM, Jaszcz W, Ambrus JL, Fauci AS, Gajl-Peczalska K, Song CW, et al. Detailed studies on expression and function of CD19 surface determinant by using B43 monoclonal antibody and the clinical potential of anti-CD19 immunotoxins. *Blood*. 1988;71(1):13-29.
139. Cooper LJ, Al-Kadhimi Z, DiGiusto D, Kalos M, Colcher D, Raubitschek A, et al. Development and application of CD19-specific T cells for adoptive immunotherapy of B cell malignancies. *Blood cells, molecules & diseases*. 2004;33(1):83-9.
140. Loken MR, Shah VO, Dattilio KL, Civin CI. Flow cytometric analysis of human bone marrow. II. Normal B lymphocyte development. *Blood*. 1987;70(5):1316-24.
141. Manzke O, Berthold F, Huebel K, Tesch H, Diehl V, Bohlen H. CD3xCD19 bispecific antibodies and CD28 bivalent antibodies enhance T-cell reactivity against autologous leukemic cells in pediatric B-ALL bone marrow. *International journal of cancer Journal international du cancer*. 1999;80(5):715-22.

142. Szatrowski TP, Dodge RK, Reynolds C, Westbrook CA, Frankel SR, Sklar J, et al. Lineage specific treatment of adult patients with acute lymphoblastic leukemia in first remission with anti-B4-blocked ricin or high-dose cytarabine: Cancer and Leukemia Group B Study 9311. *Cancer*. 2003;97(6):1471-80.
143. Mitchell P, Lee FT, Hall C, Rigopoulos A, Smyth FE, Hekman AM, et al. Targeting primary human Ph(+) B-cell precursor leukemia-engrafted SCID mice using radiolabeled anti-CD19 monoclonal antibodies. *Journal of nuclear medicine : official publication, Society of Nuclear Medicine*. 2003;44(7):1105-12.
144. Cheng WW, Allen TM. Targeted delivery of anti-CD19 liposomal doxorubicin in B-cell lymphoma: a comparison of whole monoclonal antibody, Fab' fragments and single chain Fv. *Journal of controlled release : official journal of the Controlled Release Society*. 2008;126(1):50-8.
145. Sapra P, Moase EH, Ma J, Allen TM. Improved therapeutic responses in a xenograft model of human B lymphoma (Namalwa) for liposomal vincristine versus liposomal doxorubicin targeted via anti-CD19 IgG2a or Fab' fragments. *Clinical cancer research : an official journal of the American Association for Cancer Research*. 2004;10(3):1100-11.
146. FDA approves Blincyto to treat a rare form of acute lymphoblastic leukemia (accessed on December 12, 2014) [cited 2014 December 12]. Available from: <http://www.fda.gov/NewsEvents/Newsroom/PressAnnouncements/ucm425549.htm>.
147. Lipshultz SE, Lipsitz SR, Sallan SE, Dalton VM, Mone SM, Gelber RD, et al. Chronic progressive cardiac dysfunction years after doxorubicin therapy for childhood acute lymphoblastic leukemia. *J Clin Oncol*. 2005;23(12):2629-36.
148. Altreuter DH, Dordick JS, Clark DS. Nonaqueous biocatalytic synthesis of new cytotoxic doxorubicin derivatives: exploiting unexpected differences in the regioselectivity of salt-activated and solubilized subtilisin. *J Am Chem Soc*. 2002;124(9):1871-6.
149. Xu X, Sabanayagam CR, Harrington DA, Farach-Carson MC, Jia X. A hydrogel-based tumor model for the evaluation of nanoparticle-based cancer therapeutics. *Biomaterials*. 2014;35(10):3319-30.
150. Heuser JE, Anderson RG. Hypertonic media inhibit receptor-mediated endocytosis by blocking clathrin-coated pit formation. *J Cell Biol*. 1989;108(2):389-400.

151. Plummer EM, Manchester M. Endocytic uptake pathways utilized by CPMV nanoparticles. *Molecular pharmaceutics*. 2013;10(1):26-32.
152. Benmerah A, Lamaze C. Clathrin-coated pits: vive la difference? *Traffic*. 2007;8(8):970-82.
153. Christiansen J, Rajasekaran AK. Biological impediments to monoclonal antibody-based cancer immunotherapy. *Molecular cancer therapeutics*. 2004;3(11):1493-501.
154. Fahmy TM, Samstein RM, Harness CC, Mark Saltzman W. Surface modification of biodegradable polyesters with fatty acid conjugates for improved drug targeting. *Biomaterials*. 2005;26(28):5727-36.
155. Xiang S, Tong H, Shi Q, Fernandes JC, Jin T, Dai K, et al. Uptake mechanisms of non-viral gene delivery. *Journal of controlled release : official journal of the Controlled Release Society*. 2012;158(3):371-8.
156. Jiang W, Kim BY, Rutka JT, Chan WC. Nanoparticle-mediated cellular response is size-dependent. *Nat Nanotechnol*. 2008;3(3):145-50.
157. Petros RA, DeSimone JM. Strategies in the design of nanoparticles for therapeutic applications. *Nat Rev Drug Discov*. 2010;9(8):615-27.
158. Moghimi SM, Hunter AC, Murray JC. Long-circulating and target-specific nanoparticles: theory to practice. *Pharmacological reviews*. 2001;53(2):283-318.
159. Choi HS, Liu W, Misra P, Tanaka E, Zimmer JP, Itty Ipe B, et al. Renal clearance of quantum dots. *Nat Biotechnol*. 2007;25(10):1165-70.
160. Torchilin VP. Targeted pharmaceutical nanocarriers for cancer therapy and imaging. *AAPS J*. 2007;9(2):E128-47.
161. Geng Y, Dalhaimer P, Cai S, Tsai R, Tewari M, Minko T, et al. Shape effects of filaments versus spherical particles in flow and drug delivery. *Nat Nanotechnol*. 2007;2(4):249-55.
162. Verma A, Stellacci F. Effect of surface properties on nanoparticle-cell interactions. *Small*. 2010;6(1):12-21.
163. Weissleder R, Kelly K, Sun EY, Shtatland T, Josephson L. Cell-specific targeting of nanoparticles by multivalent attachment of small molecules. *Nat Biotechnol*. 2005;23(11):1418-23.

164. Gilkey, MJ, Krishnan, V, Scheetz L, Jia, X, Rajasekaran, AK, Dhurjati, PS. Physiologically Based Pharmacokinetic Modeling of Fluorescently Labeled Block Copolymer Nanoparticles for Controlled Drug Delivery in Leukemia Therapy. *CPT Pharmacometrics Syst Pharmacol.* 2014; in press.
165. Lancet JE, Cortes JE, Kovacsics T, Hogge DE, Kolitz JE, Tallman MS, et al. CPX-351 Is Effective in Newly Diagnosed Older Patients with AML and with Multiple Risk Factors. 54th ASH Annual Meeting and Exposition; Atlanta, Georgia: Blood-ASH Annual Meeting Abstracts; 2012.

Appendix A
PERMISSION LETTERS

A.1 Reprint Permission for Chapter 1

A.2 Reprint Permission for Chapter 2

Vinu Krishnan <vinu@udel.edu>

Request for RightsLink permission to use first-author review article

2 messages

Vinu <vinu@udel.edu>
To: RightsLink@wiley.com

Tue, Jan 6, 2015 at 7:24 AM

Dear Editor,

I am writing to request for permission to reuse in my Dissertation the "Full Text including full text of the article, all tables (1, 2 and 3), all figures (1,2 and 3) and extracts" of my original first-author review article that was published in your journal "Clinical Pharmacology and Therapeutics".

The article info is as follows:

"Clinical Nanomedicine: A Solution to the Chemotherapy Conundrum in Pediatric Leukemia Therapy (pages 168–178) - V Krishnan and A K Rajasekaran; Article first published online: 5 SEP 2013 | DOI: 10.1038/clpt.2013.174"

Please let me know the appropriate procedure to credit the article and to include the copy of the RightsLink permission in both print and electronic forms of my Dissertation.

Thanks and Regards,

Vinu

--

Vinu Krishnan, M.S.E.
2013 AACR Gerald B. Grindey Memorial Scholar-in-Training
Ph.D. Candidate - Department of Materials Science and Engineering
201 DuPont Hall 127 The Green
University of Delaware
Newark, DE 19716
M: (330)780-7523
Email: vinu@udel.edu
Linkedin: <http://www.linkedin.com/pub/vinu-krishnan/10/b0a/921/>

Please consider the environment before printing this email

Wiley Global Permissions <permissions@wiley.com>
To: Vinu <vinu@udel.edu>

Wed, Jan 7, 2015 at 2:55 PM

Dear Vinu,

Permission is hereby granted for the use requested subject to the usual acknowledgements (author, title of material,

title of journal, ourselves as publisher). You should also duplicate the copyright notice that appears in the Wiley publication in your use of the Material.

Any third party material is expressly excluded from this permission. If any of the material you wish to use appears within our work with credit to another source, authorization from that source must be obtained.

This permission does not include the right to grant others permission to photocopy or otherwise reproduce this material except for accessible versions made by non-profit organizations serving the blind, visually impaired and other persons with print disabilities (VIPs).

Sincerely,

Sheik Safdar

Permissions Coordinator

Wiley

ssafdar@wiley.com

T +1 201-748-6512

F +1 201-748-6008

111 River Street, MS 4-02

Hoboken, NJ 07030-5774

U.S.

permissions@wiley.com

The Wiley logo consists of the word "WILEY" in a bold, serif font. The letter "W" is significantly larger than the other letters, which are "I", "L", "E", and "Y".

From: Vinu [mailto:vinu@udel.edu]
Sent: Tuesday, January 06, 2015 7:24 AM

[Home](#)[Create Account](#)[Help](#)**Title:**

Dexamethasone-Loaded Block Copolymer Nanoparticles Induce Leukemia Cell Death and Enhance Therapeutic Efficacy: A Novel Application in Pediatric Nanomedicine

Author:

Vinu Krishnan, Xian Xu, Sonali P. Barwe, et al

Publication: Molecular Pharmaceutics**Publisher:** American Chemical Society**Date:** Jun 1, 2013

Copyright © 2013, American Chemical Society

[LOGIN](#)

If you're a [copyright.com user](#), you can login to RightsLink using your copyright.com credentials. Already a [RightsLink user](#) or want to [learn more?](#)

PERMISSION/LICENSE IS GRANTED FOR YOUR ORDER AT NO CHARGE

This type of permission/license, instead of the standard Terms & Conditions, is sent to you because no fee is being charged for your order. Please note the following:

- Permission is granted for your request in both print and electronic formats, and translations.
- If figures and/or tables were requested, they may be adapted or used in part.
- Please print this page for your records and send a copy of it to your publisher/graduate school.
- Appropriate credit for the requested material should be given as follows: "Reprinted (adapted) with permission from (COMPLETE REFERENCE CITATION). Copyright (YEAR) American Chemical Society." Insert appropriate information in place of the capitalized words.
- One-time permission is granted only for the use specified in your request. No additional uses are granted (such as derivative works or other editions). For any other uses, please submit a new request.

[BACK](#)[CLOSE WINDOW](#)

Copyright © 2015 [Copyright Clearance Center, Inc.](#). All Rights Reserved. [Privacy statement](#).
Comments? We would like to hear from you. E-mail us at customercare@copyright.com

Appendix B

CALCULATIONS

B.1 Calculating number of anti-CD19Ab molecules conjugated per NP.

Weight of ECT copolymer taken for NP synthesis = 10 mg (0.01 g)

Density of ECT copolymer = 1.15 g/cm³

Therefore, volume of ECT copolymer taken for NP synthesis = $(0.01/1.15) \text{ cm}^3$

= 0.009 cm^3 or $9 \times 10^{18} \text{ nm}^3$

Volume of 1 NP = $4/3 \times \pi \times (40)^3 = 2.7 \times 10^5 \text{ nm}^3$

Therefore, number of NPs per formulation = $(9 \times 10^{18}/2.7 \times 10^5) \text{ nm}^3$

$\approx 3.33 \times 10^{13} \text{ NPs}$

Weight of NPs obtained per formulation = 8mg

Therefore, number of NPs per mg of formulated NPs $\approx 4.2 \times 10^{12} \text{ NPs}$

By immunoblot quantification (Fig. 3.1), number of anti-CD19Ab molecules per mg of formulated NPs $\approx 77.09 \times 10^{10}$ molecules of anti-CD19Ab

Therefore, number of anti-CD19Ab molecules per formulated NP

≈ 3.23 anti-CD19Ab molecules conjugated per NP

B.2 Calculating number of anti-CD19Ab conjugated NPs inside non-targeted REH and targeted RS4;11 leukemic cells.

Loading amount of DOX per mg of formulated NPs = 72 µg/mg \approx 132 µM DOX

Based on HPLC/MS/MS quantitation of DOX extracted from:

(A) REH cells treated with 100 nM encapsulated DOX

= 2 nM DOX or 1.09 ng DOX was extracted.

This is encapsulated within 0.015 µg of formulated NPs.

From Appendix B.1, number of NPs per mg of formulated NPs = 4.2×10^{12} NPs

Therefore, number of NPs in 0.015 µg of formulated NPs \approx 0.64×10^8 NPs

Approximately, 0.72M REH cells were treated with 0.64×10^8 DOX-NPs.

Therefore, the number of NPs internalized per REH cell is \approx **90 NPs**.

(B) RS4;11 cells treated with 100 nM encapsulated DOX

= 12 nM DOX or 6.5 ng DOX was extracted.

This is encapsulated within 0.09 µg of formulated NPs.

From Appendix B.1, number of NPs per mg of formulated NPs = 4.2×10^{12} NPs

Therefore, number of NPs in 0.09 µg of formulated NPs = 4×10^8 NPs

Approximately, 0.72M RS4;11 cells were treated with 4×10^8 DOX-NPs.

Therefore, the number of NPs internalized per RS4;11 cell is \approx **560 NPs**.

Therefore, the number of NPs internalized within RS4;11 cells are 6 times more than the number of particles internalized within REH cells.

Appendix C

ANIMAL SUBJECTS PROTOCOL REVIEW AND APPROVAL BY INSTITUTIONAL REVIEW BOARD (IRB)

RECEIVED

DEC 17 2013

University of Delaware
Institutional Animal Care and Use Committee

Application to Use Animals in Research and Teaching

IACUC CR

Title of Protocol: Drug efficacy studies in xenograft models of leukemia and solid tumors

AUP Number: 1262-2014-0

← (4 digits only — if new, leave blank)

Principal Investigator: Ayyappan K Rajasekaran, PhD

Co-Principal Investigator: Xinqiao Jia, PhD

Common Name: Mice

Genus Species: *Mus musculus*

Pain Category: (please mark one)

USDA PAIN CATEGORY: (Note change of categories from previous form)

Category	Description
<input type="checkbox"/> B	Breeding or holding where NO research is conducted
<input type="checkbox"/> C	Procedure involving momentary or no pain or distress
<input checked="" type="checkbox"/> D	Procedure where pain or distress is alleviated by appropriate means (analgesics, tranquilizers, euthanasia etc.)
<input type="checkbox"/> E	Procedure where pain or distress cannot be alleviated, as this would adversely affect the procedures, results or interpretation

Official Use Only

IACUC Approval Signature:

John Tolson, DVM

Date of Approval: 12/17/13